# REMOTE SENSING APPLICATIONS IN FORESTRY



## MONITORING FOREST LAND FROM HIGH ALTITUDE AND FROM SPACE

by



Personnel of the
Remote Sensing Research Work Unit

Pacific Southwest Forest and Range Experiment Station
Forest Service, U. S. Department of Agriculture

Annual Progress Report — 30 September 1971

*A report of research performed under the auspices of the*

Forestry Remote Sensing Laboratory,
School of Forestry and Conservation
University of California
Berkeley, California

*A Coordination Task Carried Out in Cooperation with*

The Forest Service, U. S. Department of Agriculture

*For*

EARTH RESOURCES SURVEY PROGRAM
OFFICE OF SPACE SCIENCES AND APPLICATIONS
NATIONAL AERONAUTICS AND SPACE ADMINISTRATION

# REMOTE SENSING APPLICATIONS IN FORESTRY

MONITORING FOREST LAND FROM HIGH ALTITUDE AND FROM SPACE

by



Personnel of the
Remote Sensing Research Work Unit

Pacific Southwest Forest and Range Experiment Station
Forest Service, U. S. Department of Agriculture

Annual Progress Report 30 September 1971

*A report of research performed under the auspices of the*

Forestry Remote Sensing Laboratory,
School of Forestry and Conservation
University of California
Berkeley, California
*A Coordination Task Carried Out in Cooperation with*
The Forest Service, U. S. Department of Agriculture

*For*

EARTH RESOURCES SURVEY PROGRAM
OFFICE OF SPACE SCIENCES AND APPLICATIONS
NATIONAL AERONAUTICS AND SPACE ADMINISTRATION

## PREFACE

This reporting year we have consolidated our four separate reports into one with three sections -- forest inventory, forest stress, and standardization and calibration studies. A series of papers is found in each section. We believe this new format improves the report for the reader by directing him to his particular areas of interest.

Short section summaries can be found following the listing of ACKNOWLEDGEMENTS AND COOPERATORS.

TABLE OF CONTENTS

## PERSONNEL

Salaries of all professional employees of the Remote Sensing Work Unit are contributed by the Forest Service. Employees at the Pacific Southwest Forest and Range Experiment Station assigned to these studies are:

Harry W. Camp, Assistant Director

Robert C. Heller, Supervisory Research Forester and Work Unit Leader

Robert C. Aldrich, Principal Research Forester

John F. Wear, Forester

Frederick P. Weber, Research Forester

Nancy X. Norick, Mathematical Statistician

Robert W. Dana, Physicist

Wallace J. Greentree, Forestry Research Technician

Richard J. Myhre, Photographer

Kristina A. Zealear, Geographer

Marilyn Wilkes, Mathematician

Thomas H. Waite, Forestry Technician (Research)

Anne L. Weber, Work Unit Clerk

Mary L. Chin, Clerk-typist

Summer, part-time and Work Study employees assigned to the PSW remote sensing work unit include:

| | |
|---|---|
| John Cole | James McSwanson |
| Michael Kowalski | John Noble |
| Gabriel Lugo | Steven Ramirez |
| Benno Marx | James von Mosch |

Cooperating Forest Service employees at the Rocky Mountain Forest and Range Experiment Station who assisted on these studies are:

Robert E. Stevens, Supervisory Forest Entomologist

Richard S. Driscoll, Principal Plant Ecologist

James Mitchell, Entomologist

## ACKNOWLEDGEMENTS AND COOPERATORS

These experiments are being performed under the Earth Resources Survey Program in Agriculture/Forestry under the sponsorship and financial assistance of the National Aeronautics and Space Administration, Contract No. R-90-038-002. Research and administrative direction are provided by the Pacific Southwest Forest and Range Experiment Station. Other cooperators and their contributions are:

1. R. H. Miller, Assistant to the Administrator, ARS, coordinator for Agriculture/Forestry. Provided information and guidance on program planning and status.

2. R. N. Colwell, Professor of Forestry, and G. A. Thorley, Director, Forestry Remote Sensing Laboratory, School of Forestry and Conservation, University of California, Berkeley. Consultation and integration of forestry-NASA studies.

3. Richard P. Cook, David Stark, David Hessel, Black Hills National Forest, R-2, Spearfish and Lead, South Dakota. Provided maps, vehicles, and personnel.

4. Homestake Mining Company, Forestry Department, Spearfish, South Dakota. Permitted use of property to conduct experiment.

5. Anaconda Copper and Mining Corporation, Belle Fourche, South Dakota. Permitted use of property to conduct experiment.

6. Richard Legault, Fabian Polcyn, Philip Hasell, and Fred Thomson, Willow Run Laboratories, University of Michigan. Consultation, collection, and processing of multispectral scanning data.

7. Joseph Bell, Entomologist, Forest Insect and Disease Control, Southern Area, State and Private Forestry, Forest Service, Asheville,

North Carolina. Made contacts with Georgia Forestry Commission to arrange for use of private property in Atlanta, Georgia, area.

8. Edward P. Merkel, Principal Entomologist, Southeastern Forest Experiment Station, Lake City, Florida. Provided a truck-mounted "cherry picker" from Lake City, Florida, and trained PSW personnel in its operation.

9. East Bay Municipal Utility District, Land Division. Permitted the use of the San Pablo Reservoir site for ground targets used in the aerial film test.

## SECTION SUMMARIES

## SECTION I - FOREST INVENTORY

### Microscale Photo Interpretation of Forest and Nonforest Land Classes

A test was made to determine the accuracy of interpretation for thirteen forest and nonforest land classes on 1:420,000 scale high altitude infrared color photographs. The photographs covered eight 41-square kilometer (16-square mile) study areas near Atlanta, Georgia, and were taken during a period of 10 months to represent three seasons -- early summer, late summer, and late winter. Three interpreters examined the photographs that were magnified 13 times using a projector-viewing device. On the average, the three interpreters classified 97 percent of all forest points correctly on winter photography. Seventy-one percent of the combined forest types were correct on winter photography -- 80% of the pine, 60% of the bottomland hardwood, and 70% of the upland hardwood. Only 33% of the pine and hardwood type was correctly classified. This type probably should not be used at this scale. Nonforest classification accuracy was poor but, most important to foresters, only 6% of all nonforest points were misclassified as forest. Winter photography was best for minimizing these errors. Comparisons made with the results of two independent studies indicate that microscale infrared color photography can be useful for forest area estimates and as a basis for stratifying forest area in multistage forest inventories.

### Multiseasonal Film Densities for Automated Forest and Nonforest Land Classification

Multiseasonal Ektachrome infrared color photographs taken from high

altitude and from space were scanned using an automatic recording microdensitometer. The red, green, blue, and neutral film densities were related to ground truth to develop microscale photo density signatures for thirteen forest and nonforest land-use classes. Mean densitites were plotted and examined for three seasons -- early summer, late summer, and winter. Discrimination between classes is shown to be best on winter photography using red density. However, standard deviations of the class means overlap, reducing the possibilities of discrimination based upon density alone. Two sources of unwanted density variation are examined -- film exposure variations between flights and film exposure variations caused by both differences in sun angle (season) and differences in film spectral sensitivity to varying levels of light. These sources of variation are demonstrated using mean red density for pine forest and pasture. Further research is recommended to isolate and make adjustments for this undesirable variation.

## Classification of Land Use by Automated Procedures

Automated pattern recognition methods to identify land use were used on microdensitometer scans of Ektachrome infrared photographs for each of three high altitude aircraft missions and the Apollo 9 photographic mission. Feature variables used were combinations of densities from red, green, blue, and clear filter scans. The results from two classification procedures -- linear discriminant analyses and empirical distribution analyses -- were compared for accuracy of classification. Both methods were considerably better than would be expected by random assignment. In general, the empirical analyses were better than the

linear discriminant analyses. The results from Apollo 9 photography were as good as those from the high altitude aircraft photography.

## SECTION II - FOREST STRESS

### Trend and Spread of Bark Beetle Infestations from 1968 through 1971

The spread, growth, and change of bark beetle infestations are dynamic features operating within the forest biome. We can follow these changes in the Black Hills of South Dakota on a yearly basis by counting tree mortality on medium scales of color aerial photography plus some ground checking. In four years, infestations have vacillated on a small area (8 square kilometers) from 97 in 1968, to 211 in 1969, to 96 in 1970, to 243 in 1971; over 7,000 trees have been killed within these infestation centers. A map is presented showing the clustering and periodic effects of an active uncontrolled epidemic over the four-year period. Regressions have been computed and drawn to show the relationship of photo tree counts to ground tree counts; all of the $r^2$ values were above 0.95.

### Aerial Photos Determine Optimum Levels of Stand Density to Reduce Bark Beetle Infestations

Bark beetle epidemics usually get started in pine stands that are undergoing stress of some kind -- lack of moisture, crowding, or disease. Many of the pine stands in the Black Hills are too dense and need thinning. Markets for selling the wood are just now emerging. This paper describes how aerial photos can be used to define timber stands most likely to succumb to beetle attack. The method will direct the forest

manager to those stands needing thinning first. A crown closure-crown diameter comparator was used on the aerial photos to relate the images to stand density conditions on the ground. On the ground, stand density was measured for infested stands (22), noninfested stands (16), and thinned stands (14) using basal area and number of trees per acre as criteria of stand density. We found that no recent mortality occurred in thinned stands and that tree diameters were significantly larger in infested stands. Crown closure on the photos is positively correlated with basal area while crown diameter is negatively correlated.

## The Use of Airborne Spectrometers and Multispectral Scanners for Previsual Detection of Ponderosa Pine Trees under Stress from Insects and Diseases

This report outlines the work done over the past seven years to detect stress in conifers -- both at Michigan in 1964 and in the Black Hills from 1966 to the present. Many improvements are noted in the airborne scanning instruments, but greater advances were made in digital preprocessing and analog processing techniques. Despite spectral and radiant existence differences measurable on the ground, the accuracy of airborne detection is not adequate with scanners available prior to 1971. Indications are that a single-aperture system, such as the Bendix 24-channel multispectral scanner or the new Michigan M-7 system, may provide better accuracy levels. Both the Earth Resources Program and ERTS program will share the same biophysical site where three 80-foot towers have been erected in anticipation of a multispectral flight in May 1972 and ERTS data every 18 days.

## Establishment of Earth Resources Technology Satellite Test Site in the Black Hills and Identification of Natural Resolution Targets

This report describes the location of an ERTS forest and range test site in the Black Hills of South Dakota. Natural resolution targets that will be located by mercator grid coordinates include 50 replicated samples of each of the following: (1) healthy forest, (2) insect infestations of various sizes, (3) rangeland (both natural and planted), (4) soil-rock outcrops, and (5) water bodies of various sizes. One newly infested pine stand of 54 trees was selected for installation of field instruments to interface with a data collection platform. The location of this site is shown on a test site map.

## Detection of Root Disease Impacts on Forest Stands by Sequential Orbital and Suborbital Multispectral Photography

The greatest disease impact to valuable Douglas-fir-hemlock stands of the Pacific Northwest is caused by Poria weirii root rot. To study this impact, three test sites were established in forested areas of Oregon and Washington -- two in the high Cascades and one in the Coast Range. Each test site is 9 square miles and represents a wide variety of terrain, vegetative cover, and forest and disease conditions. Color, color infrared, and black-and-white photographs at scales ranging from 1:4,000 to 1:31,680 were taken of the test sites. Interpretation of the photographs indicates that Poria disease indicators are more accurately discerned on the two test sites in the high Cascades than on the test site in the Coast Range of Oregon. Preliminary analysis of the photo interpretation results indicates a range in accuracy from 64% to 93% on

the 1:15,840 scale photographs. Accuracies of 87% and 73% were found using 1:31,680 scale photographs on the two Cascade test sites. It appears that imagery taken at much higher altitudes will also detect the presence of the root-rot disease signatures.

## SECTION III - STANDARDIZATION AND CALIBRATION STUDIES

### Calibration of Color Aerial Photography

In this report, the second by this research unit dealing with sensitometric calibration of aerial films, we have gone into detail concerning the spectral balance of the sensitometer or light source and the matching of wavelength distributions to daylight sources out to 920 nanometers. A literature survey shows notable variations in data for different combinations of direct sunlight and scattered skylight. Several system spectral distributions have been calculated for possible lamp-filter combinations, and least-square fits to the daylight curves were performed. An additional technique of electro-optically measuring the sensitometer effective exposure time and repeatability is included.

The use of calibration techniques in testing films is further exemplified in a section describing a recent flight test of new color aerial film emulsions. Useful film speed data were derived, and heretofore unobtainable details for spiral reel processing of Eastman SO-397 film are given. Eastman 2443 infrared color film was successfully tested with and without a corrective blue filter.

Finally, a discussion of the importance of sensitometry in automatic interpretation of aerial film is presented. Several hypothetical examples exhibit the probable errors introduced by working with uncalibrated density alone in the discriminant analysis of aerial infrared color film.

# MICROSCALE PHOTO INTERPRETATION OF FOREST AND NONFOREST LAND CLASSES

by

Robert C. Aldrich and Wallace J. Greentree

## INTRODUCTION

Foresters use aerial photographs to separate forest from nonforest land and to stratify forest land by types, volumes, and site classes. This is usually the first step in an extensive forest inventory such as the nationwide Forest Survey.[1] The accuracy of forest area estimates and the efficiency of forest sampling designs depend upon this first level of information.

Until recently, the interpretation of forest land has been done on prints made from panchromatic or infrared-sensitive films of scales ranging from 1:15,840 to 1:30,000.[2] The gains from using these photographs could usually be shown in terms of reduced sampling errors and reduced inventory costs. However, two factors still limit the use of aerial photographs in forest inventories: (1) the increasing cost of aerial photography and (2) the need for more frequent flights to update resource information.

---

[1]Forest Survey is a branch in the Division of Forest Economics and Marketing Research, Forest Service, U.S. Department of Agriculture, Washington, D. C. The Forest Survey was authorized by the McSweeney-McNary Forest Research Act of May 22, 1928.

[2]Color negative films are now being used for resource photography on some of the National Forests in the West.

If remote sensing of any kind is to show greater benefits for forestry, it must be up-to-date. Changes in forest area and the condition of forest lands are occurring at an increasingly rapid rate. In the more highly populated areas this rate of change is becoming alarming. To use out-of-date photographs as a basis for forest inventories causes a conflict between photo predictions of conditions and ground truth. This usually means that little gain, if any, can be shown from using them.

One possible way of reducing costs and increasing gains, while still maintaining accuracy objectives, would be to use small-scale or even microscale aerial photographs. One disadvantage of conventional aerial photographic scales is the large number of photographs required to cover an area of any size. For example, one 1:20,000 scale photograph (9- x 9-inch format) covers an effective area of approximately 5 square kilometers (2 square miles). A reduction in scale to 1:60,000 would increase the effective coverage to approximately 57 square kilometers (22 square miles) or over a 10-time increase in area coverage. One can go further and show that by using a 9- x 9-inch photograph from high altitude, or from space, taken at a scale of 1:400,000, we could effectively increase our coverage to approximately 2,460 square kilometers (950 square miles) -- over a 450-time increase.

But what kind of information will this microscale imagery provide, and with what accuracy? The research covered in this report is intended to answer these questions and to help foresters understand how microscale photography might help them in their forest inventories. However, it should be pointed out that these results are preliminary and should be

accepted only on that basis.

## METHODS AND PROCEDURES

### GROUND TRUTH

Ground truth for the Atlanta test site consists of a combination of several scales of aerial photography and ground observation points on fifteen 4-mile-square study areas. In March 1970, 1:32,000 Ektachrome infrared color film (8443)[3,4] and 1:12,000 Ektachrome (MS) color film (2448), developed to a negative, were taken over each of the study areas. These photographs, plus 1:2,000 and 1:12,000 color taken in April 1969, were used to delineate thirteen land-use and forest classes. Next, over two hundred random points representing all forest and agricultural nonforest classes were selected for ground examination. Among these points were fifty 0.24-hectare (0.6-acre) forest plots taken to establish forest volume, forest type, and site classes. Another eighty forest points were established to record forest types, species composition, crown density, and stand-size classifications. Eighty nonforest agricultural points were located on the ground to record agricultural use at the time of each high altitude overflight. The details of data collection were reported by Langley, et al (4) and Aldrich, et al (2). Final ground truth status maps were made by combining photo interpretation with observations made on the ground.

---

[3]Trade names and commercial enterprises or products are mentioned solely for necessary information. No endorsement by the U.S. Department of Agriculture is implied.

[4]This film will be referred to during the remainder of this report as IR color.

## PHOTOGRAPHY

At the outset of this study, plans were laid to obtain high altitude photography for the test site at four seasons of the year. Photography was planned for early June to represent early summer phenological development when solor radiation is at its peak. Other flights were planned for late summer, fall, and winter to represent different periods of vegetation development. Unfortunately, this planned program could not be carried out entirely. Aircraft mechanical problems and unfavoralbe weather prevented a flight scheduled for late October. Thus, only three seasons of photography were obtained. The photographic sensor data for these three flights are shown in Table 1. Photographic coverage for the 15 study areas is shown in Table 2.

As a result of poor photographic coverage for primary study blocks 1 and 3, we were forced to modify our original plans. Blocks 1 and 3 were dropped as primary study areas, and blocks 6, 8, 9, 10 and 14 were added (Figure 1). Although this meant a great deal of additional interpretation and data handling, it did result in a large increase in information for our test.

The interpretation test reported here was made using Hasselblad 1:420,000 IR color photography. One major problem for interpreters was caused by the difference in film quality and differences in atmospheric conditions at the time of photography. These caused considerable variation in quality of the film images between missions. For instance, the June (Mission 131) film emulsion had a weak cyan layer. This resulted in an overall hazy blue appearance and what appears to be a poor infrared response (Figure 2). The September (Mission 141) film was quite good,

Table 1. Photographic sensor data by season (RB-57 mission).

| Camera and focal length | Early Summer (Mission 131) June 1970 | | Late Summer (Mission 141) September 1970 | | Winter (Mission 158) March 1971 | |
|---|---|---|---|---|---|---|
| | Film | Filter | Film | Filter | Film | Filter |
| Zeiss, 12" | Ekta IR (SO-117) | W15 | Ekta IR (2443) | W15 | Ekta IR (2443) | W15 |
| Wild, 6" | Ekta (SO-397) | 2E | Ekta (SO-397) | 2E | Ekta (SO-397) | 2E |
| Wild, 6" | Ekta (SO-397) | 450 μm | Ekta IR (2443) | W15 | Ekta IR (2443) | W15 |
| Hass*, 40 mm | Ekta IR (SO-117) | W15 | Ekta IR (SO-117) | W15 | Ekta IR (SO-117) | W15 |
| Hass, 40 mm | Pan (2402) | 25A | Pan (2402) | 25A | Pan (2402) | 25A |
| Hass, 40 mm | Pan (2402) | 58 | Pan (2402) | 58 | Pan (2402) | 58 |
| Hass, 40 mm | Pan (2402) | W12 | Ekta IR (SO-117) | W15+ CC30B | Ekta IR (SO-117) | W15+ CC30B |
| Hass, 40 mm | IR (2424) | 89B | IR (2424) | 89B | IR (2424) | 89B |
| Hass, 40 mm | IR (2424) | W12 | Ekta IR (SO-117) | W15+ CC30B | Ekta IR (SO-117) | W15 |

*In this table, and elsewhere in our report, "Hass" is used as the abbreviation for "Hasselblad."

Table 2. Photographic coverage for five primary study blocks and ten secondary study blocks by season (RB-57 mission).

| Mission | Season | Date | Primary Blocks | | | | | Secondary Blocks | | | | | | | | | |
|---|---|---|---|---|---|---|---|---|---|---|---|---|---|---|---|---|---|
| | | | 1 | 2 | 3 | 4 | 5 | 6 | 7 | 8 | 9 | 10 | 11 | 12 | 13 | 14 | 15 |
| 131 | Early Summer | June 8, 1970 | X | X | | X | X | X | X | X | X | X | X | X | X | X | X |
| 141 | Late Summer | Sep. 14, 1970 | | | | X | X | X | | X | X | X | X | X | | X | |
| 158 | Winter | March 5, 1971 | | X | X | X | X | | | X | X | X | | X | | X | |

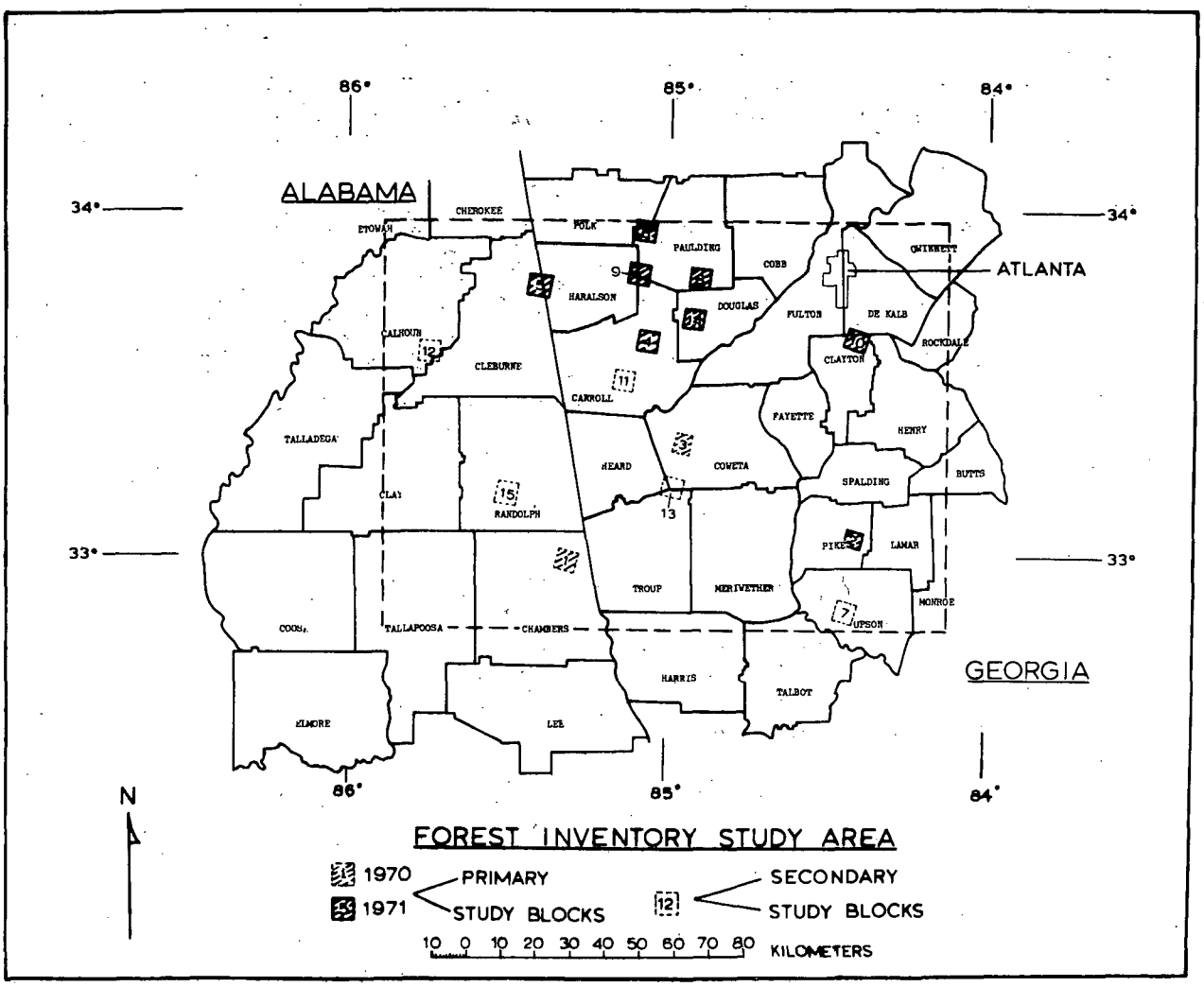


Figure 1. The Atlanta test site includes all or portions of 27 counties in Alabama and Georgia. Eight intensive study areas used in this report are shown with heavy hatch marks and solid boundaries. Two additional intensive study areas (hatch marked) were dropped because of insufficient high-altitude photographic coverage. The remaining study blocks (secondary) will be used to test interpretation models in another phase of the study.

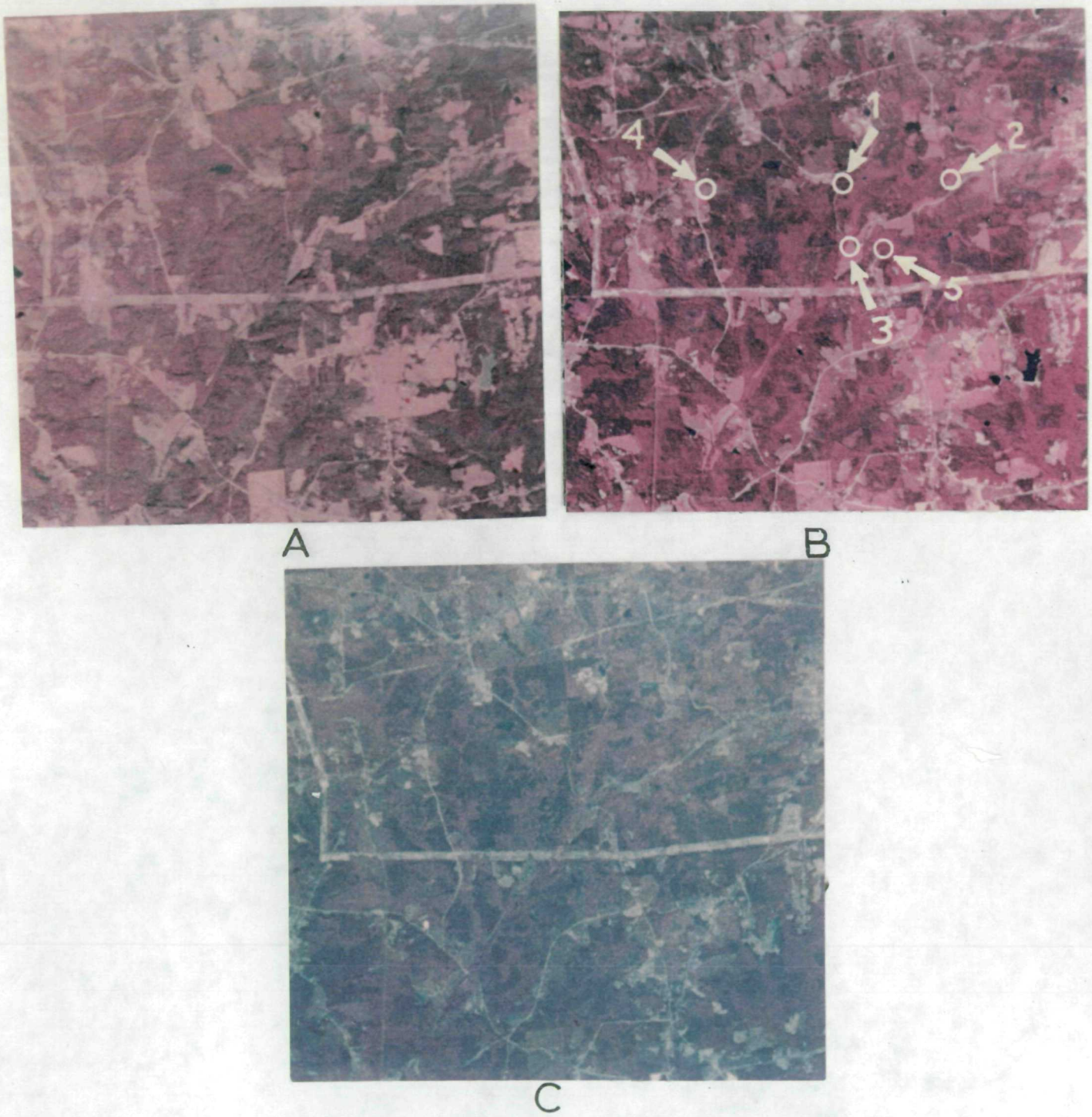


Figure 2. These three 1:420,000 scale IR color photographs for study block 14 represent the quality of imagery used in this study: (A) June 8, 1970, (B) September 14, 1970, (C) March 5, 1971. Three forest and two nonforest classes are pointed out in (B): (1) pine, (2) upland hardwood, (3) pasture, (4) abandoned, and (5) bottomland hardwood.

and the infrared response was enhanced by the addition of a CC+30B color correction filter. This same enhancement filter was used with the March (Mission 158) film, but there was a much more apparent vignetting effect causing the centers of the pictures to be overexposed. This resulted in some problems in resolving low-contrast details during interpretation.

## INTERPRETATION

Three interpreters examined the 1:420,000 IR color photographs for all primary study areas covered by each mission. One of these interpreters was a student in biological science with no previous experience in photo interpretation. The other interpreters were experienced and had worked in both the ground and photo interpretation phases of the study for two years. This experience does not bias the study results because of the interpretation techniques that we used.

Each interpreter was given a period of indoctrination and training prior to beginning the test. Two study blocks (blocks 1 and 3) not used in the test were used for training purposes. The interpreters were allowed to examine all available photography including the 1:32,000 and 1:420,000 IR color, and also were provided with ground truth to make correlations for interpretation purposes.

Because images on 1:420,000 scale imagery are much too small to interpret by normal methods, they were enlarged approximately 13 times using a projection-viewer designed for this purpose (Figure 3). The device was constructed using a Bell and Howell 35 mm slide projector, an adjustable mirror, and a Polacoat Lenscreen viewing surface. Enlargements of from 8 to 22 magnifications and adjustments for tip and tilt are


Figure 3. This projection-viewer was used to enlarge 1:420,000 scale photographs to coincide with 1:32,000 ground truth strip maps; (A) Bell and Howell 35 mm projector, (B) adjustable mirror, (C) adjustable viewing surface, (D) focusing adjustment, and (E) pulley for adjusting mirror distance for scaling purposes.

possible using the instrument as it is presently designed.

Each transparency was mounted as a 3-1/4- x 4-inch lantern slide for insertion in the projection-viewer. The position of the slide could be adjusted to project the portion of the area to be interpreted.

Interpreters, working independently, outlined and classified the 13 land-use and forest types along each of 18 sample strips. Interpretation always began with the June 1970 (Mission 131) imagery and progressed to the September 1970 (Mission 141) and March 1971 (Mission 158) imagery in that order. The appropriate slide was inserted in the projector and enlarged so that strip beginning and end points, scaled from the ground truth strip maps, coincided with the end points on the projected images. Interpreters were allowed to use magnifying glasses and filters (Wratten 15 and 25) whenever desired to enhance separations between some classes. The land classes were carefully mapped for each strip on acetate overlay material.

## ANALYSIS

Random points selected from the ground truth records were used to check the photo interpretation. The number of points in each land-use class by season is shown in Table 3.

Templates were made up for each strip to show the center of each land-use class selected to check photo interpretation. These templates were drawn to scale from the ground truth strip maps. Next, the templates were laid on top of the overlays made by each interpreter and the land-use or forest classification at each point noted and recorded.

Because of distortions inherent in small-scale photographic imagery, and because of limitations in projection systems, we made certain

Table 3. Number of random check points in each land-use class by season of photography.

| Season | Land Use[1] | | | | | | | | | | | | | Total |
|---|---|---|---|---|---|---|---|---|---|---|---|---|---|---|
| | 1 | 2 | 3 | 4 | 5 | 6 | 7 | 8 | 9 | 10 | 11 | 12 | 13 | |
| Early Summer (June) | 69 | 37 | 40 | 54 | 5 | 23 | 30 | 10 | 35 | 4 | 22 | 13 | 1 | 343 |
| Late Summer (Sept) | 59 | 33 | 16 | 45 | 7 | 8 | 20 | 6 | 22 | 0 | 18 | 7 | 0 | 241 |
| Winter (March) | 60 | 28 | 36 | 47 | 15 | 23 | 28 | 9 | 29 | 3 | 21 | 11 | 1 | 311 |

[1]
1 - Pine
2 - Pine-hardwood
3 - Bottomland hardwood
4 - Upland hardwood
5 - Crop
6 - Plowed field
7 - Pasture
8 - Idle
9 - Abandoned
10 - Orchard
11 - Urban
12 - Turbid water
13 - Clear water

concessions to the interpreter. If the classification, as shown by the interpreter was on or within 1 millimeter of the correct ground classification (on the enlarged photo), the interpreter was considered correct.

Once all data had been recorded they were punched on IBM cards for computer analysis. Computer tabluations showing the frequency of interpretation by ground classifications were used to analyze the accuracy of interpretation and to point out sources of misclassification. Because the number of observations in some classes was too small for analysis, we have combined them with the land use most closely associated. Thus, class 5 was combined with class 6, class 8 with class 9, and class 13 with class 12.

## RESULTS

While considering the results shown below, the reader should keep in mind that the photo interpretation was done on 1:420,000 scale photography. At first glance the results look rather poor. However, a comparison between these results and the results of studies made in the past using conventional 1:20,000 scale photography shows some good correlations. This comparison is made in the CONCLUSION AND DISCUSSION section of this report.

### LAND-USE CLASSIFICATION

Forest land was separated from nonforest land classes with better than 96% accuracy (Figure 4). As might have been expected the agricultural uses were least accurately identified under this land-use classification scheme. The category "active agriculture" (crops and plowed fields) was classified correctly most often on the June photography, but even then the interpreters were correct only 51% of the time, on the

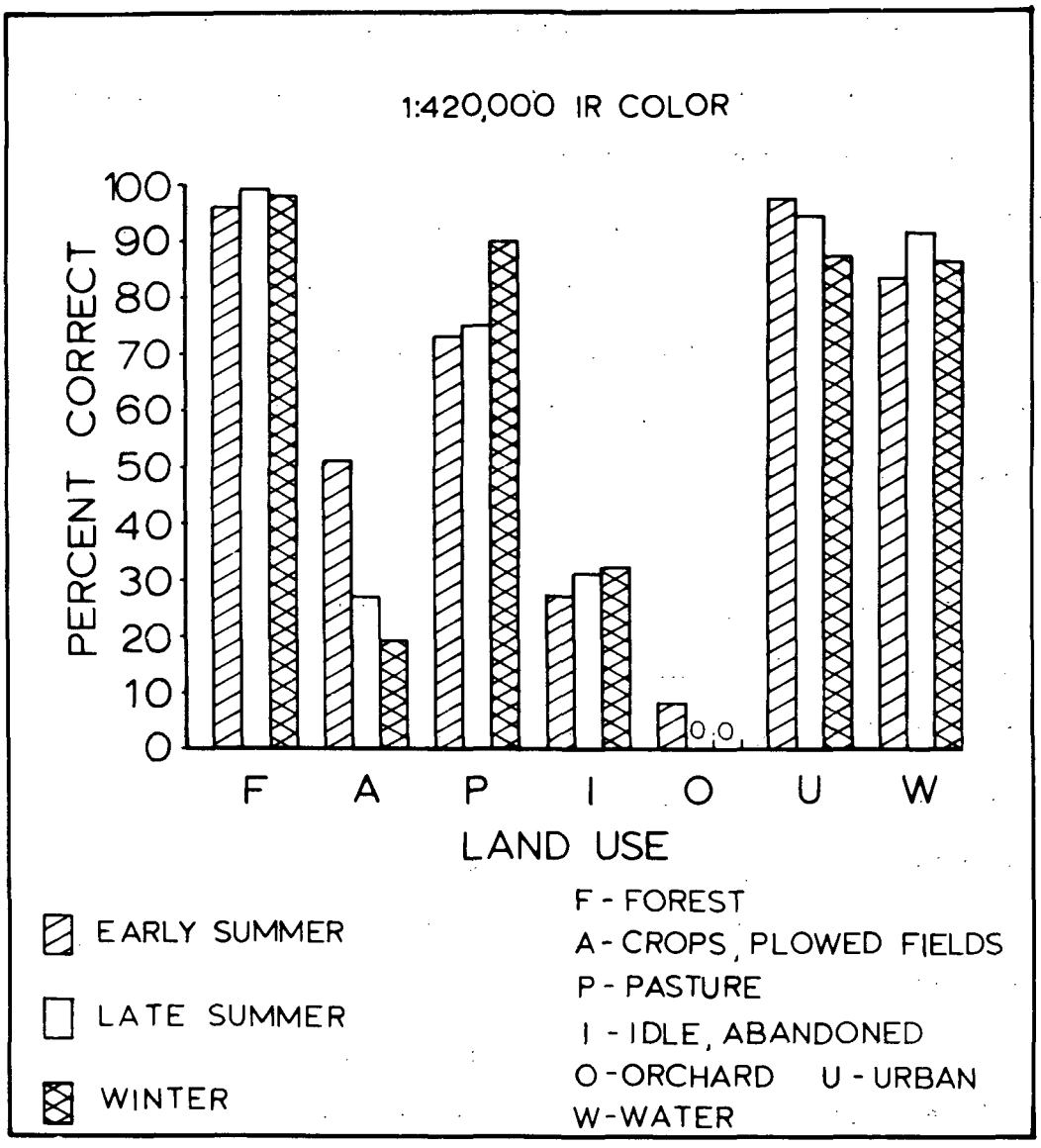


Figure 4. The average accuracy is shown for three interpreters classifying land use on 1:420,000 IR color photographs taken during three seasons. Note that only in crops and plowed fields is there a significant difference that might be attributed to season. June, or early summer photography, appears to give the greatest accuracy.

average. On March photography the accuracy dropped to a low of 19%. Pasture land is interpreted correctly in 90% of all chances on March photography. On June and September photography the accuracy drops to 73% and 75%, respectively. Regardless of the season, idle and abandoned land is mapped correctly in approximately 30% of the cases. Orchards (pecan and peach) are correct in fewer than 8% of the total number of chances.

Urban land, including improved roads, highways, power lines, pipe lines, and land areas in and around communities and cities not qualifying as forest or agriculture, is classified correctly over 97% of the time on June photography. The accuracy in September was 94%. In March the accuracy fell to 87% because some improved roads and highways could not be seen against highly reflective backgrounds.

Water, including small farm ponds, can be detected 91% of the time in September (Figure 4). Less accuracy occurs on June and March photography primarily because of poorer definition due to overexposure of center portions of the photographs.

There were very few forest points misclassified as nonforest (Figure 5). The season of photography had little effect on the results, and there is little indication that the classification errors can be attributed to anything more than random interpreter error. By taking more care and by improving our training materials we could expect to reduce these errors to almost zero.

Nonforest points were called forest quite frequently. This is a particularly serious problem in the idle and abandoned and orchard land classes. Idle and abandoned land appears a dark gray tone and moderately

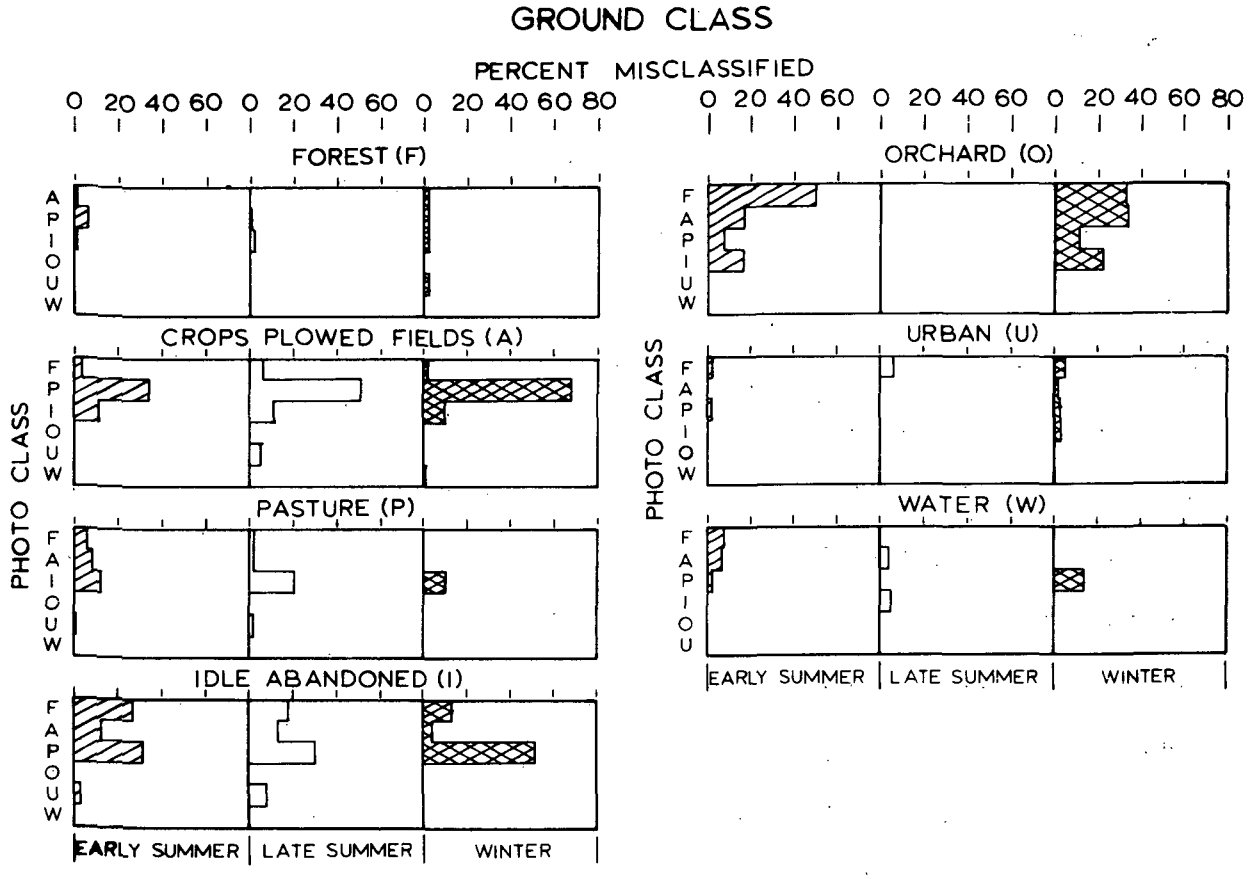


Figure 5. This chart indicates the percentage (average of three interpreters) of all nonforest points that were misclassified by land use and season of photography. Note that active cropland and plowed fields and the idle and abandoned land are most often misclassified as pasture land.

rough in texture, very much like low-stocked upland hardwood. This similarity is caused by clumps of weeds, blackberries, and noncommercial tree species scattered around with accumulated dead plant debris. It is easy to overestimate the stocking of forest trees and misclassify the land as a result. Another problem is orchards. Pecan and peach orchards look very much like upland hardwoods or abandoned agriculture. For this reason, most orchards were called either forest or idle and abandoned land. Orchards are extremely limited in the test areas, and as a result we had only a small number of samples. It is possible that with more extensive areas in this class, we could have shown better results.

There were very few misclassification errors in the urban and water classes. The most frequent cause of errors in urban classification was small wooded areas (green belts) or garden crops within urban centers (towns). Another cause of misclassification was poor contrast between roads and surrounding agricultural land caused by overexposure, particularly on the March photography. Water was misclassified in almost every instance because of the poor contrast which (turbid) water has with surrounding classes, particularly in overexposed portions of the photographs.

## FOREST CLASSIFICATION

The accuracy of forest classification varies considerably by type and by season of photography (Table 4). Photo interpreters are shown to be relatively consistent with one possible exception. Interpreter A was inexperienced and apparently had insufficient training in relating the differences in infrared response on March photography to vegetation types. Despite this, we conclude that photo interpretation on March photography

Table 4. Accuracy of forest type classification by photo interpreter and by season.

| Season[1] | Photo Interpreter | Forest Type[2,3] 1 (P) | 2 (PH) | 3 (BH) | 4 (UH) |
|---|---|---|---|---|---|
| | | - - - - percent correct - - - - | | | |
| June | A | 71 | 0 | 55 | 61 |
| | B | 70 | 11 | 25 | 72 |
| | C | 67 | 0 | 48 | 71 |
| | Mean | 69 | 4 | 43 | 68 |
| September | A | 79 | 12 | 6 | 74 |
| | B | 83 | 15 | 13 | 67 |
| | C | 81 | 33 | 6 | 71 |
| | Mean | 81 | 20 | 8 | 70 |
| March | A | 67 | 7 | 53 | 55 |
| | B | 80 | 28 | 64 | 79 |
| | C | 82 | 39 | 64 | 64 |
| | Mean | 76 | 25 | 60 | 66 |

[1]Seasons tested:

June - early summer
September - late summer
March - late winter

[2]Forest type:

Pine (P) - 1
Pine-hardwood (PH) - 2
Bottomland hardwood (BH) - 3
Upland hardwood (UH) - 4

[3]The number of observations by forest type is shown in Table 3.

resulted in the best forest type classification. Interpreters B and C were able to classify pine type correctly 81% of the time. However, these two interpreters could classify pine-hardwood type correctly only 33% of the time; this low level of accuracy is not unusual even on conventional 1:15,840 and 1:20,000 scale photography. Part of the difficulty is in defining the percentage of pine in the stand.[5] We found that with the better resolution of 1:12,000 and larger scale color and infrared color photography this classification becomes easier and more accurate to identify.

The greatest advantage of high altitude photography taken in March is found in the greater accuracy of hardwood type classifications. On the average, 60% of the stands called bottomland hardwood and 66% of the stands called upland hardwoods were classified correctly (Figure 6). In contrast to this, only 43% of the bottomland hardwood was correctly classified on June photography, and only 8% on the September photography. The accuracy of upland hardwood interpretation does not appear to vary significantly with the three seasons tested.

There were very few forest points misclassified as nonforest land (Figure 7). Regardless of the season, no fewer than 96% of forest points were correctly classified as forest. Thus, errors in forest type classification were largely errors in judgment of stand stocking. For instance, on the average, interpreters classified 19% of the pine stands as upland

---

[5]Pine-hardwood: 25-50% of the dominant stand is in pine; the remainder is composed of hardwood (deciduous) tree species.

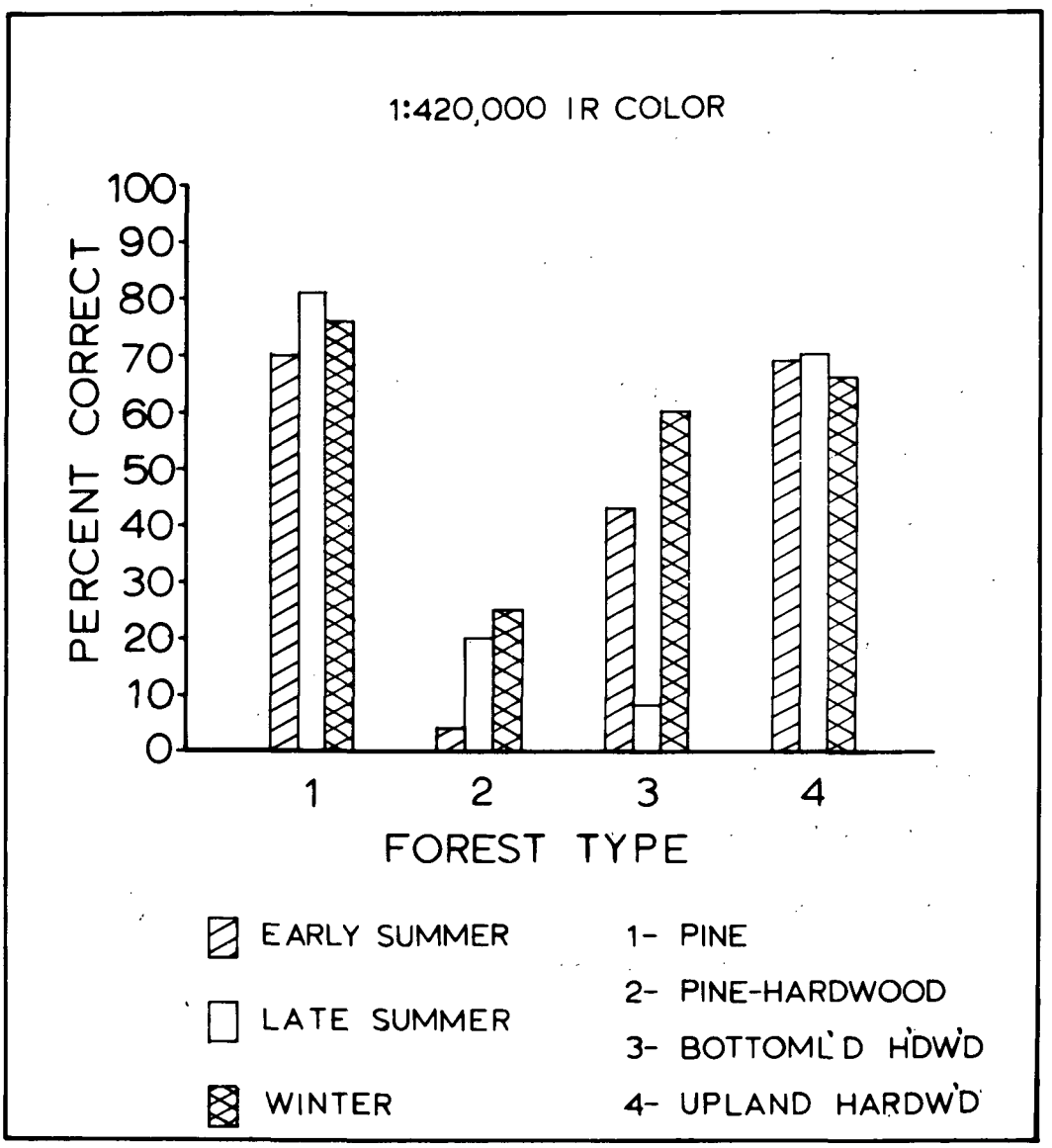


Figure 6. This chart shows the average accuracy for three interpreters classifying forest types on 1:420,000 IR color photographs taken during three seasons. Note that forest types are generally most accurately identified on March photography.

hardwood on June photography. On September photography the error was 14%, and on March photography the error was 14%. These are relatively consistent errors and should be considered the most serious errors in forest misclassification. These errors may be reduced in the future by improving photo resolution and developing better keys and definitions of forest types.

The greatest errors in pine-hardwood type classifications were in calling pine-hardwood mixtures upland hardwood (Fig. 7). Sixty-two percent of the pine-hardwood stands were called upland hardwood on June photography, 53% on September photography and 43% on March photography. It is apparent that as the percentage of pine is reduced in mixed stands, the chance for calling the stand hardwood is increased. Also, when deciduous trees (hardwoods) are leafless, there is a greater chance of seeing pine in mixed stands and a greater chance of calling the stands correctly.

Bottomland hardwood type was often called upland hardwood type (Figure 7). On the other hand, only occasionally (average of 11%) was an upland hardwood stand called bottomland hardwood. Misclassification of bottomland hardwood as upland hardwood was greatest in September and least in March -- 77% as compared to only 24%. Therefore, when we want to distinguish between upland and bottomland types, winter photography is most useful.

## CONCLUSION AND DISCUSSION

It is always difficult to evaluate the results of a study such as this without some basis for comparison. For instance, the results shown here were arrived at using 1:420,000 scale infrared color. Do we know

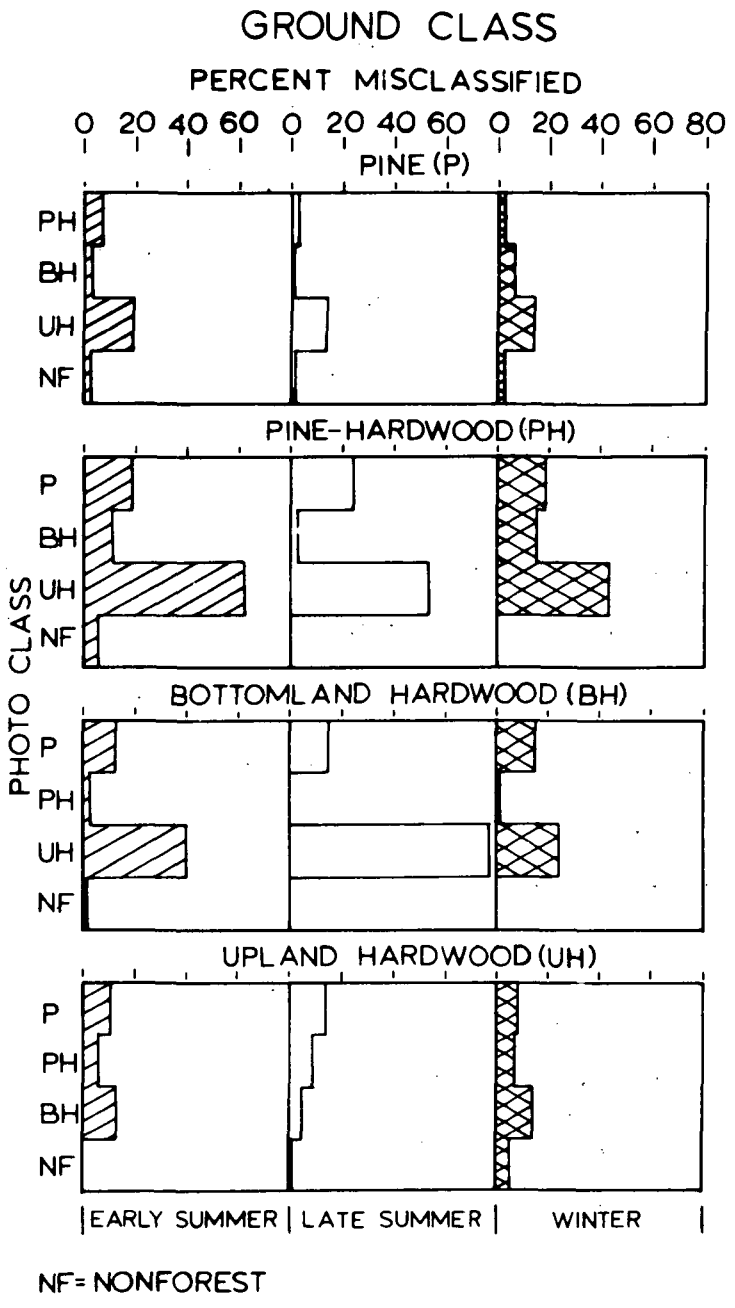


Figure 7. The percentage (average for three interpreters) of all forest points that were misclassified by type and season of photography. Note that pine-hardwood and bottomland hardwood types are most frequently misclassified. In both cases they are usually called upland hardwood by interpreters.

how well interpreters might do on conventional 1:20,000 scale panchromatic photographs?

A search of the literature shows only two studies that can be used for comparison. In the first (1), interpreters used basically the same set of criteria to classify land use in southwest Georgia on 1:20,000 panchromatic photographs. In this example 95.5% of all forest classifications were correct. This compares favorably with the 96% or better accuracy shown in this report. The second study taken from the literature shows the expected accuracy for forest type classification on 1:20,000 scale photography (3). This test made by the TVA in 1952 showed that interpreters could classify three types (pine, mixed, and hardwood) correctly 74% of the time. When the forest types used in the present study are combined in a similar way, we can show that 71% of the type classifications were correct if made on March photography.

These two comparisons can hardly be considered conclusive evidence of the benefits of 1:420,000 scale infrared color photography for forest and nonforest classification. However, they should lend some credence to the statements below.

1. Microscale IR color photography (1:420,000) can be interpreted within reasonable limits of error to estimate forest area.

2. Forest interpretation is best on winter photography, and provides 97% or better accuracy. The greatest source of error is in calling abandoned agricultural land forest land, but this error is minimized on winter photography.

3. Broad forest types can be classified on microscale photography. For instance, pine type is correctly identified more than 80% of the time on winter photography and at least 70% of the time regardless of season.

Pine-hardwood cannot be correctly identified better than 25% of the time (winter photography) and probably should not be attempted on microscale photography in the future. Bottomland hardwood is correctly classified 60% of the time on winter photography but cannot be separated from upland hardwoods at other seasons of the year. Upland hardwood is usually classified correctly 70% of the time regardless of season.

4. Active agricultural land is classified most accurately on early summer photography; in this test 51% of active cropland and plowed fields were correctly classified. The most frequent error was interpreting cropland as pasture. Fortunately, only a very small percentage of the cropland category was misclassified forest land, and on winter photography this error was at a minimum.

5. Only 6% of all nonforest observations (including urban and water) were misclassified as forest. Winter time was the best season for minimizing these errors.

During the coming year we will continue photo interpretation tests using high altitude aerial photography. These tests will include rigid statistical tests of the data presented here. For instance, a weighting scheme has been devised to assign to misclassified plots -- the magnitude of the weight depending on the seriousness of the error. An analysis of variance will be made for these weighted data to determine the levels of significance for interpretation errors.

Multiseasonal color and IR color photography taken at a 1:120,000 scale will be interpreted and analyzed in a manner similar to that used in this report. We will also concentrate on developing a photo interpretation key for microscale photo interpretation of forest and nonforest classifications.

## LITERATURE CITED


1. Aldrich, R. C. 1953. Accuracy of land-use classification and area estimates using aerial photographs. Jour. Forestry. 51(1):12-15.
2. Aldrich, R. C., W. J. Greentree, R. C. Heller, and N. X. Norick. 1970. The use of space and high altitude aerial photography to classify forest land and to detect forest disturbances. Annual Progress Report for Earth Resources Survey Program, OSSA/ NASA, by the Pacific Southwest Forest and Range Experiment Station, 36 p., illus.
3. Bateson, A. R. 1952. A test of aerial photography for forest inventory purposes in the Tennessee Valley. Report No. 205-52. Forestry Investigations Branch, Tennessee Valley Authority, 34 p.
4. Langley, P. G., R. C. Aldrich, and R. C. Heller. 1969. Multi-stage sampling of forest resources by using space photography -- an Apollo 9 case study. Second Annual Earth Resources Aircraft Program Status Review. Vol. 2. NASA Manned Spacecraft Center, Houston, Texas. 28 pp. illus.

# MULTISEASONAL FILM DENSITIES FOR AUTOMATED FOREST AND NONFOREST LAND CLASSIFICATION

by

Wallace J. Greentree and Robert C. Aldrich

## INTRODUCTION

This is the second of two reports on research started in 1969 to separate 13 forest and nonforest land-use classes using film density. The first report in October 1970 (1) was based upon fragmentary data for one study area at one season of the year. The continued research reported here is based upon data for eight study areas using photography for three seasons.

The objectives of this research are: (1) to develop microscale photo density signatures for forest and nonforest land-use classes to use in multivariate analysis techniques, (2) to examine multivariate analysis techniques to find the most effective techniques for classifying forest and nonforest land use, (3) to compare film densities by season and isolate sources of variation not caused by land use, and (4) to examine alternatives for removing undesired sources of variation to improve forest and nonforest discrimination. Research involving multivariate analysis techniques is reported by Norick and Wilkes in another section of this report. However, the association between the basic data used in these two reports should always be kept in mind.

## METHODS

To meet our study objectives we used microdensitometry methods to evaluate multiband photographs. This involved microimage density measurements using a Photometric Data Systems microdensitometer coupled with a Data Acquisition Systems digitizer, and computer processing with a Univac 1108 computer.

## PHOTOGRAPHY

Microscale (1:420,000) transparencies taken by NASA's RB-57 high-altitude aircraft were used for each of 3 seasons. The photography was taken with six Hasselblad 70 mm cameras equipped with 40 mm focal length lenses. Film and filter combinations used in this study are shown by mission date in Table 5.

The Wratten 15 and 30B color correction filter combination was used on Missions 141 and 158 because we hoped it would be better for cutting haze and would improve the infrared response of infrared color film at high altitude (4). Our hopes were justified by the results which showed a much improved image sharpness and infrared response. We did not use this film-filter combination on Mission 131, and as a result the film looked hazy and had an overall blue cast.

Master copies of 1:2,400,000 70 mm infrared color frames 3740 and 3741 from the Apollo 9 SO-65 photography experiment were also used.

## MICRODENSITOMETRY

Each of the 70 mm transparencies was run on the microdensitometer using block scanning techniques (1, 2). The density readings along our sample lines were then determined by computer programming.

Each sample line on the infrared color photography was scanned in turn with a clear, red, green, and blue microdensitometer filter.[6] The panchromatic photographs and the black-and-white infrared photographs were scanned with only a clear filter.

## ANALYSIS

The mean densities and their standard deviations were computed for each of the 13 land-use classes along each random sample line within the sample blocks. These statistics were also computed for blocks and the sum

[6] 92 - red; 93 - green; 94 - blue; clear - no filter.

of all blocks for each RB-57 mission. Density signatures for the panchromatic and black-and-white infrared photographs, processed with a clear filter, were obtained in the same manner. The combined block mean density values were then plotted for visual analysis (Figure8 ).

From these graphs it was evident that some of the density variation was the result of sources other than land use. By intuitive reasoning we felt that one source might be photographic exposure. Thus, to demonstrate the effect of exposure differences between photos, we plotted the mean red density values for pine and pasture by blocks (Figure 9). In theory, if the red, green, and blue filter are subtracted from the mean density values of the clear filter, which is unfiltered white light, we should, in effect, be normalizing for exposure differences. These values were plotted in Figure 9 for comparison with the unnormalized data.

Normalized means were computed for all forest and nonforest land-use classes and plotted for comparison in Figure 10. An examination of both the photographs and the data in Figures 9 and 10 suggests the possibility that density is affected by position of the study blocks within the individual photographs. To estimate the effect of this variable we made a first attempt by measuring the distance and the azimuth from the center of the photograph to the center of each block. The mean red density was plotted for pine and pasture by distance and by quadrant location (Figure 11).

## RESULTS

Table 6 shows the number of density data points stored on tape for each of the 13 land-use classes by season. The number of data points in each column should be multiplied by 4 to include all points for clear, red, green, and blue density signatures. The total number of data points for both the panchromatic and black-and-white infrared density signatures

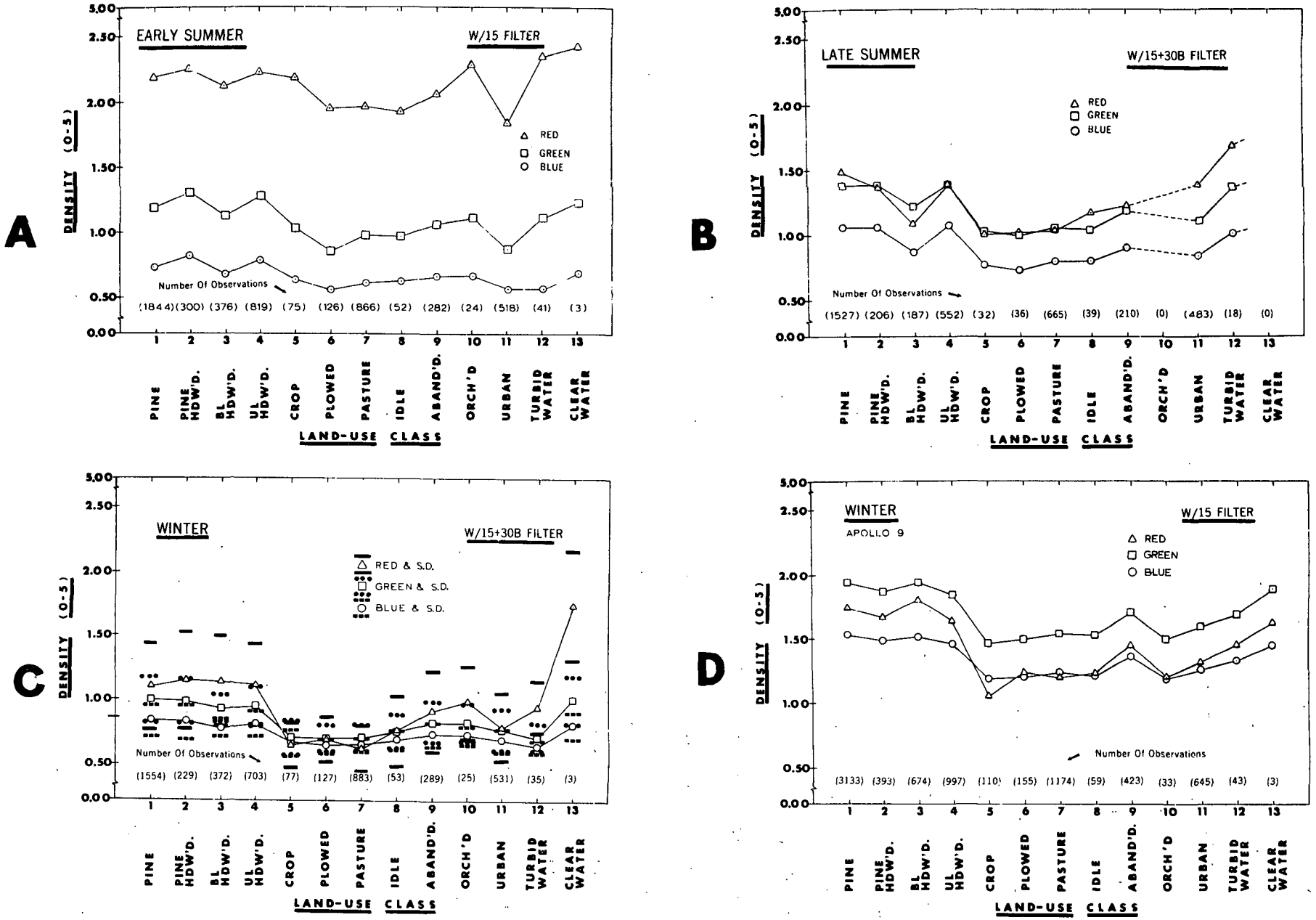


Figure 8. These graphs show a three-season comparison of mean optical red, green, and blue film densities for 13 land-use classes. The measurements were made on microscale infrared color transparencies (SO-117): (A) 1:420,000 scale taken in June 1970, (B) 1:420,000 scale taken in October 1970, (C) 1:420,000 scale taken in March 1971, and (D) 1:2,400,000 Apollo 9 taken in March 1969. Notice the magnitude of standard deviations plotted for the means in (C). Also notable is the similarity between the plotted data in (C) and (D).

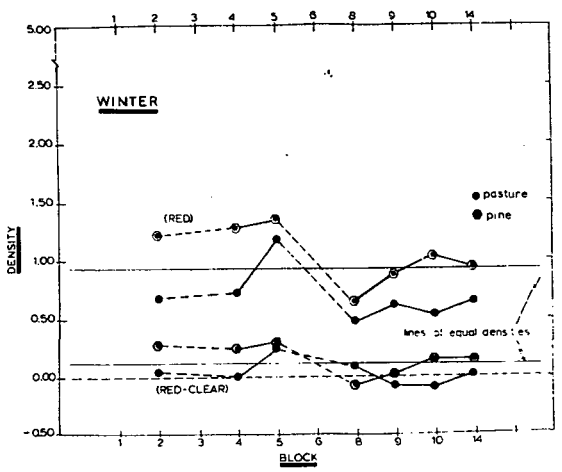


A

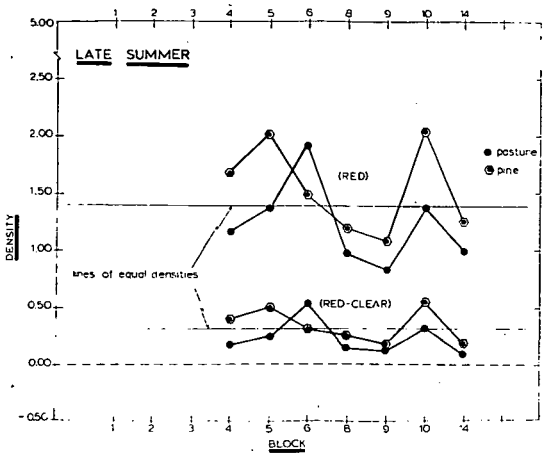


B

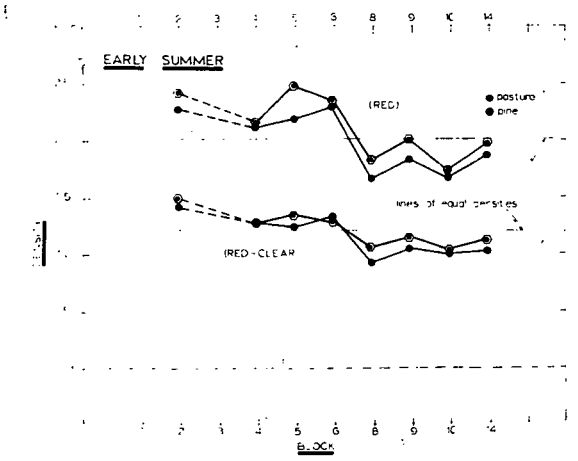


C

Figure 9. Mean red density is plotted by study block for pine and pasture to show the effects of season on film density: (A) early summer, (B) late summer, and (C) winter. The upper portion of each graph shows unadjusted red density; the lower portion of the graph shows normalized red density (red density - clear density). Notice that the scatter of density points around the horizontal line of equal density has been reduced considerably.

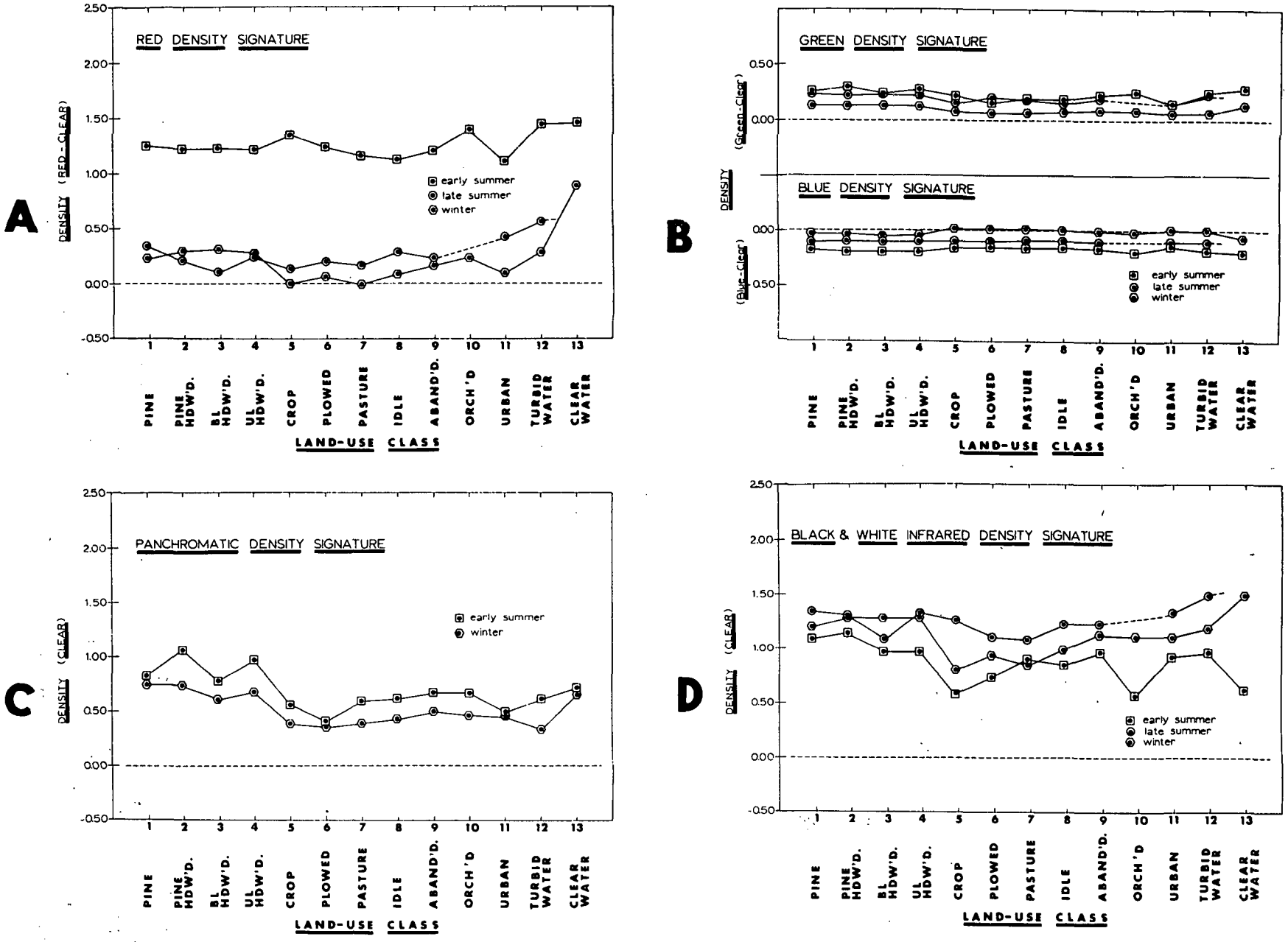


Figure 10. Normalized red density (A) and blue and green density (B) on infrared color film are compared with densities on panchromatic (C) and black-and-white infrared (D). The seasonal responses are shown and indicate that red film density on winter infrared color photography has the most information. However, density signatures on panchromatic photography would appear to be able to separate forest from nonforest with greater likelihood of success.

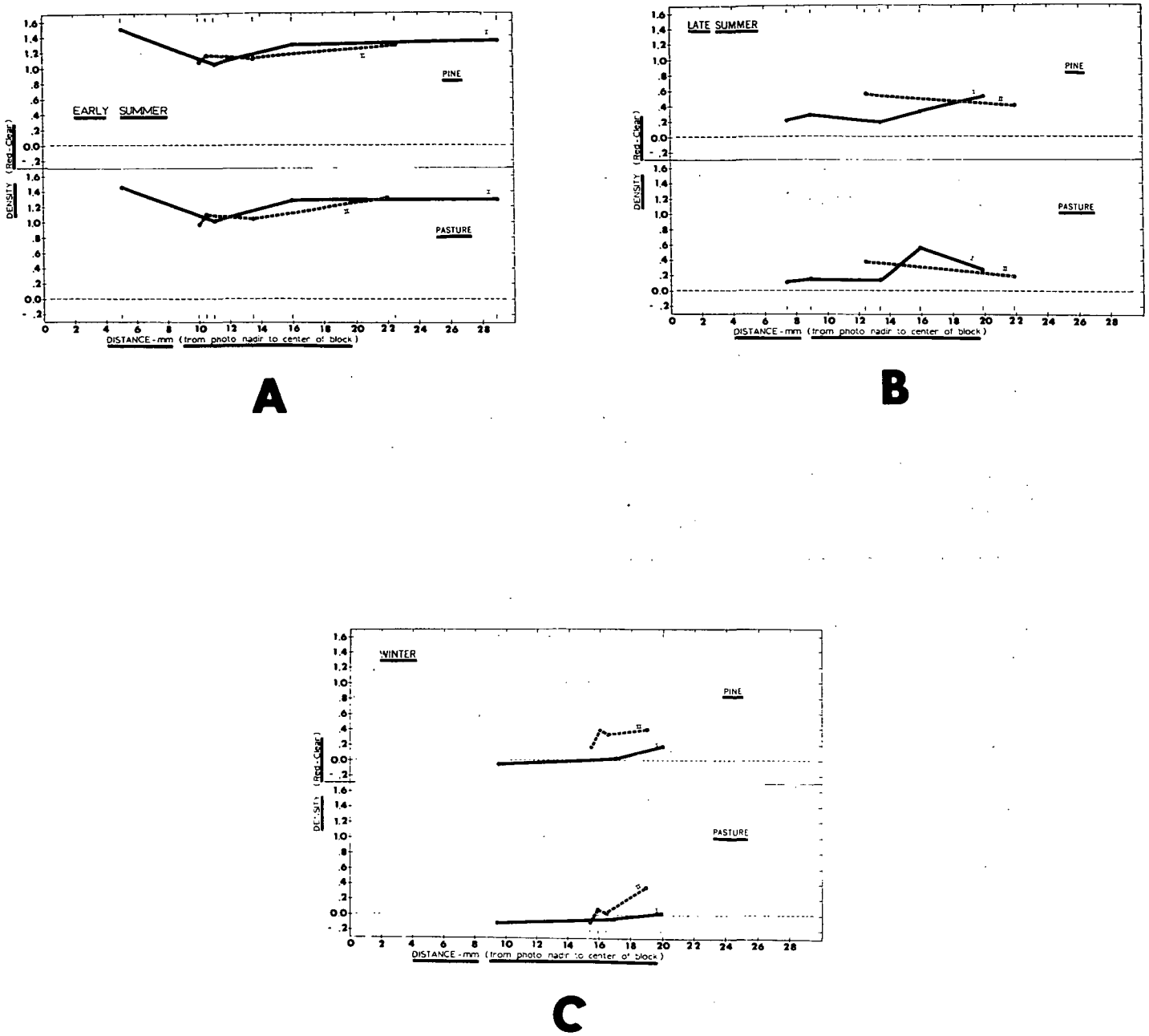


Figure 11. The mean density measured on infrared color film is plotted for pine and pasture by season, distance from the photo nadir, and quadrant location: (A) early summer, (B) late summer, and (C) winter. The solid line (I) in each graph shows data located in the two northernmost quadrants ($0^{o}$-$90^{o}$, $270^{o}$-$360^{o}$). The dashed line (II) in each graph shows the data located in the two southernmost quadrants ($90^{o}$-$180^{o}$, $180^{o}$-$270^{o}$). Notice the general increase in density with distance and the higher density for southern quadrants on winter photography (low sun angle).

Table 5. Film and filter combinations used on the various RB-57 high-altitude photographic missions.

| RB-57 Mission | Season | Film | Filter |
|---|---|---|---|
| 131 (June 8, 1970) | Early Summer | Ektachrome Infrared, SO-117<br>Panchromatic, 2404<br>Black & White Infrared, 2424 | Wratten 15<br>Wratten 25A<br>Wratten 89B |
| 141 (Sep. 14, 1970) | Late Summer | Ektachrome Infrared, SO-117<br>Panchromatic, 2404<br>Black & White Infrared, 2424 | Wratten 15+30B<br>Wratten 25A<br>Wratten 89B |
| 158 (March 5, 1971) | Winter | Ektachrome Infrared, SO-117<br>Panchromatic, 2404<br>Black & White Infrared, 2424 | Wratten 15+30B<br>Wratten 25A<br>Wratten 89B |

Table 6. Number of density data points by land use by season of photography; RB-57 and Apollo 9 infrared color. Combined study blocks.*

| Land-use Class | TOTAL NUMBER OF DENSITY DATA POINTS | | | |
|---|---|---|---|---|
| | Early Summer | Late Summer | Winter | Winter Apollo 9 |
| 1 | 1844 | 1527 | 1554 | 3133 |
| 2 | 300 | 206 | 229 | 393 |
| 3 | 376 | 187 | 372 | 674 |
| 4 | 819 | 552 | 703 | 997 |
| 5 | 75 | 32 | 77 | 110 |
| 6 | 126 | 36 | 127 | 155 |
| 7 | 866 | 665 | 883 | 1174 |
| 8 | 52 | 39 | 53 | 59 |
| 9 | 282 | 210 | 289 | 423 |
| 10 | 24 | 0 | 25 | 33 |
| 11 | 518 | 483 | 531 | 645 |
| 12 | 41 | 18 | 35 | 43 |
| 13 | 3 | 0 | 3 | 3 |
| Total | 5326 | 3955 | 4881 | 7842 |

*Early summer includes blocks 2, 4, 5, 6, 8, 9, 10, 14.

Late summer includes blocks 4, 5 (less one strip), 6, 8, 9, 10, 14.

Winter includes blocks 2, 4, 5, 8, 9, 10, 14.

Winter (Apollo 9) includes blocks 1, 2, 3, 4, 5, 6, 8, 9, 10, 14.

is approximately the same as those shown in the table.

The combined block mean density signatures for the land-use classes are shown in Figure 8. It would appear from these graphs that a separation can be made between most forest and nonforest classes. However, the standard deviations about the class means overlap one another, even though the mean densities are different.[7] This makes it difficult to separate the individual forest classes or nonforest classes from each other by using raw density alone. This result bears out the conclusions of our 1970 report which was based upon only fragmentary data (1).

Some of the overlap in standard deviations may be the result of unwanted variation that can be controlled. To explain this possibility, density signatures for pine and pasture were plotted by block, and the trend of the data was examined for possible sources of block variation (Figure 9). The plotted data shows the effects of exposure differences by season of photography. Ideally, the data would form a horizontal line of equal densities. Any differences in level between lines would be caused by variations in phenological development of the vegetation, variations in site, and differences in solar radiation at the three periods of the year. However, this is not the case, and deviations from the horizontal line of equal densities in the example must be attributed to one or more of the following: (1) variations in reflected energy received at the sensor, (2) differences in film exposure, (3) differences in film sensitivity within and between emulsions, (4) differences in spectral sensitivity of the film layers to differing light levels and (5) the position of the block within the photograph format, i.e., distance from the nadir.

[7]See Figure 8 (C) for standard deviations on winter photography.

Figure 10 is a three-season display of density signatures for all land-use classes after normalizing for exposure differences. Normalizing consisted of subtracting the mean clear density (white light) from the mean red, green, and blue densities on the infrared color.

Normalizing reduced the difference between winter and late summer red density signatures but had little effect on reducing early summer red density. The difference in infrared response is shown to be best on winter photography. Late summer and early summer red densities show fewer possibilities for discrimination even after normalizing. However, there are some interesting reversal patterns shown by season (Figure 10). For instance, crops, idle land, and urban all show red density reversals on early summer photography when compared with late summer photography. Clear water on winter photography shows a density reversal when compared with early summer photography. These patterns and others may be useful for discrimination of targets that cannot be separated on any one season of photography alone.

After the green and blue film densities were normalized, the density differences between land classes were reduced (compare Figure 10(B) with Figure 8), and the apparent seasonal differences that existed before normalizing are almost gone. From this there appears to be very little value in the blue and green densities. However, computer discriminant analysis techniques may find that differences between single-band densities, by season and between seasons, are valuable for separating some classes.

The mean densities for combined blocks indicate that forest classes can be discriminated from nonforest classes on panchromatic (25A)

photography (Figure 10). In fact, even when standard deviations are considered, there appears to be a greater potential for discrimination on this film than on infrared color. Of the two seasons for which photo coverage was available, winter was the best. Unfortunately, there is still very little possibility of distinguishing between forest types or nonforest classes.

Black-and-white infrared film (89B) alone has little value for land-use classification unless it is used together with panchromatic (25A) and infrared color film. Then it would provide some classification signatures. Some interesting density reversals are evident between seasons. However, the full potential of these must be evaluated by multivariate computer routines.

An important source of unwanted variation in film density is demonstrated in Figure 11. In this figure the normalized mean red film density has been plotted by blocks for pine and pasture for three seasons. Densities have been plotted by distance from the center of the photo and by north and south quadrants. Although the number of data points is limited there is some trend in the data that should not be ignored. For instance, quadrant location (northerly or southerly) appears to have little effect on the mean density in early summer. However, there is a slight upward trend to the data as distance from the center of the photo increases. This increase is not as dramatic as that shown for late summer and winter photography. On late summer photography the upward trend of density for pine is most apparent in the northern quadrants. The downward trend for the two southern quadrants is meaningless with only two data points, even though this could indicate a difference between the two quadrants. Winter photography shows the best separation of data in the north and south quadrants

and should give impetus to further tests -- particularly for this season. This is because winter photography shows the greatest all-around potential for forest and nonforest land classification on microscale photography.

## CONCLUSION

The use of film density to discriminate between forest and nonforest land-use classes entails many problems which must be resolved before it will be an operational technique. In another section of this report Norick and Wilkes show no better thatn 78% accuracy in classification using film density in multivariate discrimination techniques. This is rather discouraging because human interpreters can separate forest from nonforest with an accuracy of 96% or better on the same microscale photographs (see Aldrich and Greentree in the previous section of this report).

Low accuracy using film density can be attributed to several undesirable sources of variation. Two sources that may be partially controlled have been demonstrated in this report; these are also discussed on pages 170-178 in the paper by Dana and Myhre. One is the effect of exposure difference between and within the photographs and between photographic missions. This can be partially removed by subtracting clear density (white light) from raw density measured in the red, green, and blue bands. This has a normalizing effect on the data.

The second form of unwanted variation remaining results from differing sensitivities of the one or more emulsion layers in the film to variations in light intensity and quality. These variations are due to time of day, season, and camera optics, and occur within zones. Some of this zonal variation might be removed using corrections based upon

the location of sample areas within the photographs. For instance, it was demonstrated that the density of the yellow and magenta layers (red density) increases gradually in a radial direction from the photo nadir. Generally speaking, film densities are also higher in the southern quadrants on winter and late summer photography due to the low sun angle at these two seasons of the year. Thus, distance and sun angle could probably be programmed with density to increase the likelihood of success in automated photo interpretation.

## DISCUSSION

During the coming year we will continue our study of film density for discriminating land-use on high-altitude aerial photography. It is hoped that additional imagery from RB-57 mission 191 flown on November 12, 1971, will be of good quality and will complete the seasonal coverage for the Atlanta test site. This year we will also examine 1:120,000 scale RC-8 photography with the intention of using both density and spatial frequency to increase the accuracy of classification.

As a result of preliminary work reported here, we intend to make a more complete study of the effect of distance from the photo nadir and photo quadrant on film density signatures. It is our hope to develop functions for the correction of these exposure-related variations in film density and to incorporate these in multivariate discriminant analysis techniques.

## LITERATURE CITED


1. Aldrich, R. C., W. J. Greentree, R. C. Heller, and N. X. Norick. 1970. The use of space and high altitude aerial photography to classify forest land and to detect forest disturbances. Annual Progress Report for Earth Resources Survey Program, OSSA/NASA, by the Pacific Southwest Forest and Range Experiment Station, 36 p., illus.
2. Preliminary Science Report (90-day). Image evaluation, NASA RB-57 flight for Contract No. R-09-038-002. Site 217, Atlanta, Georgia, Mission 131. June 8, 1970.
3. Preliminary Science Report (90-day). Image evaluation, NASA RB-57 flight for Contract No. R-09-038-002. Site 217, Atlanta, Georgia, Missions 141 and 158. September 8, 1970, and March 5, 1971.
4. Pease, Robert W. 1968. Making color infrared film a more effective high altitude sensor. NASA Tech. Letter 117 prepared by Geological Survey, U. S. Department of Interior. Manned Spacecraft Center, Houston, Texas.

# CLASSIFICATION OF LAND USE BY AUTOMATED PROCEDURES

by

Nancy X. Norick and Marilyn Wilkes

## INTRODUCTION

Pattern recognition techniques include a variety of mathematical and statistical methods aimed at identifying particular objects of interest -- and usually automatically. Each may be optimum under certain conditions. One of the most difficult tasks is finding what features, variables, or measurements are best to use for finding differences between population types, e.g., forest and nonforest classes. The second is finding what classification techniques provide the best separation of the population types. Examples of features often used are: (1) statistical quantities such as means, variances, and other moments, (2) mathematical transforms of the data such as Fourier or Hadamard, and (3) direct untransformed measurements such as 3-color photo density measurements or digital output from a multispectral scanner. Due to time and cost restrictions on our data collection we were limited for this analysis to the use of direct measurements of image density on infrared color photos using red, blue, green, and clear filters. Until now we have concentrated on selecting among various classification procedures. For instance, we have explored this problem using multivariate linear discriminant analysis and various forms of an empirical distribution analysis. The next step will be the programming of a k-nearest neighbor procedure (k may be equal to 1, 2, 3, etc.).

The linear discriminant analysis is the optimum procedure when the data have multivariate normal distributions. It is robust, i.e., it is

nearly optimum for data which are not normal but come from continuous unimodal distributions. The empirical distribution may be better if the data are nonnormal in certain ways -- such as from multimodal distributions. A drawback is that it is necessary to have a large number of observations in the training set to adequately estimate the distribution. But, both of these methods may be totally inadequate if the data occur in strings. A method which may be better for this type of data is nearest neighbor analysis. Figure 12 shows examples of three data types and the appropriate distribution analysis. Our aim is to compare these three methods for our data (classification of land use).

LINDA is a linear discriminant analysis computer program which we wrote to handle our data. It is flexible for our use but not for general use as it requires a programmer to modify the main routine for each problem. The empirical distribution program is similar with respect to use. The number of cells and length of intervals can be changed for each run by a programmer. Both programs were written for the Univac 1108 in Fortran.

The linear discriminant method has been described by T. W. Anderson (2). This analysis chooses that classification which has the highest probability of occurrence for the values of the variables. The probabilities are based upon the training sample estimates of the normal distribution parameters. The empirical distribution method likewise chooses that classification which has the highest probability of occurrence; however, no assumptions such as those pertaining to normality are made about the probability distributions. Instead, the observed frequency distribution (often with some smoothing) of the training sample is used. Our empirical distribution analyses were done in several ways described below.

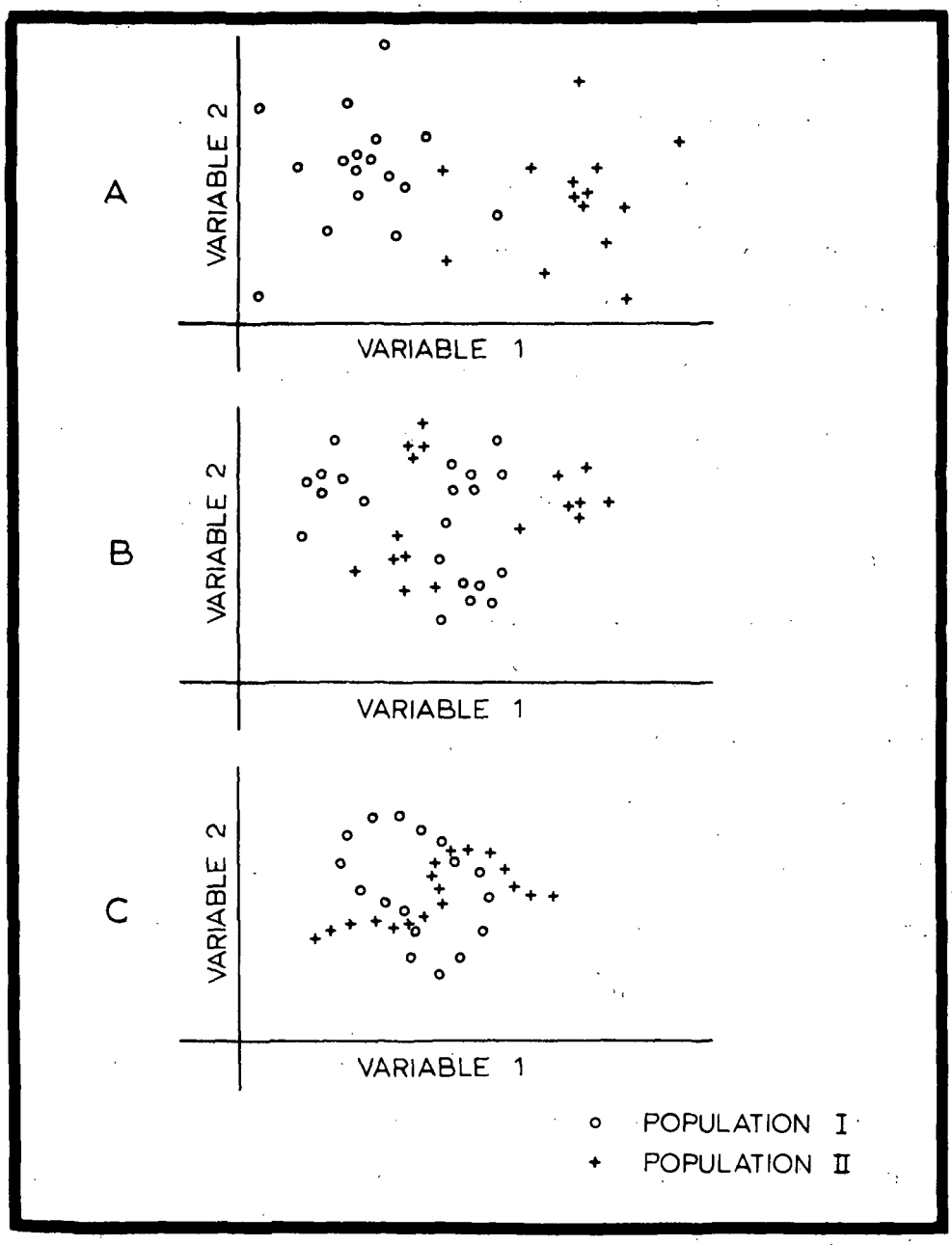


Figure 12. These three different data types may require different methods for optimum discrimination between populations: (A) a data type for which linear discriminant analysis might be chosen, (B) a data type for which empirical distribution analysis might be chosen, and (C) a data type for which the "nearest neighbor" analysis might be chosen.

## SAMPLING THE DATA

Four sets of photographic data for the Atlanta, Georgia, test site are used in this study. The aerial photography is 1:420,000 Ektachrome infrared color taken by NASA's high altitude RB-57 aircraft during three seasons -- early summer (June 1970), late summer (September 1970), and winter (March 1971).[8] Master copies of the Ektachrome infrared photographs taken from the Apollo 9 (SO-65) multiband photography experiment are also used. A full description of the photography, the photo and ground data acquisition techniques, and other analyses are given by Greentree and Aldrich in the previous section of this report and in the 1970 annual report (1).

For each photo mission two samples of data were taken. One was used as the training set for the classification analyses and the other as the new set to test the performance of the procedure. For both sets of data the sampling method was the same. A random sample of ten points was selected from each of eighteen sample strips for each land-use class. When ten exceeded the number of observations for a land-use class on a sample strip a smaller random sample was taken. This method gave equal weights to all sample strips and made the number of observations per land use as uniform as possible. The effect of this sampling scheme was to give every land use a nearly equivalent chance of being identified. For a production analysis (for example, map making) one might choose another sampling method such as a completely random sample. This would have the effect of giving greater emphasis to classes with more observations. Another sampling scheme could be devised to put greater emphasis on certain specified classes deemed more important by an investigator.

[8] Mission 131, June 8, 1970; Mission 141, September 12, 1970; Mission 158, March 5, 1971.

For each aircraft mission, information for both samples from microdensitometer scans of 1:420,000 scale Ektachrome infrared color film was written on computer tapes. Information from 1:2,500,000 scale Apollo scans was recorded as well. For each observation sampled the land use and density values for scans using red, green, blue, and clear filters were recorded. Previously we had tested the effects of using the visual versus the clear filters for normalizing the exposure differences and found they were equivalent for our purposes.

## THE ANALYSES

We tested several combinations of the original 13 forest and nonforest categories in our analyses. The simplest was all forest versus all nonforest. Another set of categories combined all forest types while all nonforest categories were kept intact -- a total of nine categories. Analyses were done also using the original 13 categories defined by Aldrich, et al (1).

The variables used to make the classifications were red minus clear densities, blue minus clear densities, and green minus clear densities. We had therefore a trivariate distribution.

The linear discriminant analysis was done in the standard way. However, the empirical distribtuion analysis was done using several models. In the first, the density range of each variable was divided into three equal length intervals. This gave 27 possible cells for observations to fall into, e.g., an observation could be in interval 1 for R minus C, 1 for B minus C, and 1 for G minus C; 1 for R minus C, 1 for B minus C, and 2 for G minus C, etc. The number of training set observations for each land-use class in each cell was tabulated. That land-use class with the

largest number of observations in a given cell was the choice for the cell. Every test data observation that fell in that cell was classified as being of that land-use class. One result of this method of choosing the interval length was that many observations fell in a few cells while most cells were empty or nearly empty.

To overcome this the range of each variable was divided into three equal frequency intervals. This improved the accuracy of the classification, and because of this success we tried other empirical models with 4, 5, and 6 intervals per variable. Each of these empirical models gave weights to land-use classes proportional to their sample size.

We also tried two other weighting systems for Mission 158 (winter) data using 9 land-use categories and 4 intervals. The first gave equal weight to each category regardless of its sample size. The second weighting system gave greater emphasis to categories with fewer observations. These models correctly classified more observations in the lightly sampled categories than the previously used models, but their overall performance, i.e., the proportion correct for all categories, was slightly poorer. Their use will depend upon the importance of the smaller categories.

For the 2-category classification problem, in addition to making the weights proportional to the sample sizes, we ran some data with the weights of forest samples doubled. As we had anticipated, this improved forest classification.

To verify that the classification procedures were having an effect we computed the number of correct classifications that would occur by chance. As a result we found that all methods were considerably better than would be expected by chance.

## RESULTS AND DISCUSSION

The major results of this investigation have been tabulated in Tables 7 through 22. Tables 7, 8, and 9 show the proportion correct over all categories for each photographic mission and each method. The proportions that would be expected if a completely random procedure had been used are also tabulated and are shown at the top of each table. All methods used are considerably better than random.

For analyses that combined observations into 13 and 9 land-use classes, the empirical distribution method yielded considerably better results than LINDA. However, when only 2 classes were used, forest versus nonforest, the methods are roughly equivalent.

One striking result is that classifications using the Apollo 9 imagery are almost as good as those for the high flight aircraft missions. This may be due to the averaging effect of the lower resoltion space imagery. If so, better results might be obtained on high altitude photography if we were to average density values for adjacent points on the scan lines and on lines scanned above and below the original scan location. We will test this procedure as the data analysis continues.

Tables 10-22 show numbers of observations by actual and predicted classes. From these data one can see which classes appear to be similar in density values.

## FUTURE WORK

The empirical distribution program is being modified to smooth the distribution curves. As a result of this, no observations will be classified as "undecided." Once this is completed the next classification method to be programmed will be the nearest neighbor method.

Thus far, our analyses have been limited to sample blocks distributed

over the entire study area. An important question which we have not yet tried to answer is: Can training samples from one block be used to classify observations from another block? We hope to answer this question during the coming year.

Another important area for investigation is the effect of the location of samples within the photo frame on classification accuracy. We hope to learn whether location can be of value to improve the normalizing procedure which has, until now, consisted only of subtracting the clear filter densities.

## LITERATURE CITED


1. Aldrich, R. C., W. J. Greentree, R. C. Heller, and N. X. Norick. 1970. The use of space and high altitude aerial photography to classify forest land and to detect forest disturbnaces. Annual Progress Report for Earth Resources Survey Program, OSSA/NASA, by the Pacific Southwest Forest and Range Exp. Sta., 36 p., illus.
2. Anderson, T. W. 1958. An introduction to multivariate statistical analysis. John Wiley and Sons, Inc., New York.

Table 7. Comparisons of methods for automated classification: Accuracy for 13 land-use classes by season of photography.

| METHOD | Mission 131 June | Mission 141 September | Mission 158 March | Apollo 9 March |
|---|---|---|---|---|
| | Proportion correct | | | |
| Expected correct if random | 0.1052 | 0.1196 | 0.1044 | 0.1066 |
| Linear Discriminant Analysis | 0.1853 | 0.1686 | 0.2288 | 0.1998 |
| Empirical Distribution Analysis | | | | |
| 3 equal length intervals | 0.2250 | 0.2532 | 0.2522 | 0.2364 |
| 3 equal frequency intervals | 0.2408 | 0.3133 | 0.2688 | 0.2565 |
| 4 equal frequency intervals | 0.2544 | 0.3187 | 0.2785 | 0.2707 |
| 5 equal frequency intervals | 0.2866 | 0.3684 | 0.3240 | 0.2737 |
| 6 equal frequency intervals | 0.2893 | 0.3594 | 0.3284 | 0.2879 |

Table 8. Comparison of methods for automated classification: Accuracy for 9 land-use classes (all forest combined) by season of photography.

| METHOD | Mission 131 June | Mission 141 September | Mission 158 March | Apollo 9 March |
|---|---|---|---|---|
| | Proportion correct | | | |
| Expected correct if random | 0.2581 | 0.2923 | 0.2413 | 0.2654 |
| Linear Discriminant Analysis | 0.3109 | 0.3178 | 0.3264 | 0.3963 |
| Empirical Distribution Analysis | | | | |
| 3 equal length intervals | 0.4781 | 0.5279 | 0.4764 | 0.5095 |
| 2 equal frequency intervals | | | 0.4737 | |
| 3 equal frequency intervals | 0.4679 | 0.5526 | 0.4982 | 0.5036 |
| 4 equal frequency intervals | 0.4843 | 0.5526 | 0.4939 | 0.5136 |
| 5 equal frequency intervals | 0.5055 | 0.5858 | 0.5289 | 0.5077 |
| 6 equal frequency intervals | 0.5130 | 0.5740 | 0.5184 | 0.5172 |

Table 9. Comparison of methods for automated classification: Accuracy for 2 land-use classes (forest versus nonforest) by season of photography.

| METHOD | Mission 131 June | Mission 141 September | Mission 158 March | Apollo 9 March |
|---|---|---|---|---|
| | Proportion correct | | | |
| Expected correct if random | 0.5028 | 0.5000 | 0.5079 | 0.5020 |
| Linear Discriminant Analysis | 0.7305 | 0.7489 | 0.7636 | 0.7571 |
| Empirical Distribution Analysis | | | | |
| 3 equal length intervals | 0.7023 | 0.6599 | 0.7338 | 0.7056 |
| 3 equal frequency intervals | 0.7155 | 0.7672 | 0.7574 | 0.7441 |
| 4 equal frequency intervals | 0.7168 | 0.7597 | 0.7758 | 0.7601 |
| 5 equal frequency intervals | 0.7339 | 0.7650 | 0.7697 | 0.7488 |
| 6 equal frequency intervals | 0.7456 | 0.7575 | 0.7715 | 0.7447 |

Table 10. Mission 158 - Color film, filter 15 + 30B. Empirical Distribution Analysis with 3 equal length intervals.

| PREDICTED TYPE | ACTUAL TYPE 1 | 2 | 3 | 4 | 5 | 6 | 7 | 8 | 9 | Total |
|---|---|---|---|---|---|---|---|---|---|---|
| 1 | 458 | 12 | 28 | 77 | 25 | 95 | 16 | 85 | 17 | 813 |
| 2 | 0 | 0 | 0 | 0 | 0 | 0 | 0 | 0 | 0 | 0 |
| 3 | 0 | 0 | 0 | 0 | 0 | 0 | 0 | 0 | 0 | 0 |
| 4 | 38 | 26 | 35 | 70 | 22 | 33 | 2 | 73 | 8 | 307 |
| 5 | 0 | 0 | 0 | 0 | 0 | 0 | 0 | 0 | 0 | 0 |
| 6 | 1 | 0 | 0 | 0 | 0 | 3 | 0 | 0 | 0 | 4 |
| 7 | 0 | 0 | 0 | 0 | 0 | 0 | 0 | 0 | 0 | 0 |
| 8 | 0 | 0 | 0 | 0 | 0 | 0 | 0 | 0 | 0 | 0 |
| 9 | 1 | 0 | 1 | 1 | 0 | 0 | 0 | 1 | 13 | 17 |
| 10 | 1 | 0 | 0 | 0 | 0 | 0 | 0 | 0 | 0 | 1 |
| Total | 499 | 38 | 64 | 148 | 47 | 131 | 18 | 159 | 38 | |

LEGEND:

1 - Forest
2 - Crops
3 - Plowed
4 - Pasture
5 - Idle
6 - Abandoned
7 - Orchard
8 - Urban
9 - Water
10 - Undecided

Table 11. Mission 158 - Color film, filter 15 + 30B. Empirical Distribution Analysis with 2 equal frequency intervals.

| PREDICTED TYPE | ACTUAL TYPE 1 | 2 | 3 | 4 | 5 | 6 | 7 | 8 | 9 | Total |
|---|---|---|---|---|---|---|---|---|---|---|
| 1 | 443 | 7 | 29 | 50 | 18 | 72 | 16 | 70 | 34 | 739 |
| 2 | 0 | 0 | 0 | 0 | 0 | 0 | 0 | 0 | 0 | 0 |
| 3 | 0 | 0 | 0 | 0 | 0 | 0 | 0 | 0 | 0 | 0 |
| 4 | 56 | 31 | 35 | 98 | 29 | 59 | 2 | 89 | 4 | 403 |
| 5 | 0 | 0 | 0 | 0 | 0 | 0 | 0 | 0 | 0 | 0 |
| 6 | 0 | 0 | 0 | 0 | 0 | 0 | 0 | 0 | 0 | 0 |
| 7 | 0 | 0 | 0 | 0 | 0 | 0 | 0 | 0 | 0 | 0 |
| 8 | 0 | 0 | 0 | 0 | 0 | 0 | 0 | 0 | 0 | 0 |
| 9 | 0 | 0 | 0 | 0 | 0 | 0 | 0 | 0 | 0 | 0 |
| 10 | 0 | 0 | 0 | 0 | 0 | 0 | 0 | 0 | 0 | 0 |
| Total | 499 | 38 | 64 | 148 | 47 | 131 | 18 | 159 | 38 | |

LEGEND:

1 - Forest
2 - Crops
3 - Plowed
4 - Pasture
5 - Idle
6 - Abandoned
7 - Orchard
8 - Urban
9 - Water
10 - Undecided

Table 12. Mission 158 - Color film, filter 15 + 30B. Empirical Distribution Analysis with 3 equal frequency intervals.

| PREDICTED TYPE | ACTUAL TYPE 1 | 2 | 3 | 4 | 5 | 6 | 7 | 8 | 9 | Total |
|---|---|---|---|---|---|---|---|---|---|---|
| 1 | 464 | 12 | 24 | 63 | 23 | 89 | 16 | 73 | 18 | 782 |
| 2 | 0 | 0 | 0 | 0 | 0 | 0 | 0 | 0 | 0 | 0 |
| 3 | 1 | 0 | 1 | 0 | 0 | 0 | 0 | 0 | 0 | 2 |
| 4 | 22 | 21 | 27 | 69 | 14 | 28 | 1 | 61 | 1 | 244 |
| 5 | 0 | 0 | 0 | 0 | 0 | 0 | 0 | 0 | 0 | 0 |
| 6 | 0 | 0 | 0 | 0 | 0 | 0 | 0 | 0 | 0 | 0 |
| 7 | 0 | 0 | 0 | 0 | 0 | 0 | 0 | 0 | 0 | 0 |
| 8 | 12 | 5 | 12 | 15 | 10 | 13 | 1 | 24 | 8 | 100 |
| 9 | 0 | 0 | 0 | 1 | 0 | 1 | 0 | 1 | 11 | 14 |
| 10 | 0 | 0 | 0 | 0 | 0 | 0 | 0 | 0 | 0 | 0 |
| Total | 499 | 38 | 64 | 148 | 47 | 131 | 18 | 159 | 38 | |

LEGEND:

1 - Forest
2 - Crops
3 - Plowed
4 - Pasture
5 - Idle
6 - Abandoned
7 - Orchard
8 - Urban
9 - Water
10 - Undecided

Table 13. Mission 158 - Color film, filter 15 + 30B. Empirical Distribution Analysis with 4 equal frequency intervals.

| PREDICTED TYPE | ACTUAL TYPE 1 | 2 | 3 | 4 | 5 | 6 | 7 | 8 | 9 | Total |
|---|---|---|---|---|---|---|---|---|---|---|
| 1 | 441 | 9 | 21 | 55 | 17 | 66 | 16 | 64 | 18 | 707 |
| 2 | 13 | 8 | 2 | 16 | 1 | 6 | 0 | 11 | 0 | 57 |
| 3 | 3 | 2 | 8 | 0 | 0 | 4 | 0 | 4 | 3 | 24 |
| 4 | 20 | 16 | 28 | 62 | 21 | 25 | 2 | 60 | 6 | 240 |
| 5 | 0 | 0 | 0 | 0 | 0 | 0 | 0 | 0 | 0 | 0 |
| 6 | 13 | 3 | 4 | 8 | 1 | 20 | 0 | 4 | 0 | 53 |
| 7 | 0 | 0 | 0 | 0 | 0 | 0 | 0 | 0 | 0 | 0 |
| 8 | 6 | 0 | 1 | 7 | 7 | 9 | 0 | 15 | 1 | 46 |
| 9 | 0 | 0 | 0 | 0 | 0 | 0 | 0 | 1 | 10 | 11 |
| 10 | 3 | 0 | 0 | 0 | 0 | 1 | 0 | 0 | 0 | 4 |
| Total | 499 | 38 | 64 | 148 | 47 | 131 | 18 | 159 | 38 | |

LEGEND:

1 - Forest
2 - Crops
3 - Plowed
4 - Pasture
5 - Idle
6 - Abandoned
7 - Orchard
8 - Urban
9 - Water
10 - Undecided

Table 14. Mission 158 - Color film, filter 15 + 30B. Empirical Distribution Analysis with 5 equal frequency intervals.

| PREDICTED TYPE | ACTUAL TYPE 1 | 2 | 3 | 4 | 5 | 6 | 7 | 8 | 9 | Total |
|---|---|---|---|---|---|---|---|---|---|---|
| 1 | 452 | 10 | 22 | 50 | 15 | 78 | 14 | 64 | 17 | 722 |
| 2 | 0 | 0 | 0 | 0 | 0 | 0 | 0 | 0 | 0 | 0 |
| 3 | 0 | 0 | 1 | 0 | 0 | 0 | 0 | 0 | 0 | 1 |
| 4 | 23 | 17 | 23 | 65 | 14 | 22 | 3 | 31 | 1 | 199 |
| 5 | 2 | 0 | 2 | 0 | 9 | 3 | 0 | 4 | 0 | 20 |
| 6 | 2 | 0 | 0 | 0 | 1 | 8 | 0 | 1 | 4 | 16 |
| 7 | 0 | 0 | 0 | 0 | 0 | 0 | 0 | 0 | 0 | 0 |
| 8 | 16 | 10 | 14 | 33 | 8 | 16 | 1 | 54 | 1 | 153 |
| 9 | 1 | 1 | 2 | 0 | 0 | 3 | 0 | 3 | 15 | 25 |
| 10 | 3 | 0 | 0 | 0 | 0 | 1 | 0 | 2 | 0 | 6 |
| Total | 499 | 38 | 64 | 148 | 47 | 131 | 18 | 159 | 38 | |

LEGEND:

1 - Forest
2 - Crops
3 - Plowed
4 - Pasture
5 - Idle
6 - Abandoned
7 - Orchard
8 - Urban
9 - Water
10 - Undecided

Table 15. Mission 158 - Color film, filter 15 + 30B. Empirical Distribution Analysis with 6 equal frequency intervals.

| PREDICTED TYPE | ACTUAL TYPE 1 | 2 | 3 | 4 | 5 | 6 | 7 | 8 | 9 | Total |
|---|---|---|---|---|---|---|---|---|---|---|
| 1 | 437 | 7 | 23 | 42 | 12 | 73 | 12 | 55 | 16 | 677 |
| 2 | 2 | 2 | 0 | 0 | 0 | 0 | 0 | 0 | 0 | 4 |
| 3 | 2 | 0 | 5 | 0 | 0 | 2 | 0 | 4 | 1 | 14 |
| 4 | 19 | 12 | 15 | 46 | 5 | 25 | 1 | 23 | 5 | 151 |
| 5 | 7 | 0 | 1 | 2 | 15 | 5 | 3 | 6 | 0 | 39 |
| 6 | 8 | 1 | 1 | 5 | 2 | 10 | 0 | 6 | 1 | 34 |
| 7 | 0 | 0 | 0 | 0 | 0 | 0 | 2 | 0 | 0 | 2 |
| 8 | 19 | 15 | 18 | 53 | 13 | 16 | 0 | 60 | 0 | 194 |
| 9 | 0 | 1 | 0 | 0 | 0 | 0 | 0 | 2 | 15 | 18 |
| 10 | 5 | 0 | 1 | 0 | 0 | 0 | 0 | 3 | 0 | 9 |
| Total | 499 | 38 | 64 | 148 | 47 | 131 | 18 | 159 | 38 | |

LEGEND:

1 - Forest
2 - Crops
3 - Plowed
4 - Pasture
5 - Idle
6 - Abandoned
7 - Orchard
8 - Urban
9 - Water
10 - Undecided

Table 16. Mission 158 - Color film, filter 15 + 30B. Weighted Empirical Distribution Analysis with 4 equal frequency intervals.

$$\text{Weight} = \frac{\text{frequency/land use in cell}}{\text{total frequency/land use}}$$

| PREDICTED TYPE | ACTUAL TYPE 1 | 2 | 3 | 4 | 5 | 6 | 7 | 8 | 9 | Total |
|---|---|---|---|---|---|---|---|---|---|---|
| 1 | 248 | 1 | 3 | 5 | 2 | 12 | 3 | 20 | 2 | 296 |
| 2 | 23 | 14 | 4 | 24 | 2 | 7 | 0 | 12 | 0 | 86 |
| 3 | 24 | 9 | 35 | 49 | 16 | 22 | 2 | 53 | 7 | 217 |
| 4 | 16 | 4 | 0 | 16 | 0 | 3 | 0 | 7 | 0 | 46 |
| 5 | 9 | 5 | 4 | 13 | 11 | 14 | 0 | 22 | 0 | 78 |
| 6 | 48 | 3 | 9 | 21 | 1 | 36 | 0 | 17 | 0 | 135 |
| 7 | 86 | 0 | 4 | 10 | 13 | 20 | 11 | 11 | 5 | 160 |
| 8 | 12 | 0 | 0 | 2 | 1 | 2 | 0 | 9 | 0 | 26 |
| 9 | 30 | 2 | 5 | 8 | 1 | 14 | 2 | 8 | 24 | 94 |
| 10 | 3 | 0 | 0 | 0 | 0 | 1 | 0 | 0 | 0 | 4 |
| Total | 499 | 38 | 64 | 148 | 47 | 131 | 18 | 159 | 38 | |

LEGEND:

1 - Forest
2 - Crops
3 - Plowed
4 - Pasture
5 - Idle
6 - Abandoned
7 - Orchard
8 - Urban
9 - Water
10 - Undecided

Table 17. Mission 158 - Color film, filter 15 + 30B. Weighted Empirical Distribution Analysis with 4 equal frequency intervals.

$$\text{Weight} = \frac{\text{frequency/land use in cell}}{(\text{total frequency/land use})^{1/2}}$$

| PREDICTED TYPE | ACTUAL TYPE 1 | 2 | 3 | 4 | 5 | 6 | 7 | 8 | 9 | Total |
|---|---|---|---|---|---|---|---|---|---|---|
| 1 | 396 | 7 | 16 | 40 | 9 | 41 | 10 | 45 | 12 | 576 |
| 2 | 17 | 10 | 2 | 16 | 1 | 6 | 0 | 11 | 0 | 63 |
| 3 | 10 | 2 | 16 | 2 | 6 | 11 | 1 | 9 | 5 | 62 |
| 4 | 13 | 14 | 18 | 58 | 14 | 17 | 1 | 53 | 0 | 188 |
| 5 | 4 | 0 | 1 | 7 | 7 | 9 | 0 | 13 | 0 | 41 |
| 6 | 26 | 3 | 8 | 16 | 1 | 29 | 0 | 12 | 0 | 95 |
| 7 | 16 | 0 | 0 | 4 | 7 | 9 | 6 | 3 | 3 | 48 |
| 8 | 12 | 0 | 0 | 2 | 1 | 2 | 0 | 9 | 0 | 26 |
| 9 | 2 | 2 | 3 | 3 | 1 | 6 | 0 | 4 | 18 | 39 |
| 10 | 3 | 0 | 0 | 0 | 0 | 1 | 0 | 0 | 0 | 4 |
| Total | 499 | 38 | 64 | 148 | 47 | 131 | 18 | 159 | 38 | |

LEGEND:

1 - Forest
2 - Crops
3 - Plowed
4 - Pasture
5 - Idle
6 - Abandoned
7 - Orchard
8 - Urban
9 - Water
10 - Undecided

Table 18. Mission 158 - Color film, filter 15 + 30B. Linear Discriminant Analysis.

| PREDICTED TYPE | ACTUAL TYPE 1 | 2 | 3 | 4 | 5 | 6 | 7 | 8 | 9 | Total |
|---|---|---|---|---|---|---|---|---|---|---|
| 1 | 118 | 0 | 1 | 4 | 4 | 12 | 0 | 13 | 1 | 153 |
| 2 | 20 | 3 | 4 | 5 | 1 | 6 | 1 | 4 | 2 | 46 |
| 3 | 0 | 0 | 0 | 0 | 0 | 0 | 0 | 0 | 0 | 0 |
| 4 | 40 | 17 | 18 | 54 | 20 | 35 | 1 | 44 | 1 | 230 |
| 5 | 1 | 0 | 0 | 0 | 1 | 1 | 0 | 1 | 0 | 4 |
| 6 | 0 | 0 | 0 | 0 | 0 | 0 | 0 | 0 | 0 | 0 |
| 7 | 24 | 0 | 1 | 0 | 1 | 0 | 1 | 2 | 0 | 29 |
| 8 | 4 | 2 | 6 | 2 | 1 | 5 | 0 | 7 | 4 | 31 |
| 9 | 59 | 1 | 5 | 10 | 5 | 13 | 9 | 9 | 21 | 132 |
| Total | 266 | 23 | 35 | 75 | 33 | 72 | 12 | 80 | 29 | |

LEGEND:

1 - Forest
2 - Crops
3 - Plowed
4 - Pasture
5 - Idle
6 - Abandoned
7 - Orchard
8 - Urban
9 - Water

Table 19. Mission 158 - Color film, filter 15 + 30B. Linear Discriminant Analysis.

| PREDICTED TYPE | ACTUAL TYPE 1 | 2 | Total |
|---|---|---|---|
| 1 | 402 | 173 | 575 |
| 2 | 97 | 470 | 567 |
| Total | 499 | 643 | |

LEGEND:

1 - forest
2 - nonforest

Table 20. Mission 158 - Color film, filter 15 + 30B. Empirical Distribution Analysis with 3 equal frequency intervals.

| PREDICTED TYPE | ACTUAL TYPE 1 | 2 | Total |
|---|---|---|---|
| 1 | 358 | 136 | 494 |
| 2 | 141 | 507 | 648 |
| 3 | 0 | 0 | 0 |
| Total | 499 | 643 | |

LEGEND:

1 - forest
2 - nonforest
3 - undecided

Table 21. Mission 158 - Color film, filter 15 + 30B. Linear Discriminant Analysis.

| PREDICTED TYPE | ACTUAL TYPE 1 | 2 | 3 | 4 | 5 | 6 | 7 | 8 | 9 | 10 | 11 | 12 | 13 | Total |
|---|---|---|---|---|---|---|---|---|---|---|---|---|---|---|
| 1 | 46 | 10 | 21 | 22 | 0 | 2 | 2 | 0 | 11 | 0 | 7 | 2 | 0 | 123 |
| 2 | 12 | 17 | 10 | 11 | 3 | 3 | 2 | 3 | 4 | 3 | 8 | 1 | 0 | 77 |
| 3 | 3 | 4 | 6 | 7 | 0 | 1 | 4 | 5 | 4 | 2 | 6 | 0 | 0 | 42 |
| 4 | 0 | 0 | 0 | 0 | 0 | 0 | 0 | 0 | 0 | 0 | 0 | 0 | 0 | 0 |
| 5 | 4 | 4 | 1 | 5 | 3 | 1 | 6 | 2 | 6 | 0 | 7 | 1 | 0 | 40 |
| 6 | 0 | 0 | 0 | 0 | 0 | 1 | 0 | 0 | 0 | 1 | 0 | 0 | 0 | 2 |
| 7 | 7 | 2 | 8 | 12 | 14 | 20 | 50 | 19 | 33 | 1 | 41 | 0 | 0 | 207 |
| 8 | 0 | 0 | 0 | 0 | 0 | 0 | 0 | 0 | 0 | 0 | 0 | 0 | 0 | 0 |
| 9 | 0 | 0 | 0 | 0 | 0 | 0 | 0 | 0 | 0 | 0 | 0 | 0 | 0 | 0 |
| 10 | 0 | 0 | 0 | 0 | 0 | 0 | 0 | 0 | 0 | 0 | 0 | 0 | 0 | 0 |
| 11 | 0 | 0 | 1 | 4 | 2 | 5 | 3 | 0 | 4 | 0 | 4 | 5 | 0 | 28 |
| 12 | 2 | 6 | 7 | 10 | 1 | 2 | 8 | 3 | 9 | 5 | 5 | 16 | 3 | 77 |
| 13 | 6 | 5 | 4 | 9 | 0 | 0 | 0 | 1 | 1 | 0 | 2 | 1 | 0 | 29 |
| Total | 80 | 48 | 58 | 80 | 23 | 35 | 75 | 33 | 72 | 12 | 80 | 26 | 3 | |

LEGEND:

1 - Pine
2 - Pine hardwood
3 - Bottomland hardwood
4 - Upland hardwood
5 - Crops
6 - Plowed
7 - Pasture
8 - Idle
9 - Abandoned
10 - Orchard
11 - Urban
12 - Clear water
13 - Turbid water

Table 22. Mission 158 - Color film, filter 15 + 30B. Empirical Distribution Analysis with 3 equal frequency intervals.

| PREDICTED TYPE | ACTUAL TYPE 1 | 2 | 3 | 4 | 5 | 6 | 7 | 8 | 9 | 10 | 11 | 12 | 13 | Total |
|---|---|---|---|---|---|---|---|---|---|---|---|---|---|---|
| 1 | 114 | 47 | 42 | 74 | 4 | 6 | 16 | 6 | 32 | 5 | 30 | 4 | 2 | 382 |
| 2 | 0 | 0 | 0 | 0 | 0 | 0 | 0 | 0 | 0 | 0 | 0 | 0 | 0 | 0 |
| 3 | 0 | 0 | 0 | 0 | 0 | 0 | 0 | 0 | 0 | 0 | 0 | 0 | 0 | 0 |
| 4 | 27 | 23 | 34 | 58 | 4 | 10 | 28 | 6 | 35 | 7 | 26 | 6 | 1 | 265 |
| 5 | 0 | 0 | 0 | 0 | 0 | 0 | 0 | 0 | 0 | 0 | 0 | 0 | 0 | 0 |
| 6 | 0 | 0 | 0 | 1 | 0 | 1 | 0 | 0 | 0 | 0 | 0 | 0 | 0 | 2 |
| 7 | 12 | 3 | 10 | 14 | 23 | 28 | 75 | 16 | 33 | 1 | 62 | 3 | 0 | 280 |
| 8 | 0 | 0 | 0 | 0 | 0 | 0 | 0 | 0 | 0 | 0 | 0 | 0 | 0 | 0 |
| 9 | 0 | 8 | 6 | 4 | 1 | 2 | 8 | 7 | 9 | 2 | 3 | 2 | 0 | 52 |
| 10 | 0 | 0 | 0 | 0 | 0 | 0 | 1 | 0 | 0 | 2 | 0 | 0 | 0 | 3 |
| 11 | 7 | 0 | 6 | 9 | 6 | 17 | 19 | 12 | 21 | 1 | 37 | 9 | 0 | 144 |
| 12 | 0 | 0 | 0 | 0 | 0 | 0 | 1 | 0 | 1 | 0 | 1 | 11 | 0 | 14 |
| 13 | 0 | 0 | 0 | 0 | 0 | 0 | 0 | 0 | 0 | 0 | 0 | 0 | 0 | 0 |
| 14 | 0 | 0 | 0 | 0 | 0 | 0 | 0 | 0 | 0 | 0 | 0 | 0 | 0 | 0 |
| Total | 160 | 81 | 98 | 160 | 38 | 64 | 148 | 47 | 131 | 18 | 159 | 35 | 3 | |

LEGEND:

1 - Pine
2 - Pine hardwood
3 - Bottomland hardwood
4 - Upland hardwood
5 - Crops
6 - Plowed
7 - Pasture
8 - Idle
9 - Abandoned
10 - Orchard
11 - Urban
12 - Clear water
13 - Turbid water
14 - Undecided

# TREND AND SPREAD OF BARK BEETLE INFESTATIONS FROM 1968 THROUGH 1971

R. C. Heller, K. A. Zealear, and T. H. Waite

Bark beetles continue to concern forest managers throughout the United States; the most damaging insects are the southern pine beetle (Dendroctonus frontalis Zimm.) in the East and South, the mountain pine beetle (Dendroctonus ponderosa Hopk.) in the Rocky Mountain and Pacific Northwest States, and the western pine beetle (Dendroctonus brevicomis LeConte) in the Southwestern States and California. The detection and location of infestations ("group kills" or spots) while they are small are still very important, so that control action can be started early before expensive epidemics get under way. For example, the costly mountain pine beetle outbreak on the Teton and Targhee National Forests and Grand Teton National Park during 1967 to 1970 (1) might have been averted if over-mature trees had been removed in the early stages of the epidemic.

Knowledge of the impact of the beetles on our national timber resource is still fragmentary and needs improvement. Studies such as those we have conducted in the Black Hills indicate that remote sensing improves our knowledge of the losses, where they are occurring, and does it more efficiently than methods used heretofore.

By following the trend of how beetle populations operate over a time period, we can expect to learn where new infestations are likely to occur and to predict roughly the size and location of new infestations.

For example, small-scale aerial color photographs (1:32,000) permit the forest manager to evaluate current losses more accurately over larger areas than he could do by ground reconnaissance methods. When the small-scale photos are used with medium-scale photography (1:8,000) and ground examination, we have a most efficient survey design (2). One of the by-products of the NASA-Forest Service cooperative studies is the collection of four years of bark beetle infestation data over one relatively small area (1.6 by 5 kilometers) where little or no effort was made to control the beetle epidemic.

The study area in the Black Hills was selected because the timber type is relatively uniform -- more than 80% ponderosa pine. The remaining species are white spruce (Picea glauca (Moench) Voss.), trembling aspen (Populus tremuloides Michx.), and white birch (Betula papyrifera Marsh). Also, there is only one generation of beetles per year in this area, which causes only one new generation of dying and discoloring trees to be present at any one time. This "once-a-year" change simplifies the separation of "old group kills" from "new group kills" on aerial photographs. From August through September of each year, these newly discolored trees offer relatively large yellow-red targets which have a fairly high contrast ratio to the uniformly green healthy forest. Since the infestations occur in random sizes and locations, they become ideal resolution targets which we have used to answer questions on film-filter-scale combinations. These known targets are also expected to be used for possible detection by the Earth Resources Technology Satellite.

## PROCEDURES

Aerial color photography was taken for three purposes over selected areas in the northern Black Hills on August 11 and 12, 1971. First, we wanted to rephotograph the 1.6 by 5 kilometer study area mentioned earlier for following the trend of the beetle epidemic. Secondly, we wished to locate prospective ERTS sites in the event we were accepted to undertake our proposed ERTS research. Finally, we wished to establish the usefulness of aerial photography to identify levels of tree density which would not support beetle infestations. These two latter studies will be reported elsewhere in this progress report.

Only one scale of photography was flown -- 1:8,000 -- with a Zeiss RMK 21/23 from the Forest Service Aero Commander. Both medium-speed Ektachrome (Type 2448) and Aerocolor (Type 2445) were exposed over most sites. The medium-speed Ektachrome was processed in our own Berkeley facility to a positive transparency. The color negative film was sent out for development in a continuous processor. Color prints were made on a color Logetronic printer at the Forest Service color lab in San Francisco.

All interpretation was carried out on the color transparencies; resolution and color fidelity were better on the transparencies than on the prints. All newly discolored trees, which were yellow to yellow-red in August, were circled in ink directly on the transparencies. The groups were numbered and the trees counted in each group. Old-killed trees (1970 faders) had to be distinguished from the new faders (discolored in 1971) and this, too, could be done more accurately on the transparencies than on the prints (Figure 13). Finally, within the 1.6 by 5 kilometer study area, all data on the transparencies were transferred to the color prints

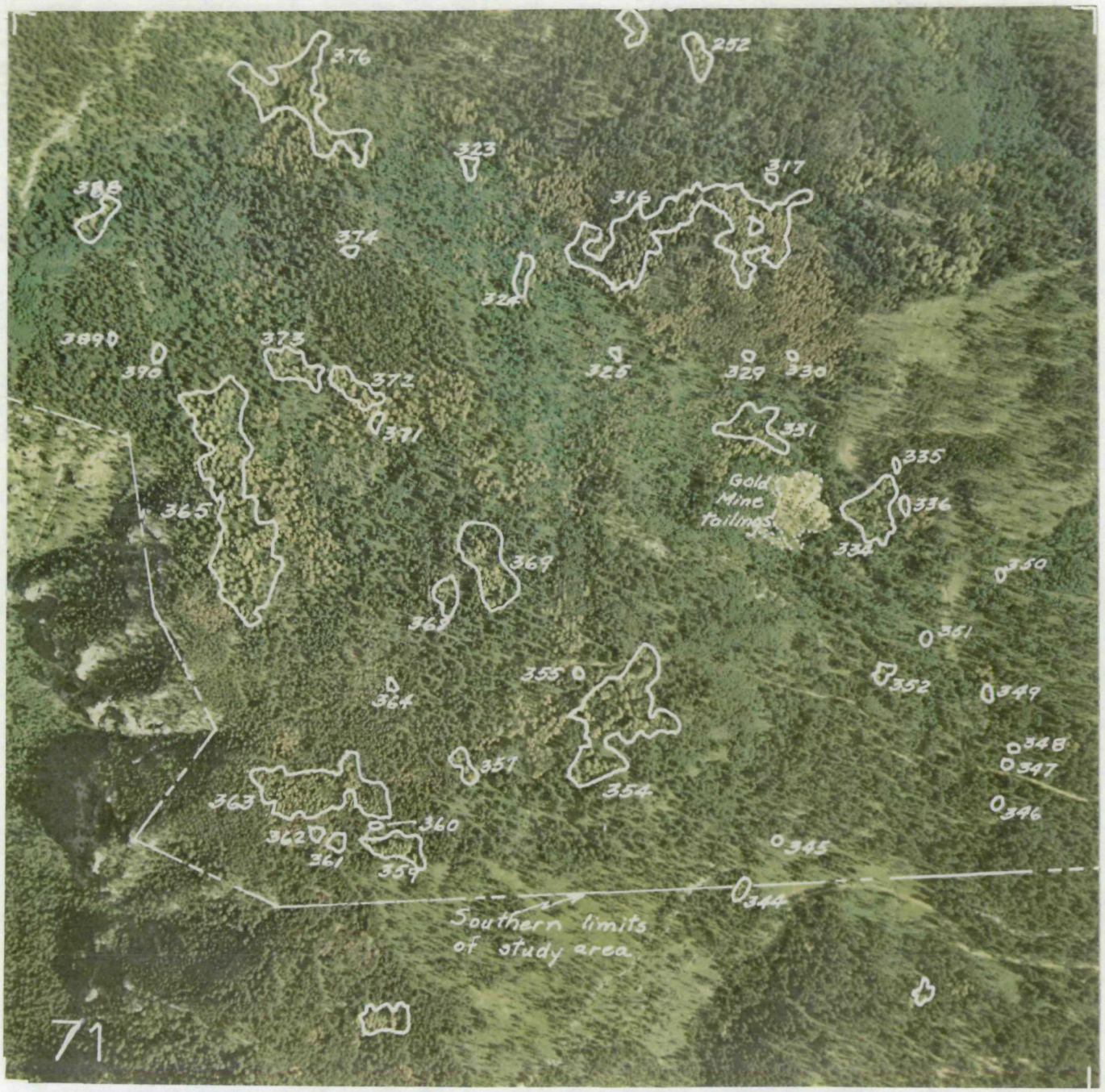


Figure 13. A portion of the 1.6 by 5 km. study area near Lead, S. D., is shown in this color print made from Aerocolor film. Scale 1:8,000, Zeiss RMK 21/23 camera. The newly dying trees are a yellow hue and are circled on this print. The infestation number shown near the circled trees can be checked in Table 8 for ground tree count. Note hue discrimination of older killed trees (yellow-red to brown) from healthy (green to green-yellow).

BLACK HILLS BEETLE STUDY

Ground Tally

Date 9/9/71 Crew KH, S.C., TW

| Spot No. | No. of Trees | DBH | Crown Class | Est. Plot Diam | Notes |
|---|---|---|---|---|---|
| 303 | 1 | 11 | 1 | 10 | |
| 304 | 1 | 9 | 1 | 10 | in cut over |
| 302 | 1 | 6 | 2 | 10' | very small crowns |
| | 2 | 7 | 2 | | |
| 301 | 1 | 9 | 3 | 20' | |
| | 2 | 10 | 2 | | |
| | 3 | 16 | 1 | | |
| | 4 | 10 | 2 | 100' | |
| | 5 | 15 | 2 | | |
| | 6 | 14 | 2 | | |
| 300 | 1 | 8 | 2 | 10' | |
| 299 | 1 | 9 | 2 | | |
| | | 11 | 1 | | |
| | | 13 | 2 | | |
| | | 8 | 3 | 40 | |
| | | 12 | 1 | 50 | |
| | | 11 | 2 | | |
| | | 13 | 2 | | |
| | | 11 | 2 | | |
| | | 12 | 1 | | |
| | 10 | 9 | 2 | | |
| | 11 | 11 | 2 | | |
| 297 | 1 | 14 | 1 | 10' | |
| 298 | 1 | 11 | 2 | | |
| | 2 | 11 | 2 | | |
| | 3 | 9 | 2 | | |

| Spot No. | No. of Trees | DBH | Crown Class | Est. Plot Diam | Notes |
|---|---|---|---|---|---|
| 298 cont. | 4 | 16 | 2 | | N |
| | 5 | 10 | 2 | | |
| | 6 | 16 | 2 | | |
| | 7 | 15 | 2 | | |
| | 8 | 13 | 2 | | |
| | 9 | 13 | 2 | | |
| | 10 | 9 | 2 | | |
| | | 12 | 2 | | |
| | | 8 | 4 | | 30' |
| | | 9 | 2 | | |
| | | 14 | 2 | | |
| | | 12 | 1 | | |
| | | 11 | 2 | | |
| | | 12 | 2 | | |
| | | 12 | 2 | | |
| | | 11 | 1 | | |
| | 20 | 14 | 1 | | |
| 296 | 1 | 12 | 2 | | 50 x 15 |
| | 2 | 14 | 2 | | |
| | 3 | 14 | 2 | | |
| | 4 | 11 | 2 | | |
| | 5 | 12 | 1 | | |
| | 6 | 15 | 2 | | |
| | 7 | 15 | 1 | | |
| | 8 | 13 | 2 | | |
| | 9 | 11 | 2 | | |

Sheet _____ of _____

Figure 14. Sample of field form used to measure size of each infestation and tally of trees within each infestation.

for field use. The interpreters were instructed to include all possible discolored trees so that there would be little likelihood of omission errors occurring. A total of 390 infestations were located on the photos.

The color prints were used stereoscopically in the field and were of incalculalable benefit in navigating through the timber. All 390 suspected infestations were ground checked for (1) presence of beetle attack, (2) number of trees within each group, (3) bole diameter in inches, (4) crown class,[9] and (5) the size of the infestation in meters (Figure 14).

## RESULTS

All trees which were found to be beetle infested were plotted on an overlay map of the study area (Figure 15). Table 23 lists these infestations by numbers of trees per group and by longest dimension of the infestation in meters. While 390 infestations were located on the photos, only 253 were found to be 1971-faded infestations when checked on the ground. Most of the 137 commission errors (390 - 253 = 137) were found to be single trees which probably faded late in 1970. The western section of this map, where the greatest amount of tree killing has occurred during the past four years (1968 through 1971), is shown in overlay form (Figure 16) for each of the years. Note particularly how the larger infestations have enlarged from one small location to merge with other large infestations. Hundreds of large trees, 25 to 30 meters tall, which were killed in 1968 are now down on the ground, changing the forest composition and environment for these sites.

Table 24 is a listing similar to Table 23 but includes only the infestations shown on the top overlay of Figure 16. The small numbers shown next

[9]Crown class is a silvicultural term relating the position of a tree to its neighbors. For example, the crown of a dominant tree receives direct sunlight from above and from three or more sides and is easily seen on air photographs. The crown of an intermediate tree receives only light from above and is often missed during photo interpretation.

Table 23. List of 1971 mountain pine beetle infestations on study area 2 by number of trees per infestation and longest dimension of the infested area.

| No. of Trees | Length Ft. | m. | No. of Trees | Length Ft. | m. | No. of Trees | Length Ft. | m. | No. of Trees | Length Ft. | m. | No. of Trees | Length Ft. | m. | No. of Trees | Length Ft. | m. |
|---|---|---|---|---|---|---|---|---|---|---|---|---|---|---|---|---|---|
| 2 | 10 | 3 | 2 | 20 | 6 | 4 | 40 | 12 | 8 | 80 | 20 | 15 | 100 | 30 | 36 | 170 | 52 |
| 2 | 10 | 3 | 2 | 20 | 6 | 4 | 40 | 12 | 9 | 30 | 9 | 15 | 150 | 45 | 37 | 200 | 61 |
| 2 | 10 | 3 | 2 | 20 | 6 | 4 | 60 | 18 | 9 | 35 | 11 | 16 | 75 | 23 | 39 | 130 | 40 |
| 2 | 10 | 3 | 2 | 20 | 6 | 5 | 15 | 5 | 9 | 50 | 15 | 16 | 90 | 27 | 39 | 150 | 45 |
| 2 | 10 | 3 | 2 | 20 | 6 | 5 | 40 | 12 | 9 | 50 | 15 | 16 | 90 | 27 | 39 | 200 | 61 |
| 2 | 10 | 3 | 2 | 20 | 6 | 5 | 40 | 12 | 9 | 60 | 18 | 16 | 100 | 30 | 44 | 150 | 45 |
| 2 | 10 | 3 | 2 | 25 | 8 | 5 | 50 | 15 | 9 | 70 | 21 | 16 | 105 | 32 | 45 | 205 | 62 |
| 2 | 10 | 3 | 2 | 30 | 9 | 6 | 30 | 9 | 9 | 75 | 23 | 17 | 35 | 11 | 47 | 125 | 38 |
| 2 | 15 | 5 | 2 | 30 | 9 | 6 | 40 | 12 | 10 | 50 | 15 | 19 | 70 | 21 | 61 | 200 | 61 |
| 2 | 15 | 5 | 3 | 10 | 3 | 6 | 40 | 12 | 10 | 60 | 18 | 19 | 80 | 24 | 64 | 330 | 100 |
| 2 | 15 | 5 | 3 | 10 | 3 | 6 | 50 | 15 | 10 | 70 | 21 | 19 | 90 | 27 | 81 | 210 | 64 |
| 2 | 15 | 5 | 3 | 15 | 5 | 6 | 100 | 30 | 10 | 90 | 27 | 19 | 90 | 27 | 82 | 220 | 67 |
| 2 | 15 | 5 | 3 | 15 | 5 | 7 | 30 | 9 | 11 | 45 | 14 | 19 | 130 | 39 | 86 | 260 | 79 |
| 2 | 15 | 5 | 3 | 20 | 6 | 7 | 32 | 10 | 11 | 50 | 15 | 19 | 190 | 58 | 90 | 265 | 81 |
| 2 | 15 | 5 | 3 | 20 | 6 | 7 | 40 | 12 | 11 | 65 | 20 | 20 | 80 | 24 | 104 | 330 | 100 |
| 2 | 15 | 5 | 3 | 30 | 9 | 7 | 50 | 15 | 11 | 100 | 30 | 24 | 132 | 40 | 108 | 125 | 38 |
| 2 | 15 | 5 | 3 | 30 | 9 | 7 | 50 | 15 | 12 | 60 | 18 | 27 | 70 | 21 | 143 | 250 | 76 |
| 2 | 15 | 5 | 3 | 30 | 9 | 7 | 55 | 17 | 12 | 65 | 20 | 27 | 90 | 27 | 173 | 400 | 122 |
| 2 | 15 | 5 | 3 | 35 | 11 | 7 | 75 | 23 | 13 | 70 | 21 | 27 | 150 | 45 | 214 | 700 | 210 |
| 2 | 15 | 5 | 4 | 15 | 5 | 8 | 30 | 9 | 14 | 40 | 12 | 29 | 150 | 45 | 236 | 470 | 143 |
| 2 | 15 | 5 | 4 | 15 | 5 | 8 | 40 | 12 | 15 | 60 | 18 | 31 | 100 | 30 | 337 | 470 | 143 |
| 2 | 20 | 6 | 4 | 30 | 9 | 8 | 60 | 18 | 15 | 70 | 21 | 33 | 87 | 27 | 347 | 950 | 290 |
| 2 | 20 | 6 | 4 | 30 | 9 | 8 | 60 | 18 | 15 | 100 | 30 | 35 | 80 | 24 | 948 | 550 | 168 |

*A total of 115 single tree infestations is not listed; single tree infestations averaged 3 m. (10 ft.) in diameter.

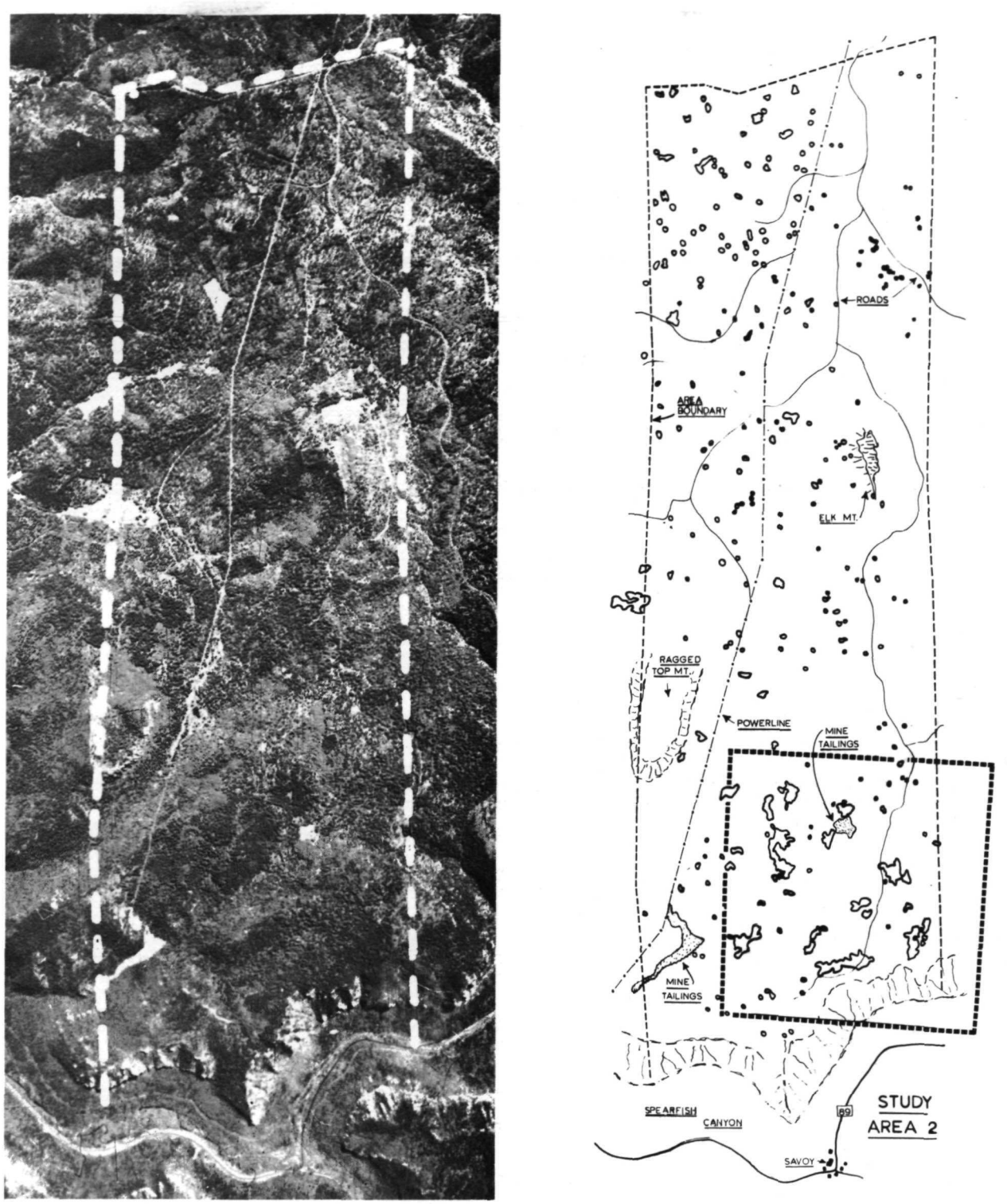


Figure 15. Aerial mosaic on left of 1.6 by 5 km. study area near Lead, S. D. On right, 253 infestations of various sizes (3 to 200 meters) are plotted at same scale. Outlined area on right refers to photo coverage shown in Figure 13 and the overlay shown in Figure 16.


Figure 16. Overlay of four years of mountain pine beetle infestations within selected portion of study area (same coverage as photo shown in Figure13). Hardwoods are shown on base map as being crossed-hatched. 1971-killed trees are shown on top overlay in red; 1970 in orange; 1969 in blue; 1968 in green. Note the grouping of the infestations. Most of the pine timber has been killed in this small area. Size and number of each infestation in 1971 are referenced in Table 24. Scale 1:8,000.

Table 24. Infestations by spot number, number of trees, and longest dimension of the infestation.

| Spot No. | No. of Trees | Length Ft. | m. | Spot No. | No. of Trees | Length Ft. | m. |
|---|---|---|---|---|---|---|---|
| 252 | 29 | 150 | 45 | 354 | 236 | 470 | 143 |
| 316 | 948 | 550 | 168 | 355 | 1 | 10 | 3 |
| 317 | 7 | 30 | 9 | 357 | 24 | 132 | 41 |
| 323 | 9 | 60 | 18 | 359 | 81 | 210 | 64 |
| 324 | 10 | 90 | 27 | 360 | 1 | 10 | 3 |
| 325 | 3 | 30 | 9 | 361 | 14 | 40 | 13 |
| 329 | 2 | 15 | 5 | 362 | 7 | 32 | 10 |
| 330 | 1 | 10 | 3 | 363 | 337 | 470 | 173 |
| 331 | 61 | 200 | 61 | 364 | 1 | 10 | 3 |
| 334 | 90 | 265 | 81 | 365 | 347 | 950 | 290 |
| 335 | 1 | 10 | 3 | 368 | 33 | 87 | 27 |
| 336 | 3 | 30 | 9 | 369 | 104 | 330 | 9 |
| 344 | 7 | 55 | 17 | 371 | 10 | 70 | 21 |
| 345 | 1 | 10 | 3 | 372 | 39 | 200 | 61 |
| 346 | 1 | 10 | 3 | 373 | 45 | 205 | 62 |
| 347 | 1 | 10 | 3 | 374 | 1 | 10 | 3 |
| 348 | 1 | 10 | 3 | 376 | 303 | 375 | 114 |
| 349 | 4 | 30 | 9 | 388 | 19 | 190 | 58 |
| 350 | 1 | 10 | 3 | 389 | 2 | 25 | 8 |
| 351 | 1 | 10 | 3 | 390 | 2 | 15 | 5 |
| 352 | 8 | 80 | 24 | | | | |

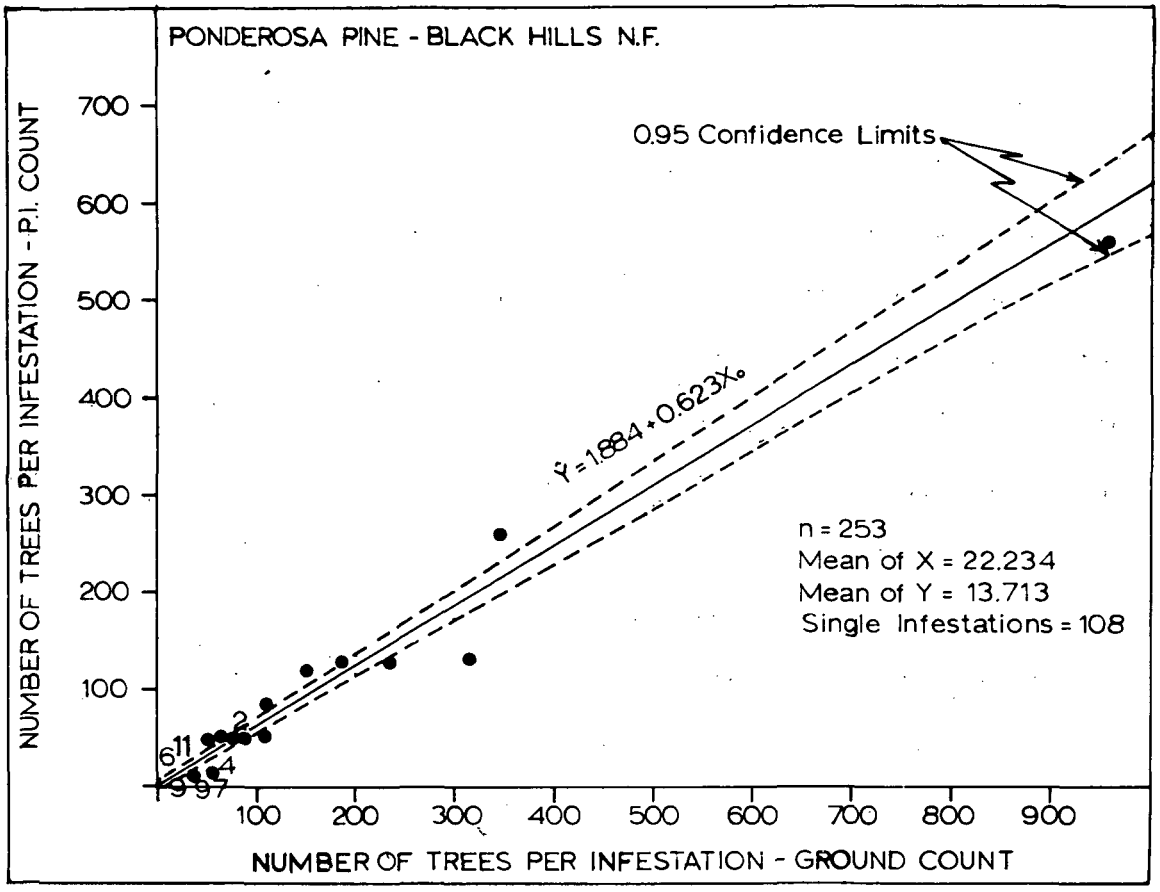


Figure 17. Regression of ground counts to photo counts. Confidence bands at the 95% level are shown on each side of regression line. For 1:8,000 scale color transparencies. Includes all crown classes.

to the circled infestations on the color print (Figure 13) refer to the listed infestation numbers in Table 24.

Photo interpreters cannot see all trees in a stand of timber. Usually fewer trees are counted on photos as scale becomes smaller. Also, small-crowned single trees are frequently missed both on the photos and on the ground. These facts have been documented in several other studies (3, 4). However, usually a relationship between ground counts and photo counts can be developed from which a ground count can be estimated and a level of confidence can be expressed for any selected photo count. A linear regression was developed for these data (Figure 17) which should be helpful in making total mortality estimates over large areas when 1:8,000 color photography is used as the sampling frame. One can use Figure 17 by entering the ordinate (or photo count) reading across to the regression line and down to the ground count. For example, a photo count of 25 trees per infestation would yield a ground count of 38 trees with an estimated possible error of $\pm$ 6 trees, 19 out of 20 times. The reason for the increase of the ground count over the photo count is that the photo interpreter cannot see all trees in the overtopped and intermediate crown classes.

Figure 18 is a plot of three regressions. The lowest curve (all crown classes) is identical to Figure 17 on which the confidence bands have been superimposed. Note that as the suppressed and intermediate tree crown classes are removed from the ground count, the regression slope approaches 1.0. Undoubtedly the confidence limits would be even closer to the plotted regression than in Figure 17.

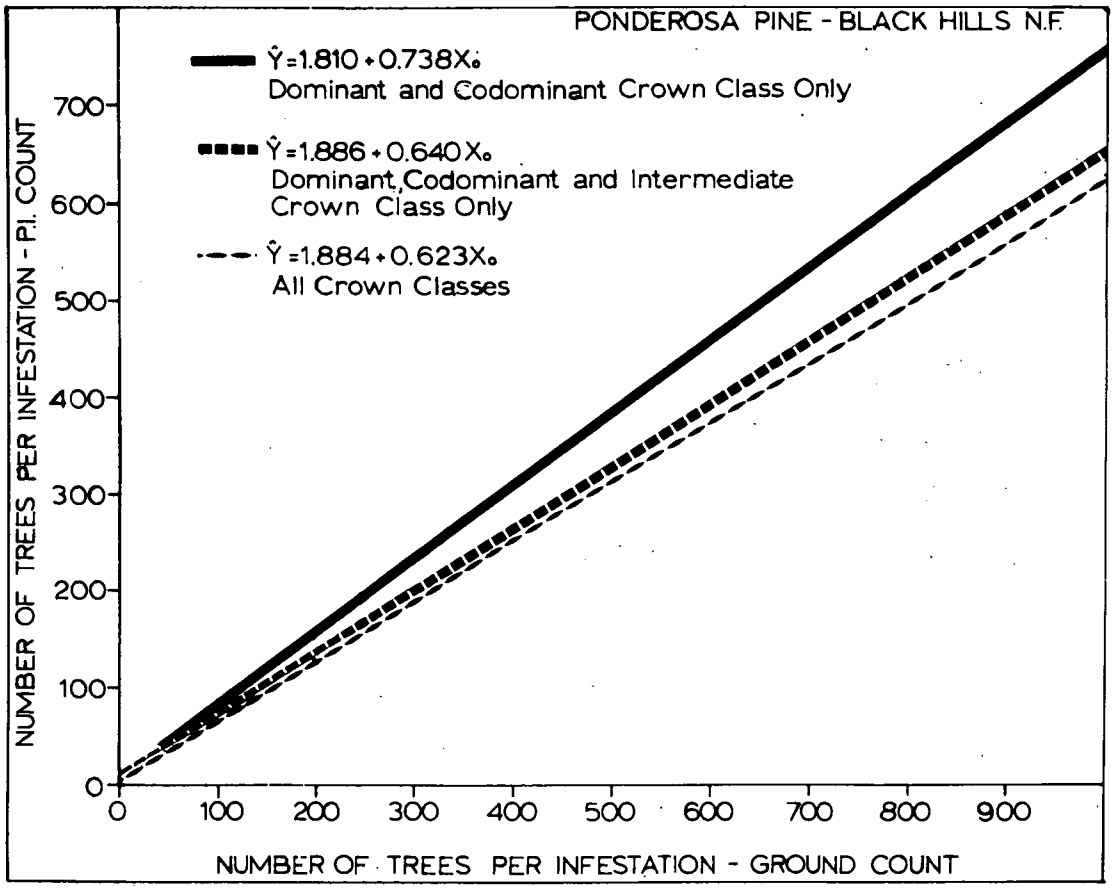


Figure 18. Comparison of ground tree counts to photo tree counts of discolored ponderosa pine infestations on 1:8,000 color transparencies. The lower line is identical with Figure 17 and includes all crown classes. The middle line -- dashed -- includes dominant, codominant, and intermediate crown classes. The upper solid line is for the largest trees in the dominant and codominant crown classes only.

When assessing the detectability of stressed trees from ERTS imagery, the map of 1971 infestations will be extremely helpful in providing natural resolution targets whose size we know quite accurately. These data will be useful until July 1972; however, by mid-August 1972, new infestations will appear and provide a different set of resolution targets. These new targets will have to be assessed on the ground at that time. Additional discussion on the probability of detection of stressed trees from ERTS imagery can be found in the report by Weber and Heller, which follows.

## LITERATURE CITED


1. Forest insect and disease conditions in the Intermountain States during 1970. 1971. Div. of Timber Management, Forest Service, U.S. Dept. of Agric., Ogden, Utah. Resource Report.
2. Heller, R. C., and J. F. Wear. 1969. Sampling forest insect epidemics with color films. Proceedings of Sixth International Symposium on Remote Sensing of Environment, University of Michigan, Ann Arbor, Mich. October 13-16, 1969.
3. Heller, R. C., R. C. Aldrich, and W. F. Bailey. 1959. An evaluation of aerial photography for detecting southern pine beetle damage. Photogrammetric Eng. 25(4): 595-606.
4. Young, H. E. 1953. Tree counts on air photos in Maine. Tech. Note No. 21, University of Maine Forestry Dept., Orono, Maine.

# AERIAL PHOTOS DETERMINE OPTIMUM LEVELS OF STAND DENSITY TO REDUCE BARK BEETLE INFESTATION

by

T. H. Waite, R. C. Heller, and R. E. Stevens

## INTRODUCTION

Large bark beetle infestations have been and will continue to be costly until adequate management practices are adopted. They are costly not only in terms of timber production but are damaging to watershed, wildlife, and recreational resources as well.

For years experienced field men have noted an apparent relationship between low stand basal area and resistance to bark beetle attack. Field observation of ponderosa pine (Pinus ponderosa Laws.) stands in the Black Hills indicates that stands which have been thinned appear resistant to beetle attack. This same relationship was evident on our aerial photographs of the area.

Because aerial photographic techniques may permit more rapid selection of stands needing thinning, this study is designed to show the relationship between beetle attack and stand basal area. It should provide evidence to determine if thinning is a viable treatment for bark beetle control.

The objectives of this study were twofold. The first was to determine whether aerial photographs can be used to identify various stand density levels. The second was to determine what density levels will reduce the likelihood of beetle attack.

## PROCEDURES

In August 1971, new photography was flown over the Black Hills study area (1:8,000 Aerocolor 2445 and MS Ektachrome 2448). Five separate areas were flown in order to insure broad coverage of infested, uninfested, and thinned areas.

To obtain a representative sample of the study areas, two photographs were selected at random from each of the five areas photographed. In study area II an exception was made. The photos were selected purposely to include areas of heavy infestation. A grid having 63 one-inch squares was placed over the selected photos. The outside 1- x 9-inch strip on each side of the photograph, and parallel to the flight line, was eliminated in order to reduce distortion in the x direction. Each square inch (approximately 10 acres) of the sample was stratified into one of two categories: (1) pine type with no infestations and (2) pine type with infestations; nonpine type was not sampled. Each stratum was listed by the photo of origin and the identifying square inch. From this list, 40 sample one-inch squares were chosen at random from each stratum. These one-inch squares were further divided into four 1/4-inch (2 1/2-acre) squares; one was selected at random and listed by corner (NE, SE, SW, NW), square, and photo number. The final random sample of twenty 1/4-inch squares was drawn from each stratum, giving a total field sample of 40 (two were rejected in the field as being out of type, giving a field sample of 38; 22 were infested, and 16 were uninfested).

The sample of the thinned stands was obtained in a different manner. Again, all 1971 photography taken of each of the five areas was considered. The thinned areas on the photos were delineated. Recently thinned areas

(defined by the presence of fresh haul roads, equipment or active landings) were not considered. On each of the thinned areas two 1-acre plots were selected at random (avoiding road edges and openings). A pinprick was placed on the photo in the center of the plot, and estimates of crown closure (density) and average crown diameter were made using a crown closure comparator (1). In all, sixteen plots were located on thinned areas.

All 54 plots (38 nonthinned and 16 thinned stands) were visited on the ground. The stereo color prints used in the field were of incalculable value in locating the points. Each of the 54 plots was recorded in the same manner. The center point pricked on the photo was visited, and the photo and point numbers were recorded on the field form. A ten-point plot cruise using a 40 B.A. prism was done at each sample point. In addition, at each point the D.B.H., the crown diameter, crown class, and species were recorded; species other than pine were included in the tree count only, as it was felt that these factors contributed to basal area and thus to stress. At 5 of the 10 points, dominant tree height was recorded.

## RESULTS

Three separate analyses were made of the data.

1. To determine the relationship of crown comparator measurements (crown closure and crown diameter) to basal area. Are they highly correlated? To what accuracy?

2. To test the null hypothesis that thinned stands are from the same population as natural stands.

3. To test the null hypothesis that the basal area of non-infested stands is from the same population as the basal area of infested stands.

In order to determine the relationship between crown closure and crown diameter measurements on the photographs and stand basal area measurements on the ground, two simple linear regressions were made (Figures 19 and 20). Figure 19 shows the linear relationship between basal area and crown closure. The regression coefficients were tested using Student's "t" test and were found to be significant at the 95% confidence level. This means that if there is in fact no relationship between the two variables, given this many observations, the chance of getting coefficients this different from zero is 5%. A more intuitive explanation would be: This result indicates that a significant amount of the variation in the basal area values is explained by the fitted linear regression. However, its value as a predictive tool at this point is questionable. For instance, the coefficient of determination $r^2$ was only 0.47. Although this value is significant at the 95% confidence level, it implies that only 47% of the variation in the basal area values is associated with the crown comparator measurements. Furthermore, the standard error of the basal area estimate is $\pm$40.72 square feet. This value is quite high and is an indication of the rather large variation of the basal area values about the mean.

Figure 20 shows the linear relationship between basal area and crown diameter. As we expected, the regression slope coefficient is negative, indicating that as stand basal area decreases crown diameters increase. Both regression coefficients were significant at the 95% confidence level.

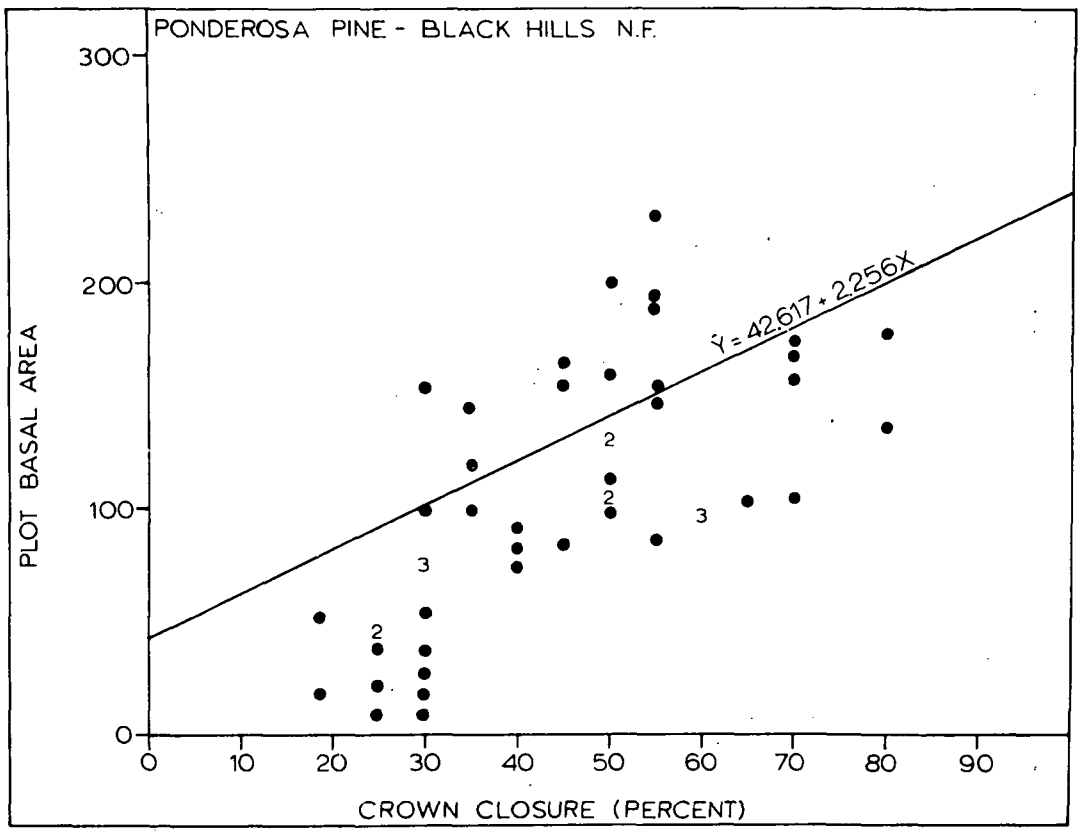


Figure 19. A simple linear regression showing the relationships of stand basal area as measured on the ground to average crown cover as measured by the crown comparator.

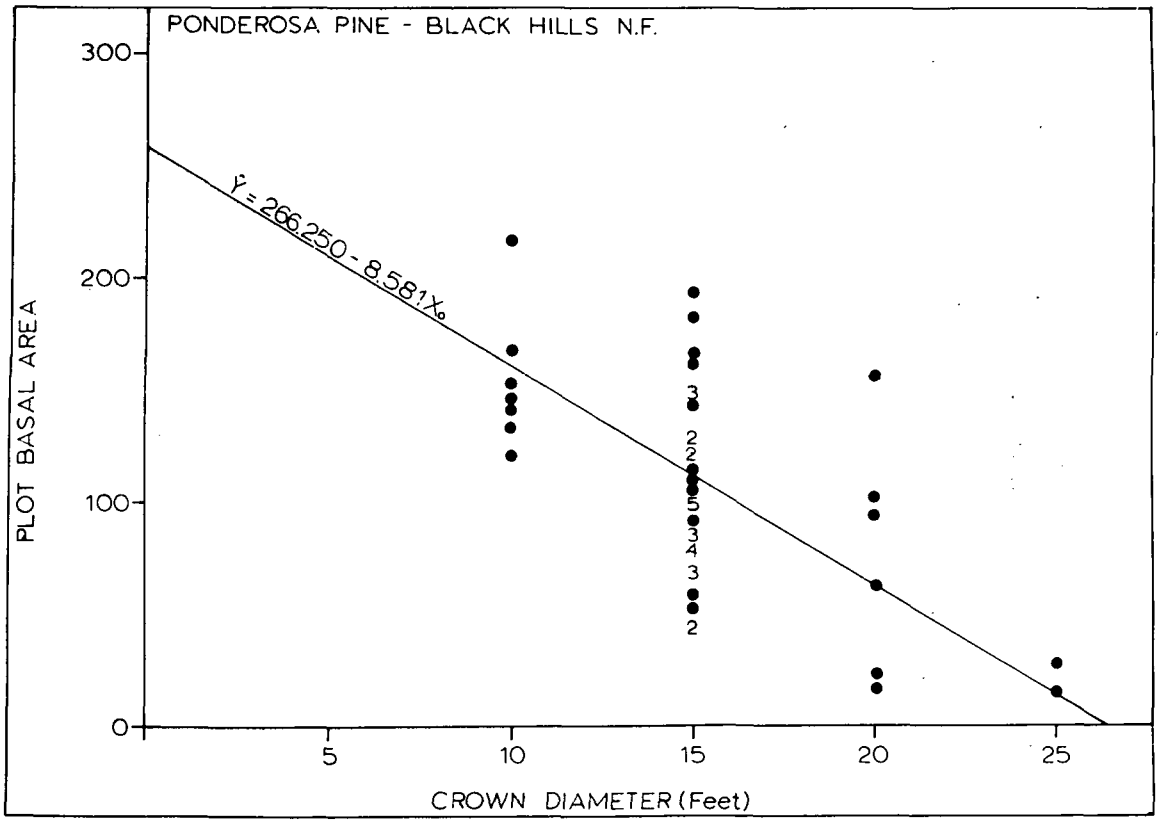


Figure 20. A simple linear regression showing relationship of stand basal area as measured on the ground to average crown diameter as measured by the crown comparator.

The implications in terms of the model are the same as that for Figure 19, i.e., a significant amount of variation in basal area can be explained by the fitted linear regression. The coefficient of determination, $r^2$, for these data is only 0.29 -- indicating that only 29% of the variation in the basal area values is associated with the crown diameter measurements. However, this value is significant at the 95% confidence level. On this basis we reject the null hypothesis that there is no relationship between the variables. In addition to the low $r^2$ value, the large variation about the fitted line is further substantiated by the high standard error of the basal area estimate which is $\pm$49.27 square feet.

Figure 21 is a plot showing the relationship between basal area and d.b.h. for both infested and uninfested plots. All thinned plots were uninfested and as such were included in the uninfested group. In view of the distribution of the plotted data, it was decided that a simple linear regression analysis was inappropriate. A Student's "t" test was done on the differences between mean d.b.h.'s and mean basal areas of the infested and uninfested plots. The mean d.b.h. for the infested plots is 12.64 inches and for the uninfested plots is 9.63 inches. Student's "t" test indicates that this difference is significant at the 95% level. This means that if there is no difference between these groups, given this number of observations, a difference this large would arise 5% of the time. In other words, the probability is very high that these groups are from different populations. The mean basal area for the infested plots is 149.33 square feet and for the uninfested plots is 113.64 square feet. Again, Student's "t" test indicates that the difference is significant at the 95% confidence level. The implication is the same as that for the mean d.b.h.'s, i.e., the probability is very high that these two

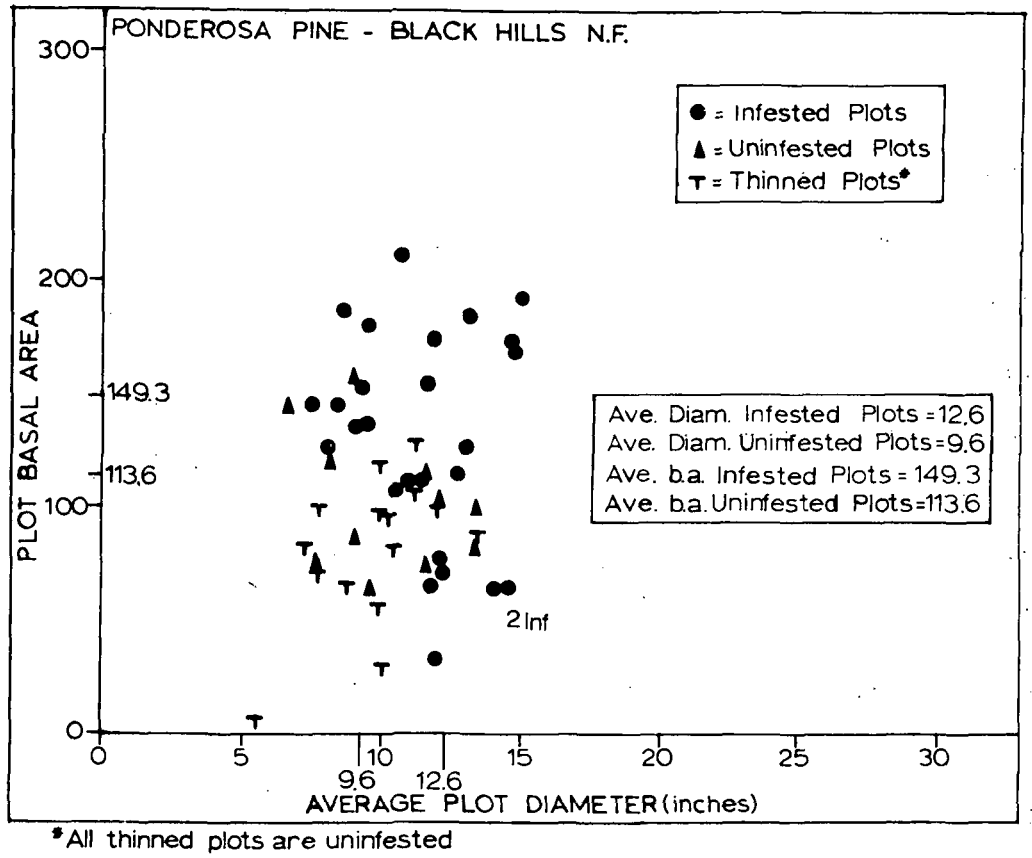


Figure 21. A plot showing the distribution of infested, uninfested and thinned stands by average basal area and average stand diameter.

groups are from different populations.

## CONCLUSIONS AND DISCUSSION

The crown comparator has shown itself to be a photo interpretation tool with substantial development potential. Further experience in its use should reduce the variability found in this study. The elementary analysis conducted on the thinning data indicates that reducing stand basal area will increase resistance to beetle attack. However, this phenomenon is probably more complex than our elementary analysis indicates. Our studies in the future will look toward a more complex analysis of the effects of basal area on insect attack. For instance, a multivariate approach would be suitable for this purpose. It would allow us to determine the contributions made by other variables such as slope, aspect, soil, and microsite to the susceptibility of stands of beetle attack. Some of these data are available to us, and we expect to continue the analysis.

## LITERATURE CITED

1. Aldrich, R. C. Stratifying photo plots into volume classes ... by crown closure comparator. U.S.D.A. Forest Service. Pacific Southwest Forest and Range Experiment Station. Research Note PSW-151.

# THE USE OF AIRBORNE SPECTROMETERS AND MULTISPECTRAL SCANNERS FOR PREVISUAL DETECTION OF PONDEROSA PINE TREES UNDER STRESS FROM INSECTS AND DISEASES

F. P. Weber

Several times during the last seven years we have looked at the application of optical-mechanical infrared line scanners for previsual detection of stress and loss of vigor in pine trees. In the original feasibility study undertaken by the Forest Service (4), we tried fifteen individual spectral channels of data from the University of Michigan's original AAS-5 scanners. Because the focus of the supporting field study was to detect temperature differences between healthy and low-vigor trees, a group of forty-year-old red pine trees (Pinus resinosa Ait.) were artificially stressed with injections of an herbicide. A temperature rise in the affected trees was measured in the field and was related to the decline in tree vigor. The same temperature difference was recorded by the Michigan thermal scanner, prior to the time the stressed trees were detected by a change in color on large-scale color and color infrared photography.

Because of the success with the feasibility study in Michigan, we established a cooperative pilot study with NASA in the Black Hills in 1966 to determine if trees attacked by the mountain pine beetle (Dendroctonus ponderosae Hopk.) and an associated blue stain fungus could be detected on thermal infrared imagery prior to identification on large-scale color photography. Test sites were established and trees were instrumented to measure data on the biophysical responses and physiological differences of healthy and beetle-attacked ponderosa pine (5).

The airborne fire detection and mapping group from the Northern Forest Fire Laboratory in Missoula, Montana, flew our Black Hills test sites in 1966 and 1967 with their bispectral thermal infrared scanner. Missions were flown both in daytime and at night and with various meteorological conditions. In spite of the concerted effort by our joint research groups, we were not able to identify the beetle-attacked trees on thermal infrared imagery (1, 2).

In 1968 and 1969, we again worked closely with the Infrared and Optics Laboratory (IROL) of the University of Michigan. They had developed an improved scanner capability with the addition of a 12-channel spectrometer. This development opened the door to sophisticated multispectral processing, at least for data in the visible and near infrared portions of the spectrum. New test sites were established in the Black Hills to provide base-line biophysical data and calibration to support the Michigan multispectral scanner data.

Although our results with Michigan demonstrated the capability to identify bark beetle infestations, two findings were most noteworthy. First, although thermal infrared (8 to 14 μm) data contributes to the detection of beetle-attacked pine, reliable detection requires the use of simulataneous visible, reflective infrared, and thermal infrared data collected in narrow-band channels selected from a broad-band multispectral system (0.4 to 14.0 μm). Secondly, hybrid multispectral processing is required which utilizes the best features of a digital computer for optimum channel selection in concert with a specialized analog computer which actually does the recognition process (7).

Two recent instrument developments improve the potential for furthering our stress detection capabilities in 1972. Both the Bendix 24-channel multispectral scanner and the Michigan (M-7) 12-channel multispectral scanner incorporate design features which we have determined are necessary to improve our present level of success in previsual stress detection. The principal improvement in both systems is the integrated design which permits simultaneous registration of all spectral channels of data. This we know is the single most important requirement of our work.

Until now our position has been that for optimum detection of forest stress conditions where automated feature recognition is desired, it may be necessary to design and construct special systems. There have been few alternatives to this belief until now. The requirement of high spatial resolution for coniferous trees with small crown diameters as well as for deciduous trees with large crown diameters has been achieved with high sampling rates. Moreover, this work would have to be done without sacrificing signal-to-noise ratio (S/N) capability which relates to the minimum detectable differences in temperature. In general, improving the spatial resolution for a scanner by a factor of 2 reduces the detector sensitivity by a factor of 4. This reduction means that a 3 milliradian (mr) resolution system (with, for example, a $0.5^{\circ}F$ Noise Equivalent Temperature sensitivity (NET), when converted to 1.5 mr systems by changing detectors may have only a $2^{\circ}F$ NET. As has been shown by extensive ground measurements, this temperature is within the normal range of differences between stressed and unstressed trees. Therefore, such a conversion would not provide sufficient S/N capability for reliable identification of tree conditions.

This resolution dilemma can be alleviated now in two ways. First,

we can use one or more of the new systems which provide truly registered multispectral data in narrow spectral bands over a broad portion of the spectrum. Secondly, we can specify flights at low altitudes to achieve better ground resolution.

As part of our continued participation in the Earth Resources Program during 1972-73, we anticipate getting several supporting flights by the NASA C-130 aircraft with the Bendix 24-channel Multispectral Scanner Data System (MSDS). Our program is in part designed to test the capability of the MSDS for detecting green beetle-infested trees in the Black Hills. As a minimum, we expect to demonstrate large gains in the area of automatic thematic mapping and landscape feature recognition. Additionally, the MSDS flights will be a coordinated part of the ERTS experiment for the Black Hills test site (226A). Baseline biophysical and calibration data needed for processing the MSDS imagery will be collected at the test site and transmitted to ERTS for correlation with satellite-collected imagery.

The focal point of the MSDS missions in early 1972 (within the 3,000-square-mile ERTS test site) is the site selected for establishment of the Data Collection Platforms (DCP). This location (N44° 16', 103° 47'W) was selected primarily because it includes new bark beetle activity of the type required for a good test of the 24-channel scanner. The general location of the new study area is shown in Figure 22. By cross checking with Figure 26 (page 111) of the section of this report by Weber and Heller, the reader can see how the MSDS study site and DCP location tie in with a larger portion of the ERTS experiment test site.

Within the MSDS study site, we have located one group of 54 large ponderosa pine trees which were attacked by the mountain pine beetle in

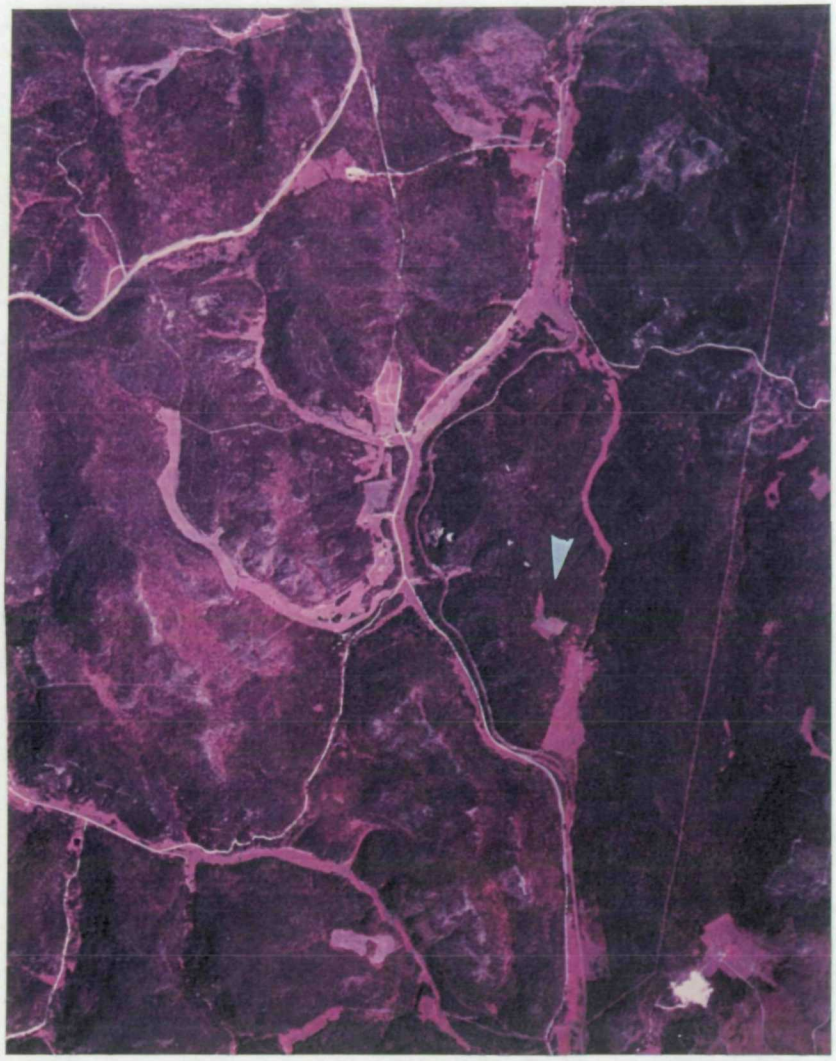

Figure 22. The location of the MSDS study site and the data collection platforms (within the larger ERTS test site) are shown on this 1:55,000 scale photography.

late August 1971. This is in an area where there have been few beetle infestations for several years; this makes it ideal for the test. The newly attacked trees were green when the site was selected in September 1971 and will remain that way until after the first requested flight support (April 1972) by the NASA C-130 aircraft. Subsequent support flights throughout early spring and summer should provide a good test of the capability of the MSDS for previsual detection of stress in conifers.

An important part of the pre-experiment study site establishment was the construction of a three-tower tramway system in September 1971 (Figure 23). The tramway was established so that the south half of the north-south sample line runs above healthy pine and the north half above the newly attacked pine. The purpose of the tramway system is to provide a means of transporting sensors for measuring spectral radiance and other important biophysical data. Sensor data will be recorded much the same as that reported by Weber and Wear (6). In addition, some data that are recorded by our digital data logger will be multiplexed and transmitted via two DCP's to ERTS.

In past studies we have measured many radiation parameters to discover the implications to remote sensing of reflected and emitted energy differences between healthy and stressed trees. Always, a missing link has been the lack of spectral energy differences measured at the target. This past season we have built and calibrated a small portable field spectrometer which currently operates with four ERTS-matched channels. The first prototype model was constructed with the intent that it be suspended from the tramway system to provide baseline spectral information both for ERTS and for the MSDS flights. The operating prototype of the


Figure 23. The alignment of the three-tower tramway system (A) and the DCP location (B) are shown in this September 1971 aerial photo. The group of 54 new beetle-attacked trees is also shown (C).

field spectrometer was checked out in the laboratory and the results were better than expected. It will be field tested the first week in November as a coordinated effort with the flight of the Michigan M-7 scanner system over our Atlanta test site (NASA Site 217).

The 1:8,000 scale aerial color photograph (Figure 24), taken of the Black Hills MSDS study site in August 1971, shows several of the landscape features which will be instrumented for the coordinated ERTS-MSDS experiment. Spectral data, in addition to other critical biophysical and physiological information, will be gathered at a range site and a soil outcrop site in addition to the forest site. The range site was selected by R. S. Driscoll, Principal Range Ecologist from the Rocky Mountain Forest and Range Experimental Station, who will assist in collection and analysis of range data.

We look forward to the opportunity in 1972 for a field trial of the Multispectral Scanner Data System for previsual detection of green bark beetle-attacked trees in the Black Hills. We have spent much of the last seven years defining our multispectral scanner requirements and are eager to try the Bendix 24-channel system and the Michigan 12-channel M-7 system. During the same period we have developed a good scheme for evaluating bark beetle impact on forests, using a combination of high-resolution aerial color photography and probability statistics (3). However, current photographic analysis techniques do not lend themselves readily to automatic data processing. Although some automatic photo analysis can be done with film, it can be done more easily if the data are stored initially on magnetic tape. Moreover, multispectral scanner techniques seem to provide the best means for previsual detection of stress in forests. The efficiency

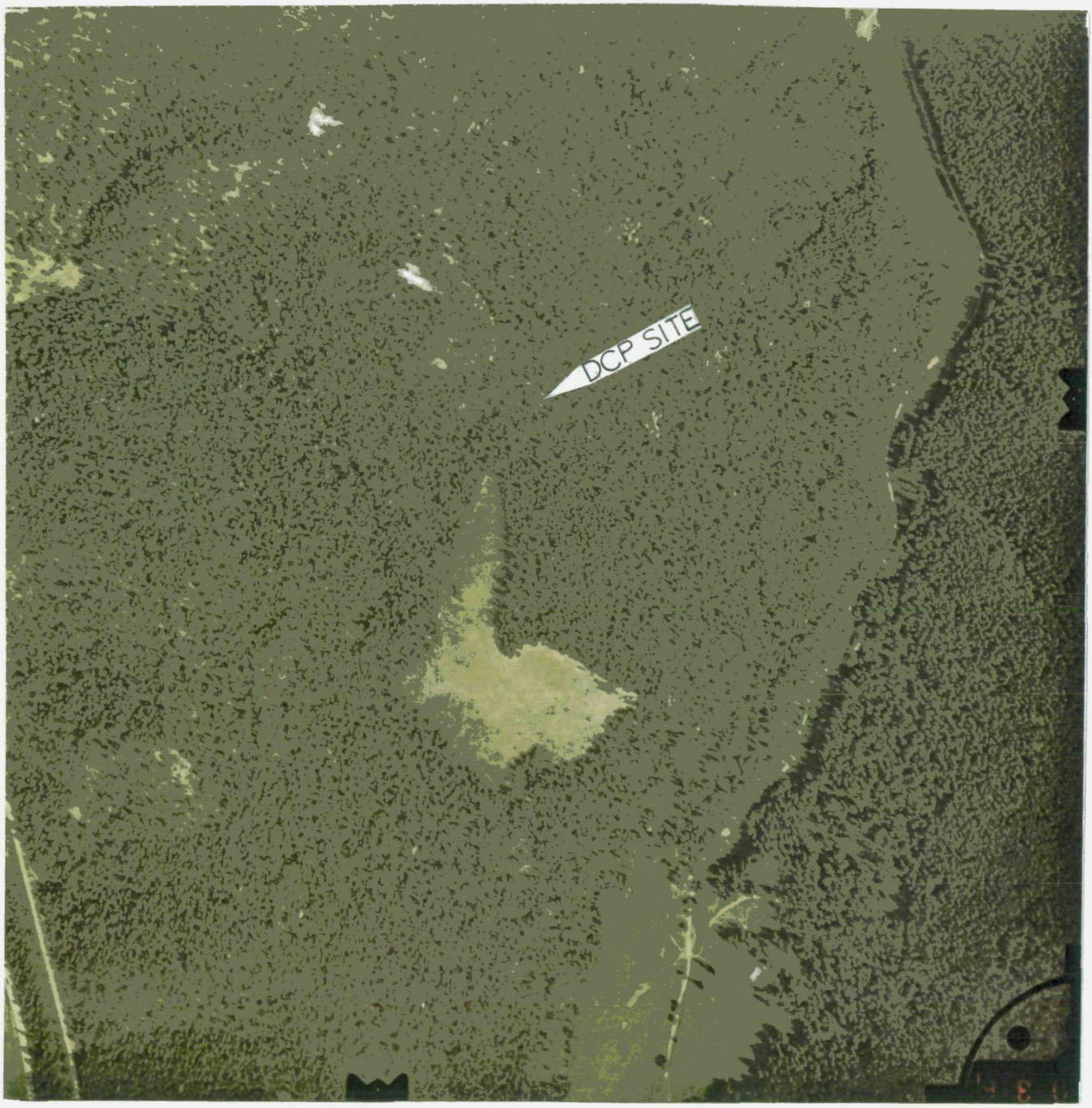


Figure 24. The focal point of the Black Hills MSDS study site is shown on a 1:8,000 scale aerial color photograph taken in August 1971. The pasture in the center of the photo and the light, soil-rock outcrop just above the field will be instrumented in addition to the forest site just to the right of the upper end of the pasture.

and reliability of scanner techniques in comparison to photography remains to be demonstrated.

## LITERATURE CITED


1. Heller, R. C., W. F. McCambridge, R. C. Aldrich, and F. P. Weber. 1966. The use of multispectral sensing techniques to detect ponderosa pine trees under stress from insect or pathogenic organisms. Annual Progress Report for Earth Resources Survey Program, OSSA/NASA, by the Pacific Southwest Forest and Range Experiment Station.
2. Heller, R. C., R. C. Aldrich, W. F. McCambridge, and F. P. Weber. 1967. The use of multispectral sensing techniques to detect ponderosa pine trees under stress from insect or pathogenic organisms. Annual Progress Report for Earth Resources Survey Program, OSSA/NASA, by the Pacific Southwest Forest and Range Experiment Station.
3. Heller, R. C., and J. F. Wear. 1969. Sampling forest insect epidemics with color films. Proceedings of the Sixth International Symposium, Remote Sensing of Environment, Univ. of Mich., Ann Arbor, Mich., Oct. 13-16, 1969. pp. 1157-1167.
4. Weber, F. P. 1965. Exploration of changes in reflected and emitted radiation properties for early remote detection of tree vigor decline. Master's Thesis, Univ. of Mich., Ann Arbor, Mich. 101 pp. Available on microfilm from University Microfilms, Inc., Ann Arbor, Mich.
5. Weber, F. P. 1969. Remote sensing implications of water deficit and energy relationships for ponderosa pine attacked by bark beetles and associated disease organisms. Doctoral Dissertation, Univ. of Mich., Ann Arbor, Mich. 143 pp. Available on microfilm from University Microfilms, Inc., Ann Arbor, Mich.

6. Weber, F. P., and J. F. Wear. 1970. The development of spectro-signature indicators of root disease impacts on forest stands. Annual Progress Report for Earth Resources Survey Program, OSSA/NASA, by the Pacific Southwest Forest and Range Experiment Station.

7. Weber, F. P., and F. C. Polcyn. 1971. Remote sensing with optical-mechanical line scanners to detect stress in forests. Proceedings of the 37th Annual Meeting, American Society of Photogrammetry, Washington, D. C. pp. 123-152.

# ESTABLISHMENT OF EARTH RESOURCES TECHNOLOGY SATELLITE TEST SITE IN THE BLACK HILLS AND IDENTIFICATION OF NATURAL RESOLUTION TARGETS

F. P. Weber and R. C. Heller

The Black Hills National Forest test site (NASA site 149) encompasses a 3,000-square-mile forest and rangeland area in western South Dakota and eastern Wyoming (Figure 25). For the past seven years we have maintained an intensive aerial and ground study in the Black Hills for learning how to use multispectral sensing techniques to detect trees under stress from insect or disease attack. During that period of time we have observed several phenomena of change, such as the manifestation of dead trees from insect attack, that have occurred over a large enough area or resulted in sufficient spectral change to suggest the feasibility of change detection from space.

In mid-September 1971, after an extensive survey of the northern Black Hills, we selected a location for the ERTS data collection platforms (DCP). The site -- N44° 16', 103° 47'W -- is a central location which embraces all of the physical characteristics of the landscape we hope to study with ERTS imagery. Features such as range grass, soil-rock outcroppings, and beetle-attacked and health pines are close enough to the DCP site so that biophysical data from each target, e.g., spectral radiance, can be measured and recorded via land lines to the central data collection site.

An important consideration in the site selection was the location of a new mountain pine beetle infestation in the area to be used as an indicator of tree stress. The new infestation includes 54 large trees grouped in roughly a circular pattern with an area of approximately 1,260 square

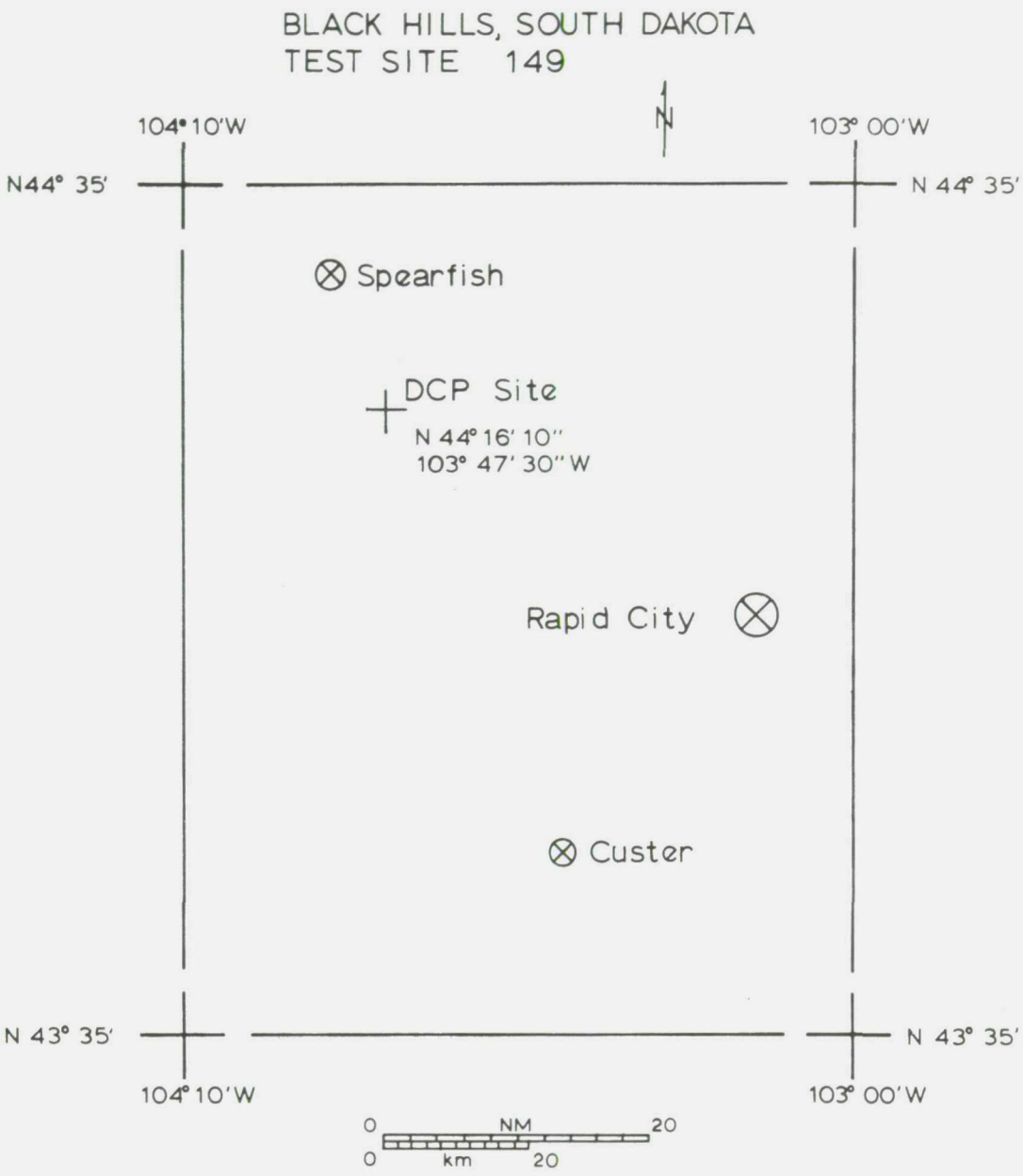


Figure 25. The Black Hills National Forest test site in western South Dakota and eastern Wyoming. Notice the location of the ERTS data collection platform (DCP).

camera lens (1). Each distribution was integrated by the trapezoidal rule from 400 to 700 nm and normalized to the same bandpass value. The definition is

$$(1) \qquad \frac{1}{2}\left[D_{400} + D_{700}\right] + \sum_{\lambda=420}^{680} D_{\lambda} \equiv 25.00$$

where $D_{\lambda} = \log_{10}$ relative daylight irradiance,

$\lambda$ = wavelength in nanometers.

Another way of expressing the meaning of these data is that they represent the relative daylight distribution passing through a lens onto film, normalized to the average value in the 400-700 nm range.

For infrared-sensitive film which is almost always used with a minus-blue filter, we attenuated the curves by the density of the Eastman Wratten 12 filter and chose 500-920 nm as the representative bandwidth. The normalization equation is

$$(2) \qquad \frac{1}{2}\left[D_{500} + D_{920}\right] + \sum_{\lambda=520}^{900} D_{\lambda} \equiv 50.00.$$

The data of reference 5 extend only to 830 nm so that distribution was extrapolated to 920 nm using the sunlight data of reference 2. Skylight does not appreciably alter the shape of the daylight curve between 830 and 920 nm.

Each daylight distribution D is denoted by the reference number from which the data were drawn. D1A is a composite sun + sky distribution as

meters. The beetle attacks occurred in late August 1971, so that at the time of the expected launch and first data collection by ERTS, the attacked trees will still be green. However, during the first five months of the ERTS experiment, the study trees should discolor from green to yellow-green and finally to yellow-red by August 1972.

During our September visit to the Black Hills, 10 large groups of beetle-killed trees were selected within our existing study area II for observation and study during the ERTS experiment (Table 25). See Figure 13in the paper by Heller, Zealear, and Waite of this report showing these infestations (page 74). After we had carefully examined the infestation spots on aerial color photography, each spot was assigned a relative probability of detection on ERTS imagery. The assignment of a relative value -- low, moderate, or high -- is based on three characteristics: (1) spot size, (2) spot geometry, and (3) spectral contrast of the spot in relation to the surrounding landscape features.

The assignment of detection probabilities based on appearance on the August 1971 photography is a relative entity attached to a dynamic process. That is, the trees continue to change in color and texture between August 1971 and launch time, March 1972. The prediction considers that beetle-killed trees that were yellow-red this past summer may be indistinguishable from other old-killed trees by the spring and early summer of 1972. Spots in this situation would have a low detection probability in contrast to spots which were completely surrounded by healthy trees. Our main purpose here is to determine various beetle spot sizes that can be recognized on space imagery relative to spectral contrast with the surrounding landscape features. This objective implies that one moderate-size spot in

Table 25. Numbers of trees and size of mountain pine beetle infestation spots identified for the ERTS experiment.

| Spot Number[1/] | Number of Attacked Trees | Longest Dimension (meters) | Area (meters$^2$) | Probability of Detection[2/] |
|---|---|---|---|---|
| 176 | 108 | 38 | 1,090 | low |
| 229 | 214 | 214 | 9,750 | moderate |
| 309 | 173 | 124 | 4,840 | low |
| 311 | 143 | 76 | 2,240 | low |
| 316 | 948 | 225 | 10,125 | moderate |
| 354 | 236 | 147 | 11,700 | high |
| 363 | 337 | 147 | 5,900 | moderate |
| 365 | 347 | 290 | 17,700 | high |
| 369 | 104 | 110 | 3,380 | low |
| 376 | 303 | 155 | 6,975 | moderate |

1/ These infestations ("group kills") are circled and numbered on the color print (Figure 13).

2/ Probability of detection is based on total size and shape of beetle spot in addition to spectral contrast with healthy pine, old-killed pine, and other landscape features.

a green forest of healthy pines may be more readily identifiable than, say, a group of large spots in an area of intense insect activity where spot aggregation is prevalent.

Initially, there are three additional physical features which we would like to be able to identify and evaluate on ERTS imagery in addition to bark beetle-killed trees. They are: (1) range grass and pasture land (both natural and planted), (2) soil and rock outcroppings, and (3) water storage areas and water courses (Figure 26). Within our ERTS study site we have identified three natural targets within each of the three categories (Table 26). Once again, each target was assigned a detection probability based on size, shape, and spectral contrast with surrounding features. The evaluation for deriving the detection probabilities was done on 1:220,000 scale color photography obtained from the August 1969 RB-57 flight over the Black Hills.

Scientists worldwide look forward to the availability of the first satellite-collected space imagery next year. We have tried to establish a forest test site, based on our experience in the Earth Resources Program in the Black Hills, which will reveal any possible utility to resource managers from current space imagery. We feel competent to make the evaluation of applicability; however, it remains to be seen just how good and useful the ERTS imagery will be.

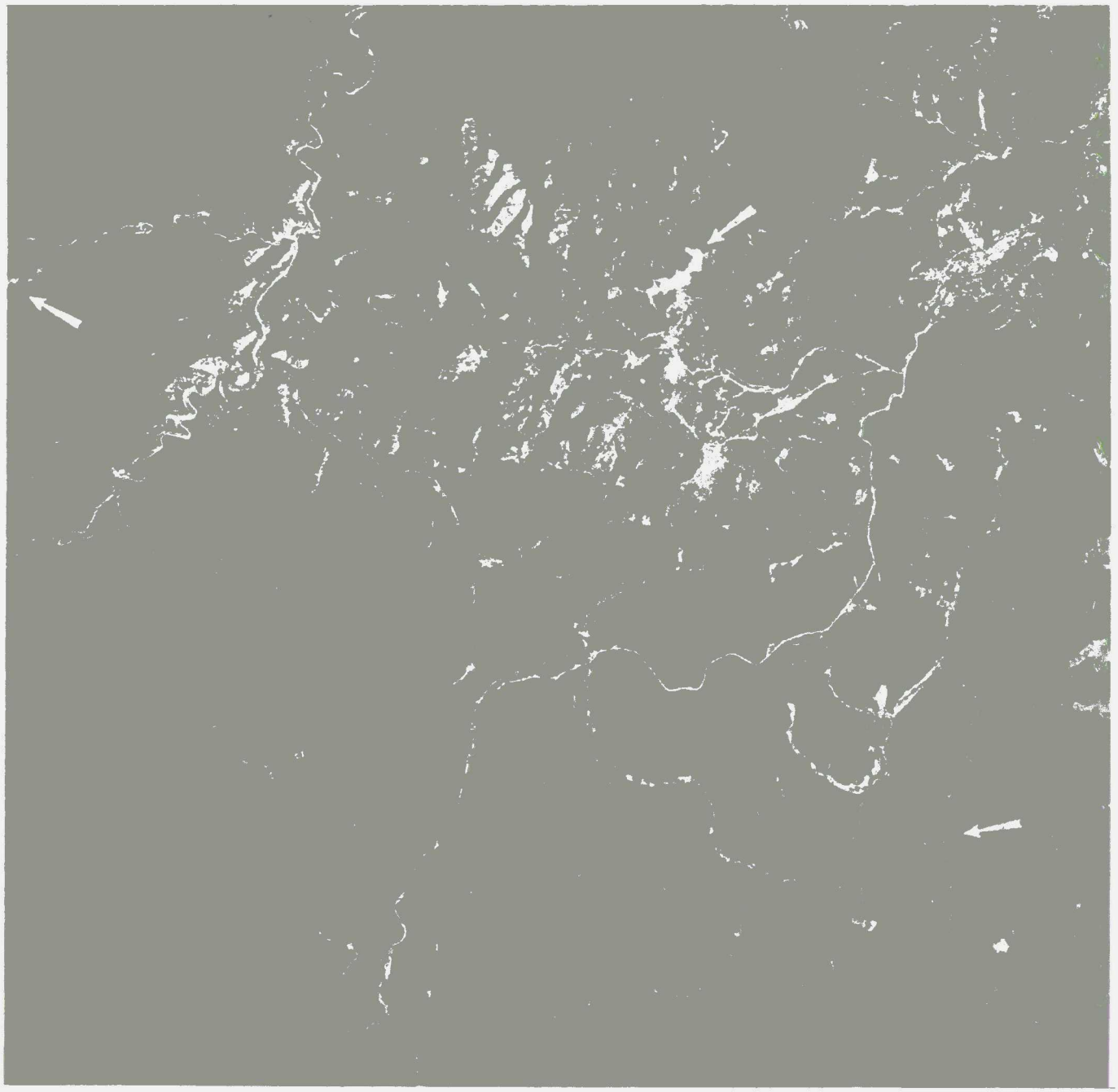

Figure 26. A portion of the Black Hills test site for the ERTS experiment is shown on 1:110,000 RB-57 photography. Image annotations show several of the targets which are listed in Table 26. These targets represent the three major landscape features of interest, other than bark beetle-killed trees, which will be our focus for ERTS image analysis.

Table 26. Black Hills landscape features selected as natural resolution targets for the ERTS experiment.

| Natural Target | Longest Dimension (meters) | Area (meters$^2$) | Probability[1/] of Detection |
|---|---|---|---|
| Range grass | | | |
| Pasture A (planted) | 403 | 64,722 | moderate |
| Pasture B (planted) | 905 | 200,093 | high |
| Pasture C (natural) | 2,262 | 135,720 | low |
| Soil-rock Outcrop | | | |
| Gravel pit | 295 | 68,349 | moderate |
| Mine tailings | 940 | 197,400 | high |
| Rock outcrop | 195 | 11,700 | low |
| Water | | | |
| Reservoir | 8,850 | 1,371,600 | high |
| Lake | 440 | 152,053 | moderate |
| River | 7,280 | - - - - | low |

1/ Probability of detection is based on total size and shape of target in addition to spectral contrast with surrounding features.

# DETECTION OF ROOT DISEASE IMPACTS ON FOREST STANDS BY SEQUENTIAL ORBITAL AND SUBORBITAL MULTISPECTRAL PHOTOGRAPHY

John F. Wear

## INTRODUCTION

The feasibility of detecting and measuring the impact of root-rot diseases on our forest resources by applying remote sensing techniques from aircraft and earth satellites is an important study of the Remote Sensing Work Unit in the U. S. Forest Service. Earth resources managers are greatly concerned about the continuing timber losses over extensive forest areas caused by forest diseases. Satisfactory aerial surveying techniques are needed to acquire data on the distribution of disease centers in order to salvage distressed timber and alter management plans to minimize the impact of tree mortality on our valuable forest resources.

Remote sensing research conducted over the past six years has attempted to previsually discriminate root-rot (Poria weirii) infected Douglas-fir trees from healthy trees in the Pacific Northwest. Unfortunately, the foliar color characteristics of healthy and diseased trees are so similar that aerial photographic techniques in the visible and near infrared portions of the spectrum (.34 micrometer to .90 micrometer) are unable to differentiate affected trees. Thermal infrared detection of incipient root-rot infection centers was not successful with the University of Michigan's multispectral scanner (3), although some earlier success was reported with a nonimaging radiometer from a low-flying helicopter (1 and 2).

Results of two years of biophysical studies at the Wind River test site revealed that when infrequent tree crown temperature differences occur

in Douglas-fir they are not necessarily due to differences in tree vigor. Consequently, it was not possible to separate the diseased from healthy trees on the basis of infrared temperature.

To better relate ground data to airborne remote sensing, we installed a comprehensive network of biophysical and tree physiological instruments. Sensors were placed in the trees as well as over the trees (on a double aerial tramway system) to record data on all parameters of stress in healthy and diseased trees. Details of the construction and operation of the aerial tramway system, the collection of data through the Vidar 5403 digital data logger at the test site, and the analysis of the ground data collated with the multispectral data collected by the University of Michigan airborne optical-mechanical line scanner system are discussed in our 1969 and 1970 Annual Reports. More sensitive multispectral data collecting, processing, and analyzing systems with higher resolution capabilities are needed to discriminate small biophysical differences between individual trees.

A promising aerial survey technique has been discovered that may detect well-established root-rot disease centers in certain areas from orbital as well as suborbital altitudes. Openings in the forest canopy (not the trees per se) caused by root-rot diseased and fallen timber are proving to be positive signatures for surveying large forested areas to detect disease infection centers. This report discusses a new approach which is being developed and tested in the Douglas-fir-hemlock types of of Oregon and Washington.

## CURRENT RESEARCH ACTIVITIES

Openings in forest stands have distinctive characteristics that can

be frequently identified on aerial photographs and may be exploited as a new type of information by resource managers. Recent photo interpretation and ground examination of 1:15,840 scale photos prove conclusively that Poria weirii root-rot disease has a distinctive signature which has been found in many forested areas of the Northwest. This signature appears as variable-sized circular openings (ranging from 50 to 700 feet in diameter) in the form of infection centers which may be observed on small photo scales and possibly on orbital imagery.

The major objectives of the Poria weirii remote sensing study during the past year were (1) to determine the criteria for detecting root-rot centers or openings, (2) to investigate the distribution of signature indicators on existing photographs covering the Douglas-fir types in Oregon and Washington, (3) to cooperate with various forestry agencies in developing an intensive survey program on selected test sites in Oregon, (4) to determine the optimum photographic scale for detecting infection centers, and (5) to compare various types of multispectral imagery, i.e., color, color infrared, and panchromatic photography, for discriminating disease infection centers or openings from healthy trees.

## DETECTING ROOT-ROT CENTERS

The criteria for identifying openings in the forest canopy that can be attributable to the root-rot disease, Poria weirii, vary with topography, vegetative types, elevational range, soil and site characteristics, and environmental factors. The interrelationships of these different characteristics to identify broad differences between openings occuring in various parts of the Douglas-fir subregion can only be inferred at this time. Further remote sensing research is contemplated to determine meaningful

characteristics of root-rot centers or openings in localized areas.

The primary signature indicator of Poria weirri root-rot was discovered in the high Cascade Mountains of Oregon on 1:15,840 scale photographs. The signature consists of an unusual phenomenon of bare ground in a half-round circular shape surrounded by trees. A conglomerate of openings gives the appearance of a ringworm pattern (Figure 27). Determining the cause of the openings in the forest canopy involved a multidisciplinary group of scientists and foresters. Openings could be the result of insect or disease activity, unusual geomorphological features such as rock outcrops or soil and water deficient strips. The team ground-checked several openings in different age classes of the Douglas-fir-hemlock type. The preliminary interpretation that the openings were caused by root-rot disease was verified by the multidisciplinary team and has been further substantiated by ground surveys with many plots this year.

Not all openings in the forest canopy are caused by root-rot disease so that good interpretative judgments are required to identify Poria openings in different parts of the Douglas-fir subregion. The striking appearance of the circular bare ground signature indicator in the high Cascades of Oregon was the primary criterion for identifying root-rot centers in other forested areas of the Pacific Northwest. In the early stages of development, a Poria signature appears on the aerial photo as a circular opening (or "hole") in the forest stand with dead and down trees jackstrawed in the center and standing trees in various stages of deterioration at the edges of the opening. Stand openings increase radially in size from the center of infection. Where brush and other vegetative species do not invade rapidly (as in the Waldo Lake Test Site


Figure 27. 1:31,680 scale color imagery shows characteristic pattern of Poria weirii root-rot disease in forest stands of high Cascades in Oregon (Waldo Lake test site). At (1) a new center can be observed; at (2) an older enlarging center; at (3) a series of coalescing centers. Note how residual trees of less susceptible types (white and true fir, western red cedar, and white pine) fill in initial openings.

in the high Cascades), the circular bare ground signature is readily discerned. At lower elevations and on better timber sites, small trees (primarily hardwoods) and brush invade rapidly to obscure down trees and increase the problem of positively identifying root-rot disease centers. Both large and small pockets of bark beetle-killed trees in various stages of deterioration in the forest stand may also confuse interpretation. Considerable field experience is needed by the photo interpreter to delineate root-rot disease-caused openings.

## LOCATION OF PROBLEM AREAS

As a first step in establishing test sites for further research and development of survey methodology in detecting Poria weirii root-rot centers in the Douglas-fir subregion, it was considered desirable to know where (based on the general distribution of root-rot signature indicators) tree mortality was in progress. Existing photographs covering approximately 30 million acres on 12 National Forests in Oregon and Washington were carefully scrutinized by two interpreters for the presence or absence of discrete signature indicators. Interpretations on some 8,200 photographs at scales ranging from 1:10,000 to 1:15,840 indicated good disease indicators on four National Forests and likely indicators on eight others.

From this broad overview of root-rot disease in the Northwest, three test sites were selected (Figure 28) for more detailed examination, photographic coverage, and analysis. Each test site encompasses 9 square miles (3-mile x 3-mile block) of pole and sawtimber stands. A variety of disease, stand, and climatic conditions, slope and elevations, and forest types would thus be sampled.

1. The Waldo Lake Test Site (William N. F.) is in the high Cascades of Oregon, has some brushy areas, and moderate to easy terrain accessibility.

2. The Olallie Lake Test Site (Mt. Hood N. F.) is in the Oregon Cascades, brushy with areas of dense reproduction, and moderate terrain accessibility.

3. The Divide Lookout Test Site (Siuslaw N. F.) is in the Coast Range of Oregon, brushy with extensive understory of vine maple, rhododendron, and red alder, and has extremely rough terrain with deeply dissected slopes of 80 to 90%.

## INTERAGENCY COOPERATION

The interest by forest resource managers in the new root-rot disease signature has stimulated a strong cooperative research and development program to evolve a survey method for detecting and evaluating the impact on the forest resources of the Northwest. The following Federal and State agencies are contributing manpower and/or financial help to assist in the collection of ground truth and in obtaining aerial photography: Forest Insect and Disease Control, Timber Management, R-6, U. S. Forest Service; Remote Sensing Work Unit, Pacific Southwest Forest and Range Experiment Station, U. S. Forest Service; Earth Resources Survey Program, National Aeronautics and Space Administration; Forest Disease Research, Pacific Northwest Forest and Range Experiment Station, U. S. Forest Service; and the Oregon State Board of Forestry. This interagency cooperative effort will increase the likelihood of developing a practical airborne survey sensing system in the shortest possible time. A well-developed survey system (orbital or suborbital) can assist in the


Figure 28. Forest map of Oregon and Washington shows location of three 9-square-mile test sites -- two in the high Cascades and one in the Coast Range -- that are utilized for developing aerial photo graphic survey techniques from orbital or suborbital altitudes. Areas of Douglas-fir and hemlock forest types susceptible to the root rot disease are located in the shaded areas.

protection of one of our most valuable natural resources in the Pacific Northwest -- our National Forests.

## PROCEDURES

### SUBORBITAL MULTISPECTRAL PHOTOGRAPHY

Preliminary interpretations of panchromatic photos at the 3 test sites (9 square miles each) indicated a wide range of terrain, vegetative conditions, and appearance of root-rot disease openings. This necessitated a preliminary ground evaluation of the different sites to determine the feasibility of testing minimum and maximum photographic scales. The vegetative complexity of the Coast Range test site clearly indicated the need for maximum ground detail to delineate root-rot openings. Consequently, photo scales larger than 1:15,840 were considered essential for the initial tests in the Divide Lookout test site of the Coast Range (Figure 29). Because of the more easily discerned signature indicators in the high Cascades of Oregon (Waldo Lake and Olallie Lake) much smaller scale photography (including orbital imagery) should be useful in detecting Poria weirii disease centers.

Subsequently, plans were made to secure aerial imagery at the respective test sites using the following scales of photography, camera systems, and film-filter combinations.

1. Photo Scales

| Divide L. O. (Coast Range) | Waldo Lake (Cascades) | Olallie Lake |
|---|---|---|
| 1:4,000 (USFS) | | |
| 1:8,000 (USFS) | 1:8,000 (USFS) | 1:8,000 (USFS) |
| 1:15,840 (USFS) | 1:15,840 (USFS) | 1:15,840 (USFS) |


Figure 29. 1:8,000 scale color photography shows two types of openings in forest stands of the Coast Range in Oregon. Plots 1 and 2 are caused by Poria root rot. Dead Douglas-fir trees, killed in past years by the Douglas-fir bark beetle, remain standing in some openings (Plot 3). Large numbers of dead trees in a pocket indicate beetle activity rather than incidence of root-rot spread.

Photo Scales, continued

| Divide L. O. (Coast Range) | Waldo Lake (Cascades) | Olallie Lake |
|---|---|---|
| | 1:30,000 (USFS) | 1:30,000 (USFS) |
| | 1:60,000 (NASA) | 1:60,000 (NASA) |
| | 1:125,000 (NASA) | 1:125,000 (NASA) |
| | 1:250,000 (NASA) | 1:250,000 (NASA) |

2. Film-filter Combinations

Each test site was photographed with Aero color negative film (2445) which provides either color or black-and-white prints, and with Color Infrared film (2443) using a Wratten #15 filter.

3. Camera Systems

The U. S. Forest Service used a Zeiss 8 1/4" focal-length camera for all film and scale combinations. NASA expects to use two RC-8 cameras (6" and 12" focal lengths) and four 70 mm cameras, 1.57" (40 mm) focal length to 6" focal length (2 1/4" x 2 1/4" format) from an RB-57 or U-2 jet type aircraft.

Multiscale photography was taken by the U. S. Forest Service using the PSW Forest and Range Experiment Station's Aero Commander and the Region 6 Cartographic Section's twin Beechcraft. Scheduling constraint for the NASA aircraft in 1971 prevented our obtaining small-scale photographic coverage. Plans were to analyze and compare the accuracy of interpreting several film-filter and photo scales taken at suborbital altitudes at the three test sites. This photo coverage has been rescheduled for NASA aircraft in July 1972.

## COLLECTION OF GROUND TRUTH

A plan to collect ground truth requires a knowledge of the general distribution of disease infection centers on each test site. Thus, criteria were developed to identify the appearance and characteristics of Poria weirii root-rot openings on aerial photographs using some preliminary ground inspections. Then, with these criteria, two photo interpreters scrutinized the currently available 1:15,840 scale panchromatic photos taken in 1967-69 of each 9-square-mile area selected for the study. Openings and type areas suspected as indicative of root-rot centers were classified into two categories: good Poria signatures and possible Poria signatures. Each suspect area was circled and numbered on a frosted acetate overlay attached to each photo. Areas of timber that did not appear infected with Poria were also marked on the photos to serve as control checks.

From these interpretation data, 25 or more areas in each of the above categories were selected for ground visitation on each test site. Areas to be checked were chosen largely on the basis of accessibility. The extremely adverse terrain on the Divide Lookout test site (Siuslaw N. F.) necessitated that plots be within a few chains of a road. Presence or absence of Poria root-rot was determined by the examination of several living, dead, and down trees for diagnostic symptoms and signs of the fungus, including ectotrophic mycelium, setal hyphae, and laminated decay. Check plots were at least 1/5 acre in size and located at least 2 chains from known Poria centers. Two 2-man teams under the direction of a trained forest pathologist visited designated plots on the three test sites from July 6 to September 22, 1971.

## PHOTO INTERPRETATION

Photo interpretation on this study consisted of four phases that ranged from a comprehensive overview for the large problem area (the Douglas-fir-hemlock timber resource in the Pacific Northwest) to more intensive and detailed interpretations of specific plots within each of the three test sites. The first phase was mentioned earlier and involved the inspection of some 8,200 panchromatic photos covering approximately 30 million acres to detect any type of signature indicators in the forest types of Oregon and Washington that might be caused by a root-rot forest disease.

The second phase was the intensive photo interpretation on 1:15,840 scale panchromatic photographs of three selected test sites in Oregon. The three test sites represent signature indicators ranging from simple to complex degrees of interpretability. Two experienced photo interpreters received field training on different types of openingsin forest areas of the high Cascades and Coast Range before interpreting Poria signatures on photos of the three test sites. From the large array of interpreted areas, more than 75 plots were chosen for field examination in each test site. Good accessibility was the primary concern for final plot selections. Photo interpreters from the two field crews greatly enhanced their ability to discriminate root-rot centers on the photos as the field visitations progressed during the summer.

The third interpretation phase developed toward the end of the summer as new photo coverage on each test site with black-and-white, color, and color infrared films and at different photo scales became available. The two most experienced interpreters examined all test site areas, first on small scale and then progressing to large scale with a random selection from the available film types.

The fourth and final phase of the photo interpretation for the 1971 season is now in progress. A more complete analysis of all film-filter and scale combinations is needed to make statistically valid and meaningful comparisons that can be utilized in establishing sound aerial photographic survey procedures. In order to achieve this objective, it was considered appropriate to devise a photo interpretation testing technique that would minimize or remove almost entirely the bias that is commonly found in multiple and sequential photographic interpretations of the same areas with different films and scales.

The large number of plots selected and field-checked on each test site provided a sound basis for using a randomized block design with a factorial feature at each of the three test sites. Nine combination treatments are possible at each test site -- three types of photography and three photo scales. An even distribution of plots within each combination treatment for all three tests (dictated by total field plots) gave eight replications. Thus, from a total of 72 plots in each test site, (there were from 75 to 100 plots on each of the three test sites) eight were randomly selected for each film-scale combination. Photo interpretation will be made by five interpreters. Each of the 72 plots will be interpreted only once by each interpreter, thus removing a possible source of interpreter bias. Prior to making the random selection, the 72 plots were delineated and numbered on each film-scale combination at the three test sites -- a total of 1,944 plots. The interaction between photo type scale combinations (nine) and interpreters (five) is used as the error term for testing significance. Tests of significance will be performed for film types, photo scales, and the photo-scale film interaction.

## RESULTS

The results of the photo interpretation are not complete at this time because color prints, panchromatic prints, and color IR transparencies were not available for interpreting all photo scales and test sites before the end of the field season. However, the results shown in Table 27 are encouraging. Interpretation of each circled plot included in the field check indicated whether or not root-rot disease was present or absent. A few of the field plot openings in the Waldo Lake and Olallie Lake test sites were caused by another root rot, Fomes annosus. Characteristics of Fomes root rot in Douglas-fir are indistinguishable from Poria weirii root rot on aerial photography and are included in the interpretation results. This distinction must be made on the ground.

An inspection of the above photographic interpretation accuracy of rating stand openings shows that differences in photo scale do not materially affect accuracy. Relatively small differences in accuracy are indicated between scales for each of the high Cascade test sites. It is apparent that, with the excellent signature indicators in the Waldo Lake test site area, a high degree of accuracy should be attainable in detecting Poria centers in this part of the high Cascades. Somewhat less accuracy was obtained in the Olallie Lake test site area.

## FUTURE RESEARCH ACTIVITIES

### DETERMINATION OF OPTIMUM FILM-SCALE COMBINATION

Our major effort for the immediate future will be to complete the interpretations (five) of the 216 selected Poria root-rot plots on the three test sites. Upon completion, the statistical analysis of the data will determine optimum combinations of films and photo scales that would

Table 27. Photo interpretation accuracy in detecting root-rot disease on three test sites in Oregon with several film types and scales of photography.

| Type of Photography | Scale | Waldo Lake | Olallie Lake | Divide L. O. |
|---|---|---|---|---|
| Pan | 1:15,840 | 93% | 80% | 64% |
| Color | 1:31,680 | 87% | 73% | --* |
| Color | 1:15,840 | --* | --* | 61% |
| Color | 1:8,000 | 89% | 76% | 62% |
| Color | 1:4,000 | --* | --* | 50% |

*Not included in the photographic coverage

be applicable to surveys in the Douglas-fir region or in particular test site areas in the Cascades or Coast Range of Oregon and Washington. Further remote sensing tests may be necessary if variable results for a particular test site occur. Preliminary data indicate good potentials for photo survey techniques in the high Cascades of Oregon using small-scale sub-orbital photography.

Additional aerial photographic imagery will be secured over the three test sites from NASA RB-57 overflights, if possible, in July 1972. Imagery would simulate orbital and suborbital photo scales not currently available for analysis and projection into further survey methodology. Analysis of these data, coupled with photography currently on hand and in the interpretation and analysis stages, should provide corroboration on optimum film-scale combinations. This should indicate success-ratio likelihood for forest disease aerial survey techniques from orbital and suborbital altitudes.

## PHOTO SURVEY TEST IN HIGH CASCADES IN 1972

The results of the preliminary interpretations in the high Cascades of Oregon are sufficiently encouraging so that an attempt will be made in 1972 to implement an aerial photographic trial survey in the forest types of the high Cascades in and adjacent to the Waldo Lake test site. An interagency cooperative survey development program (mentioned previously) is being planned for (1) administering this aerial survey, (2) designing the aerial survey methodology, (3) procuring, processing, and interpreting aerial photographic imagery, (4) collecting the ground truth according to specific sampling procedures, (5) assigning responsibilities to qualified personnel in all phases of the survey program, and (6) developing logistics

and setting time schedules to accomplish the aerial photographic survey in an expeditious manner. Details of the survey program will be developed during the winter period.

## IMPROVING PHOTO INTERPRETATION IN THE COAST RANGE TEST SITE

Additional remote sensing research is being considered for improving photo interpretation capabilities in the Coast Range test site areas. A major problem in interpreting imagery in the Coast Range of Oregon and Washington is the abundance of brush and hardwood tree species which when fully foliaged preclude seeing details in down trees and on the ground. Hence, there is a need to utilize photography taken in these areas prior to spring growth, which is before April 15. Attempts will be made from mid-March to early April to determine whether a higher interpretation success ratio can be obtained at this time. Additional photo tests may also be scheduled in early October when normal leaf drop of vegetation (hardwoods and deciduous brush species) occurs. As a part of this endeavor, more detailed criteria will be investigated and developed for classifying root disease openings in the Coast Range forest canopy. These criteria would be applicable to the Oregon Coast Range and the Washington Olympic areas.

## ESTIMATING CHANGES IN PORIA CENTERS

Investigations will continue on comparing older photography taken over the past 30 years of the Olallie Lake and Waldo Lake test sites to determine whether or not Poria root rot changes shape and size rapidly, gradually, or remains static. More survey information is being gathered on the distribution of root-rot disease centers to establish a base map from which comparative measurements can be obtained. Disease enlargement

comparisons will be made on sequential photography using a Zeiss stereotape-Olivetti computer program. A time sequence for rephotography may also be ascertained from this investigation.

## ERTS IMAGERY MAY BE IMPACT SURVEY TOOL

Because of the relatively large size of the root-rot infection centers, there is a good possibility that ERTS imagery might detect the incidence of advanced stages of Poria. The three Poria weirii test sites in Oregon are included in the Oregon State University ERTS proposal. Plans have been made to look at the ERTS imagery of these test sites when it becomes available and to collate the data with suborbital imagery taken in 1971. A multistage probability sampling design may be an effective means to determine the impact of the root-rot disease on the forest resource using ERTS imagery as the first stage.

## LITERATURE CITED


1. Wear, J. F. 1967. The development of spectro-signature indicators of root disease on large forest areas. Annual Progress Report for Earth Resources Survey Program, OSSA/NASA, by the Pacific Southwest Forest and Range Experiment Station.
2. Wear, J. F. 1968. The development of spectro-signature indicators of root disease impacts on forest stands. Annual Progress Report for Earth Resources Survey Program, OSSA/NASA, by the Pacific Southwest Forest and Range Experiment Station.
3. Weber, F. P. and J. F. Wear. 1970. The development of spectro-signature indicators of root disease impacts on forest stands. Annual Progress Report for Earth Resources Survey Program, OSSA/NASA, by the Pacific Southwest Forest and Range Experiment Station.

# CALIBRATION OF COLOR AERIAL PHOTOGRAPHY

by

R. W. Dana and R. J. Myhre

## INTRODUCTION

The guiding premises behind film calibration work by this group are that film response data would aid in the design of remote sensing experiments and provide the photographer with film speed data of new film emulsions. The capability to relate film density to irradiance level and reflectivity of ground targets is also of great interest. Furthermore, it is reasonable to assume that calibration of this sort can be a valuable tool in the automatic recognition of forest and range type classes and their associated patterns.

The acquisition of these capabilities requires good instrumentation -- a sensitive, versatile densitometer, which we have purchased, and a repeatable uniform light source (sensitometer) which we are developing. The subject of a large portion of this report is the design of filter combinations for the sensitometer that will yield a close fit to typical daylight spectral distributions in the visible and near infrared region. A detailed radiometric measurement of the sensitometer exposure time and repeatability was made, and a brief description of the techniques and results should be of interest.

During a lull in the summer flying schedule, we were able to field-test some new film emulsions, using sensitometry to monitor the exposure and processing. Two of the film types were new to us (Eastman 2443 and SO-397) and the others were new emulsions of film types with which we had much previous experience. Most of the qualitative analysis can be presented.

While the quantitative phases are still under way, only the methods of analysis can be described in this report.

## SENSITOMETER DEVELOPMENT

The instrumentation work involved with sensitometry is a continuation of work described in a previous special report (2). The important requirements of an aerial film sensitometer which we have strived for are the following:

1. Daylight spectral balance in the range 400-900 nanometers.
2. Radiometric repeatability approaching the densitometer accuracy of $\pm$ 0.02 density units.
3. Exposure time of under 20 milliseconds.
4. Compact size.
5. Filter interchangeability.

This section discusses the quantitative work toward accomplishing requirements 1, 2 and 3.

## SPECTRAL DISTRIBUTION

If one were to choose one particular spectral distribution for his light source in aerial film calibration, it should be the daylight that illuminates his targets. But daylight takes so many forms as evidenced by the variations in irradiance with wavelength that have been discovered by several authors. Gates (3 and 4) has published numerous daylight spectra of direct sunlight from various solar zenith angles and with various atmospheric effects present. He has also presented the distribution of skylight, which is largely Rayleigh scattering by air molecules, and "cloudlight" due to overcast conditions. The latter two are much stronger in the blue end of

the spectrum than direct sunlight. The effect of sun angle is shown in Figure 30. Each curve is normalized to the same value at 480 nm to allow comparison of general shape. A low sun situation (large zenith angle and large air mass) is richer in longer wavelength radiation than a noon sun situation except in the very strong absorption bands.

The sunlight spectrum is characterized by approximately 5900°K blackbody radiation undergoing strong absorption by ozone and oxygen in the ultraviolet, a moderate molecular oxygen absorption band at 760 nanometers, and a strong water vapor band centered at 930 nm (Figure 30). Gates (3) has computed these attenuation effects as well as Rayleigh scattering by air molecules and Mie scattering by aerosols. The aerosol levels expected in aerial photography are rather hard to predict, and the effect of water vapor concentration is generally no greater than the variation of Figure 30. The moderate slant path represented by m = 1.5 would seem to be the best bet for consideration as a typical direct sunlight curve.

The effect of adding skylight to the sunlight distribution is shown in Figure 31, revealing a general increase with decreasing wavelength in the 400-900 nm band. Here, as with all spectra in this section, distributions are shown as log plots in terms of relative energy per unit area-time-wavelength.

Data from two other sources (6 and 12) are tabulated in Tables 28 and 29 at 20 nm intervals along with the Gates data (3, 4). For the visible range covered by panchromatic and normal color films, the daylight values were lowered at the short wavelength end by the attenuation of a typical

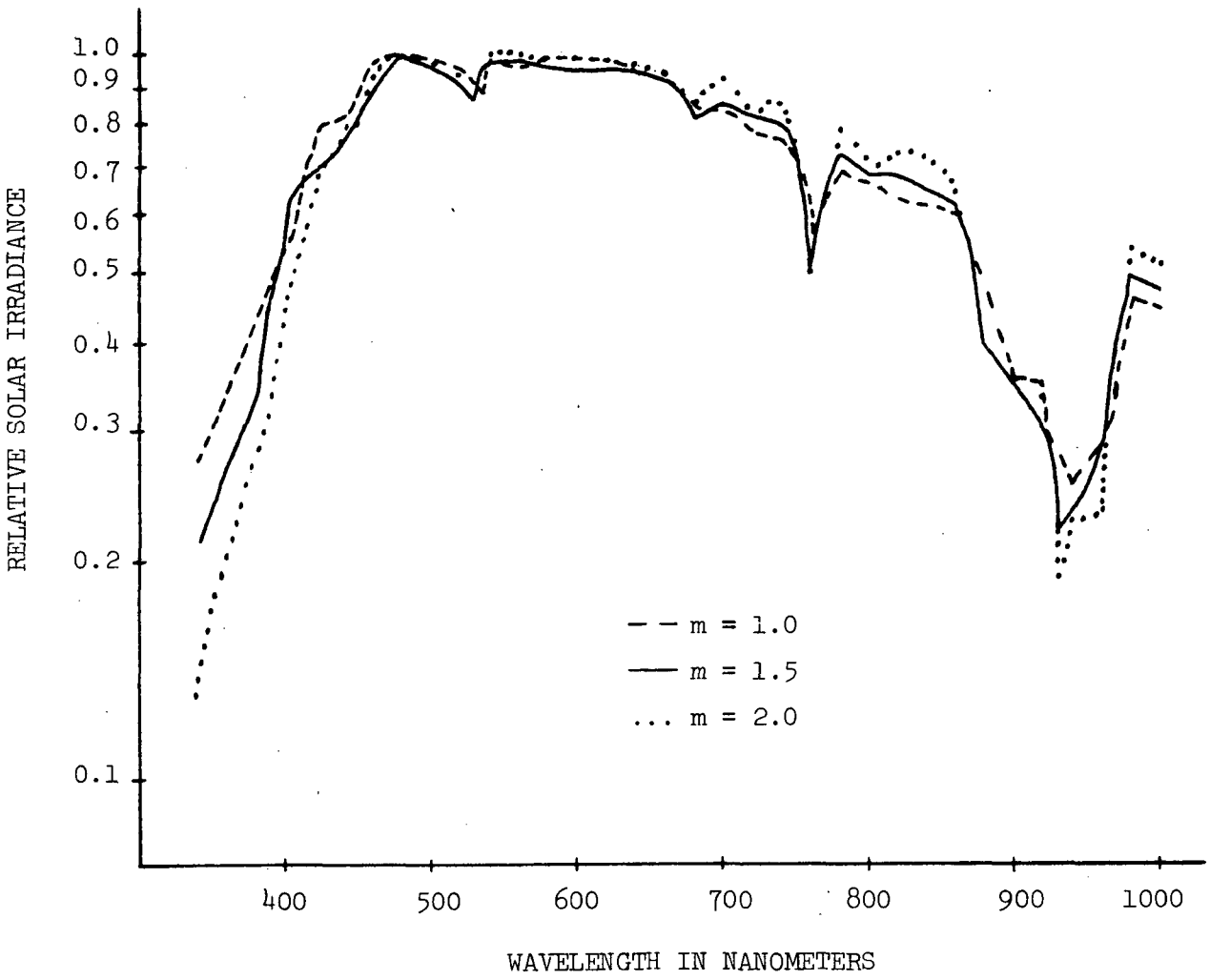


Figure 30. Relative spectral irradiance at sea level from direct sunlight with air mass m of 1.0, 1.5, and 2.0. The corresponding sun angles are $0^{o}$, $48^{o}$ 11', and $60^{o}$ from the vertical. Precipitable water concentration -- 1 centimeter; aerosol concentration -- 200 particles per cubic centimeter; ozone concentration -- 0.35 centimeter. Data derived from reference no. 3.

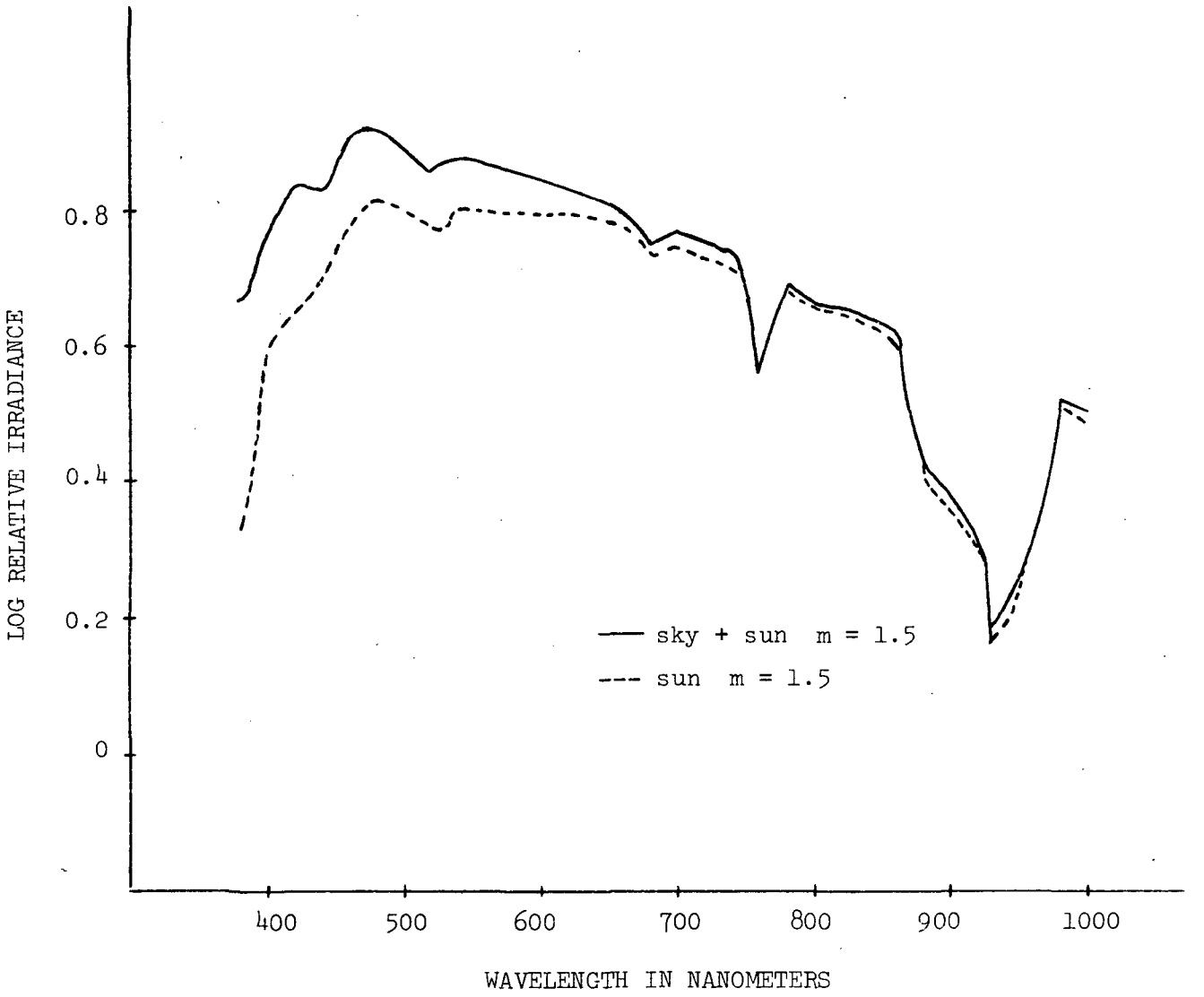


Figure 31. Relative spectral irradiance at sea level of direct sunlight at m = 1.5 and sunlight plus skylight. Data derived from references no. 3 and no. 4.

Table 28. Daylight spectral distributions for the visible region normalized to the same integrated 400 to 700 nm value.

| Wavelength (nm) | Log Relative Irradiance | | | | | | |
|---|---|---|---|---|---|---|---|
| | D1A | D1B | D2 | D3A | D3B | D4A | D4B |
| 400 | 1.53 | 1.43 | 1.44 | 1.43 | 1.67 | 1.45 | 1.54 |
| 420 | 1.64 | 1.58 | 1.54 | 1.53 | 1.68 | 1.61 | 1.70 |
| 440 | 1.64 | 1.59 | 1.60 | 1.62 | 1.72 | 1.67 | 1.71 |
| 460 | 1.74 | 1.81 | 1.69 | 1.70 | 1.76 | 1.74 | 1.75 |
| 480 | 1.75 | 1.93 | 1.72 | 1.72 | 1.74 | 1.74 | 1.75 |
| 500 | 1.72 | 1.95 | 1.70 | 1.71 | 1.72 | 1.72 | 1.73 |
| 520 | 1.69 | 1.96 | 1.68 | 1.71 | 1.70 | 1.70 | 1.70 |
| 540 | 1.71 | 1.91 | 1.71 | 1.72 | 1.70 | 1.70 | 1.69 |
| 560 | 1.70 | 1.83 | 1.71 | 1.71 | 1.68 | 1.71 | 1.67 |
| 580 | 1.69 | 1.73 | 1.70 | 1.71 | 1.66 | 1.68 | 1.65 |
| 600 | 1.68 | 1.60 | 1.70 | 1.69 | 1.63 | 1.66 | 1.63 |
| 620 | 1.66 | 1.54 | 1.70 | 1.68 | 1.62 | 1.65 | 1.61 |
| 640 | 1.65 | 1.46 | 1.69 | 1.68 | 1.60 | 1.63 | 1.63 |
| 660 | 1.63 | 1.39 | 1.68 | 1.67 | 1.58 | 1.62 | 1.62 |
| 680 | 1.58 | 1.39 | 1.63 | 1.66 | 1.57 | 1.62 | 1.62 |
| 700 | 1.60 | 1.37 | 1.65 | 1.63 | 1.53 | 1.60 | 1.63 |
| Total | 25.06 | 25.07 | 24.99 | 25.04 | 24.96 | 24.97 | 25.05 |

D1A - sunlight + skylight

D1B - cloudlight

D2 - sunlight m = 1.5

D3A - 5500°K correlated color temperature

D3B - 6500°K correlated color temperature

D4A - 6000°K sunlight + skylight

D4B - 6500°K overcast skylight

Table 29. Daylight spectral distributions for the visible-infrared region normalized to the same integrated 500-920 nm value.

| Wavelength (nm) | Log Relative Irradiance | | | |
|---|---|---|---|---|
| | D1A | D1B | D2 | D3A |
| 500 | 0.83 | 1.26 | 0.77 | 0.79 |
| 520 | 2.36 | 2.83 | 2.31 | 2.35 |
| 540 | 2.57 | 2.97 | 2.53 | 2.55 |
| 560 | 2.58 | 2.91 | 2.55 | 2.56 |
| 580 | 2.57 | 2.81 | 2.55 | 2.56 |
| 600 | 2.57 | 2.69 | 2.55 | 2.55 |
| 620 | 2.55 | 2.63 | 2.55 | 2.54 |
| 640 | 2.54 | 2.55 | 2.54 | 2.54 |
| 660 | 2.52 | 2.48 | 2.53 | 2.53 |
| 680 | 2.47 | 2.48 | 2.48 | 2.52 |
| 700 | 2.49 | 2.46 | 2.50 | 2.49 |
| 720 | 2.47 | 2.42 | 2.48 | 2.42 |
| 740 | 2.46 | 2.40 | 2.47 | 2.50 |
| 760 | 2.28 | 2.23 | 2.28 | 2.29 |
| 780 | 2.41 | 2.25 | 2.43 | 2.43 |
| 800 | 2.38 | 2.18 | 2.40 | 2.40 |
| 820 | 2.38 | 2.18 | 2.40 | 2.39 |
| 840 | 2.36 | 2.09 | 2.38 | 2.37 |
| 860 | 2.34 | 2.01 | 2.37 | 2.35 |
| 880 | 2.15 | 1.95 | 2.17 | 2.16 |
| 900 | 2.10 | 1.88 | 2.11 | 2.10 |
| 920 | 2.04 | 1.83 | 2.06 | 2.05 |
| Total | 49.98 | 49.94 | 49.99 | 50.02 |

D1A - sunlight + skylight

D1B - cloudlight

D2 - sunlight m = 1.5

D3A - 5500°K correlated color temperature

is D4A which is further defined as having a 6000°K color temperature. D1B and D4B are overcast sky distribution. The color temperature of D3A is 5500°K while the somewhat more blue distribution D3B is for color temperature 6500°K. Distribution D4B, also said to have a 6500°K color temperature, is plotted with D1B and D3B in Figure 32 to show how daylight expressions can vary in the literature. D4B has more strength in the red and less strength in the blue than D3B. By comparison the D1B cloud-light is very strong in the green wavelengths.

The filter matching technique used to obtain sensitometer filter combination to match daylight distribution was to start with some of the filters commonly used to convert tungsten light to daylight in the visible region and to reduce the 700-900 nm region. We computed their effect on the system and tried several other filters in the same series that showed from their own transmission curves some promise of bending the system curves in the right directions. The products of three major glass and gelatin filter suppliers were tried, and several more sources are to be investigated in the future.

Spectral irradiance data for tungsten lamps at two different temperatures were digitized and combined with data for the sensitometer wedge, neutral density attenuators (for overall adjustment of light level for different speed films) and the various prospective conversion filters, again at 20 nm intervals. Base 10 logarithms of these functions, with uncertainty $\pm$ 0.01, were used to compile the product functions $F(\lambda)$ wavelength by wavelength. Equation 3 gives the general form of the spectral product functions.

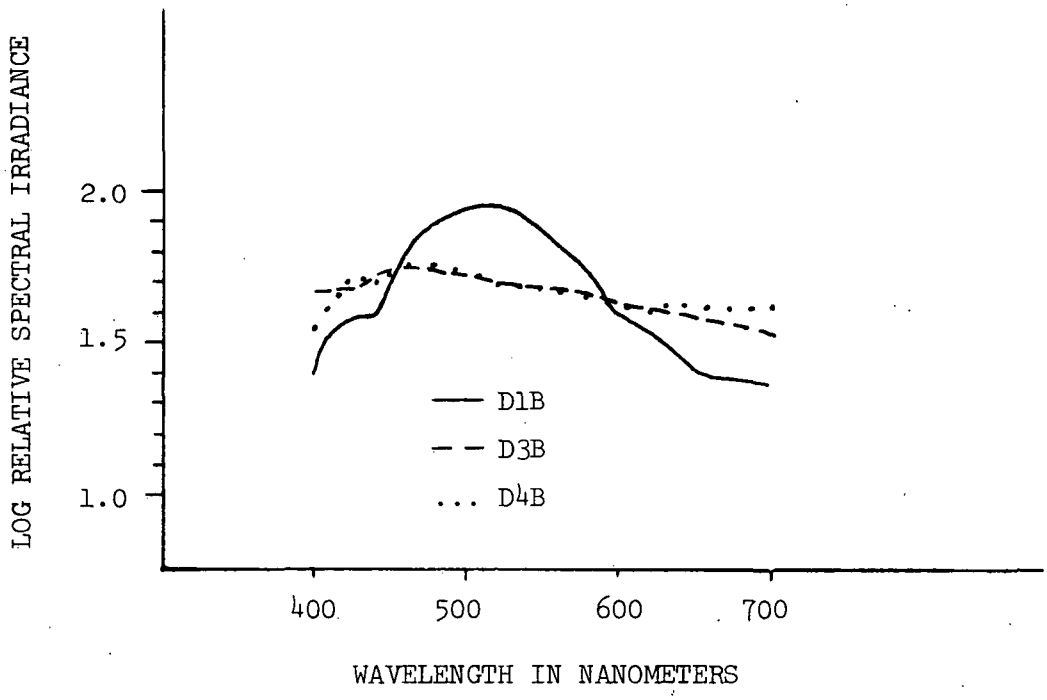


Figure 32. Spectral distributions from three sources which might be used as typical curves of overcast conditions. D1B, D3B, and D4B are from references no. 4, 6, and 12, respectively.

(3) $$F(\lambda) = L(\lambda)\ F(\lambda)\ F_n(\lambda)\ \prod_i F_c^i(\lambda),$$ where

$L(\lambda)$ = lamp irradiance

$W(\lambda)$ = sensitometer wedge transmissivity

$F_n(\lambda)$ = neutral density attenuator transmissivity

$\prod_i F_c^i(\lambda)$ = product of all conversion filter transmissivities.

The logarithmic form is normalized by equation 4.

(4) $$F(\lambda) = L(\lambda) + W(\lambda) + F_n(\lambda) + \sum_i F_c^i(\lambda) \equiv \begin{matrix} 25.00 \text{ for visible range} \\ 50.00 \text{ for IR film range} \end{matrix}$$

The eight best filter combinations for which reasonably reliable transmission data were available are described in Table 30. The resultant distributions from equation 4 are displayed in Tables 31 and 32. Combination F1 is somewhat idealized in that a perfectly neutral wedge and general attenuator were assumed. This appears to be the assumption made for the sensitometry of Kodak Aerochrome Infrared Film 2443 and 3443 as shown in the manufacturer's specifications (9). While combinations F1 and F3 include correction filters which total 7 mm in thickness and must be mounted rigidly and close to the lamps, combination F2 has the advantage of having 5 mm of glass filters and a gelatin-based filter (Agfa 144 Mired), which can be mounted in a curved holder. The curved configuration helps to maintain uniformity at the film plane. Tests of uniformity with these filter combinations have not as yet been performed.

Having normalized the distributions for daylight and sensitometer light sources for the bandwidths of interest, we found it a simple step to compute root-mean-square deviations between distributions. These are shown in Tables 33 and 34 and are representative of the closeness of fit

Table 30. Description of lamp-filter combinations for artificial daylight sources.

| Combination | Lamp Color Temp °K | Filters | |
|---|---|---|---|
| | | Visible Region 400-700 nm | Infrared Film Region 500-920 nm |
| F1 | 2850 | Corning 5900 + Corning 3966 | F1 (visible) + Kodak Wratten 12 |
| F2 | 3100 | Carbon wedge + Kodak neutral density + Agfa 144 Mired correction filter + Corning 3966 + Corning 4602 | F2 (visible) + Kodak Wratten 12 |
| F3 | 3100 | Carbon wedge + Kodak neutral density + Corning 5900 + Corning 3966 | F3 (visible) + Kodak Wratten 12 |
| F4 | 3100 | Carbon wedge + Kodak neutral density + Kodak Wratten 38 + Kodak CC 20 blue | - - - - - - - - - - |
| F5 | 3100 | - - - - - - - - - - | Carbon wedge + Kodak neutral density + Corning 5900 + Corning 4602 + Kodak Wratten 12 |

Table 31. Artificial daylight distributions for the visible region. Tungsten lamps in combination with various filters as described in Table 30. Normalization is for the whole 400-700 nm band.

| Wavelength (nm) | Log Relative Irradiance | | | |
|---|---|---|---|---|
| | F1 | F2 | F3 | F4 |
| 400 | 1.53 | 1.23 | 1.50 | 1.39 |
| 420 | 1.68 | 1.52 | 1.70 | 1.66 |
| 440 | 1.74 | 1.61 | 1.73 | 1.78 |
| 460 | 1.75 | 1.64 | 1.68 | 1.81 |
| 480 | 1.76 | 1.70 | 1.70 | 1.85 |
| 500 | 1.78 | 1.71 | 1.71 | 1.85 |
| 520 | 1.73 | 1.72 | 1.70 | 1.89 |
| 540 | 1.70 | 1.72 | 1.67 | 1.87 |
| 560 | 1.74 | 1.77 | 1.80 | 1.86 |
| 580 | 1.72 | 1.82 | 1.74 | 1.81 |
| 600 | 1.64 | 1.79 | 1.68 | 1.73 |
| 620 | 1.58 | 1.80 | 1.63 | 1.62 |
| 640 | 1.54 | 1.72 | 1.58 | 1.39 |
| 660 | 1.48 | 1.62 | 1.51 | 1.32 |
| 680 | 1.56 | 1.53 | 1.58 | 1.27 |
| 700 | 1.59 | 1.53 | 1.59 | 1.25 |
| Total | 24.96 | 25.05 | 24.96 | 25.07 |

Table 32. Artificial daylight distributions for the region of infrared film. Tungsten lamps in combination with various filters as described in Table 30. Normalization is for the 500-920 nm band.

| Wavelength (nm) | Log Relative Irradiance | | | |
|---|---|---|---|---|
| | F1 | F2 | F3 | F5 |
| 500 | 1.99 | 0.73 | 0.90 | 1.06 |
| 520 | 2.57 | 2.30 | 2.45 | 2.63 |
| 540 | 2.66 | 2.49 | 2.61 | 2.71 |
| 560 | 2.72 | 2.56 | 2.70 | 2.79 |
| 580 | 2.70 | 2.61 | 2.70 | 2.79 |
| 600 | 2.63 | 2.58 | 2.65 | 2.74 |
| 620 | 2.57 | 2.60 | 2.60 | 2.70 |
| 640 | 2.53 | 2.52 | 2.55 | 2.59 |
| 660 | 2.47 | 2.42 | 2.48 | 2.59 |
| 680 | 2.55 | 2.33 | 2.55 | 2.66 |
| 700 | 2.58 | 2.33 | 2.56 | 2.66 |
| 720 | 2.50 | 2.47 | 2.47 | 2.57 |
| 740 | 2.42 | 2.65 | 2.38 | 2.45 |
| 760 | 2.31 | 2.72 | 2.29 | 2.35 |
| 780 | 2.29 | 2.68 | 2.28 | 2.29 |
| 800 | 2.25 | 2.57 | 2.26 | 2.22 |
| 820 | 2.20 | 2.44 | 2.22 | 2.14 |
| 840 | 2.18 | 2.31 | 2.20 | 2.05 |
| 860 | 2.14 | 2.19 | 2.18 | 1.98 |
| 880 | 2.10 | 2.05 | 2.16 | 1.88 |
| 900 | 2.06 | 1.88 | 2.12 | 1.75 |
| 920 | 2.12 | 1.70 | 2.19 | 1.76 |
| Total | 49.91 | 49.92 | 49.95 | 49.95 |

Table 33. Root mean square deviations between light sources F1, F2, F3, and F4 and the daylight curves D1A, D3A, D3B, D4A, D4B, and D1B for the wavelength range 400-700 nm. The log values of Table 31 were used.

| | D1A | D3A | D3B | D4A | D4B | D1B |
|---|---|---|---|---|---|---|
| F1 | .06 | .09 | .05 | .06 | .06 | --- |
| F2 | .09 | .07 | .12 | .09 | .12 | --- |
| F3 | .06 | .08 | .05 | .06 | .06 | --- |
| F4 | --- | --- | --- | --- | --- | .09 |

Table 34. Root mean square deviations between light sources F1, F2, F3, and F5 and the daylight curves D1A, D2, D3A, and D1B for the wavelength range 500-920 nm. The log values of Table 32 were used.

| | D1A | D2 | D3A | D1B |
|---|---|---|---|---|
| F1 | .11 | .13 | .12 | --- |
| F2 | .15 | .16 | .16 | --- |
| F3 | .09 | .11 | .10 | --- |
| F5 | --- | --- | --- | .12 |

between sensitometer and daylight spectra. With one exception (F2 - D3A in Table 33), the F3 distribution is the best fit in all comparisons with daylight curves, and F2 is the poorest. In Figure 33, F3 is plotted along with two daylight curves for the 400-700 nm band and in Figure 34 for the 500-920 nm band. Daylight curves D1A and D4A in the visible region are fairly well correlated as are D3A and D2 in the 500-920 nm band. Therefore, the latter members of these pairs are not shown in the figures. Figures 35 and 36 illustrate the matching of F4 and F5 with the rather hard-to-fit D1B cloudlight distribution.

## EXPOSURE TIME MEASUREMENTS

*The exposure time of a sensitometer used with aerial film should be* short enough to avoid reciprocity differences between data derived from sensitometry and actual imagery taken at 1/200 to 1/2000 second. To insure that enough light will be available for slow films and changes in filtration, the effective exposure time cannot be quite that fast in our instrument. Indications are that an adequate trade-off exists at 1/50 second.

The primary problem of measurement of effective exposure time is that the total or integrated exposure of the light pulse must be determined because the pulse is not simply a square step function. Total exposure E is defined as:

(5) $$E = \int_0^\infty H(t)\, dt$$ where H(t) is the irradiance of the time-varying pulse. The effective exposure time $\bar{T}$ is given by equation 6 in terms of the maximum value $H_{max}$ of irradiance in the pulse.

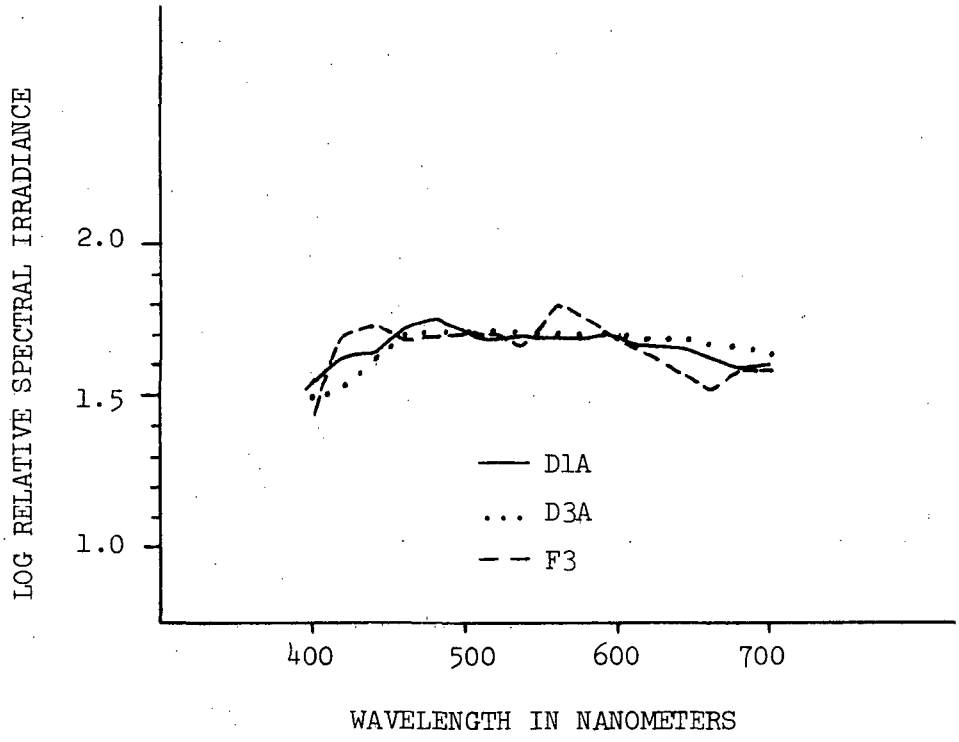


Figure 33. Sensitometer spectral distribution, F3, for the visible wavelength region plotted with two typical daylight curves.

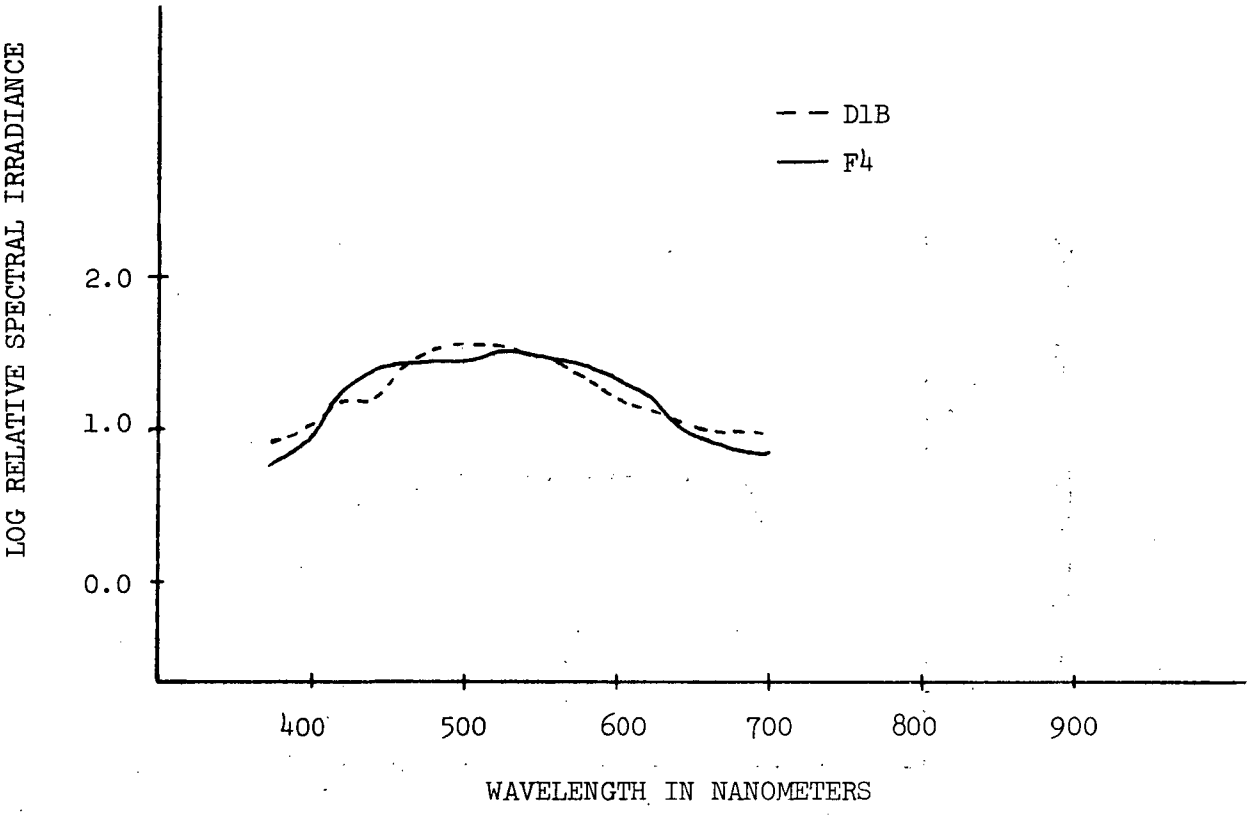


Figure 35. Cloudlight distribution, D1B, and a matching sensitometer spectral distribution, F4, for the visible region.

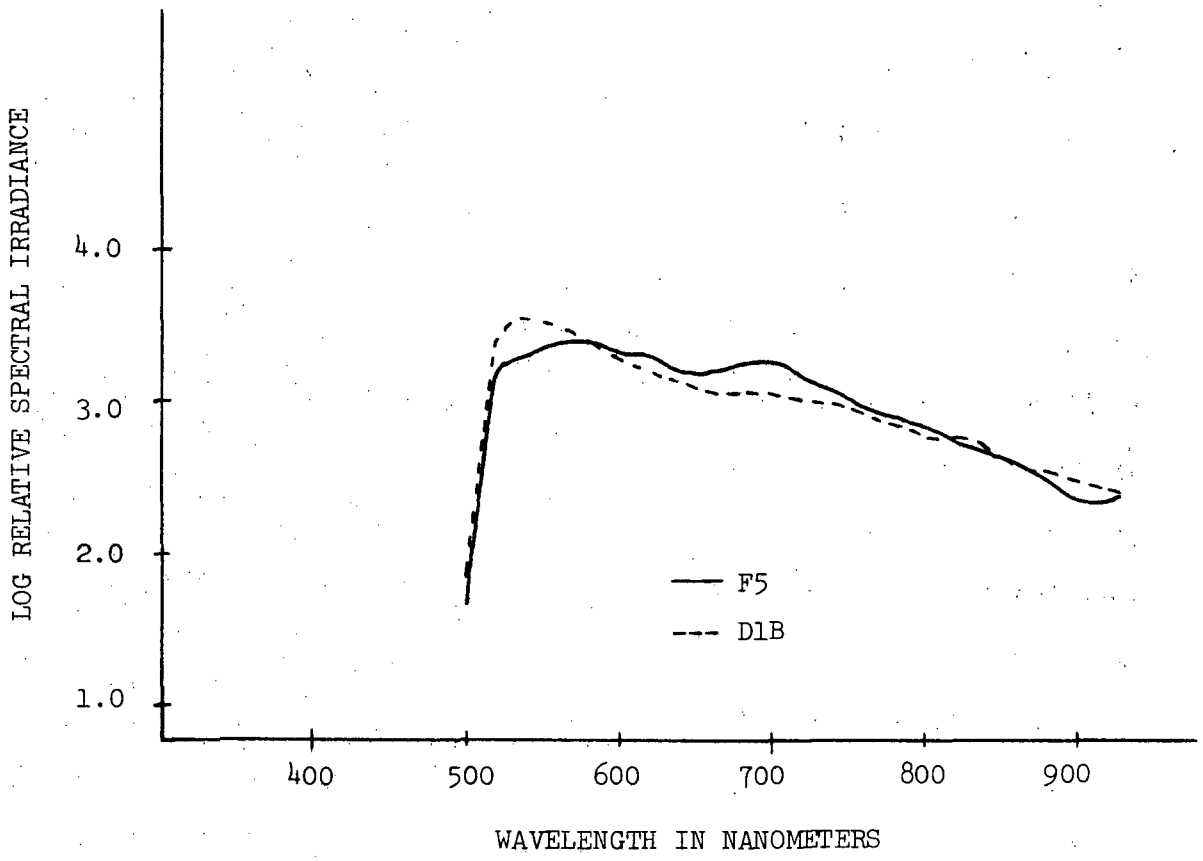


Figure 36. Cloudlight distribution, D1B, and a matching sensitometer spectral distribution, F5, for the infrared film region.

(6) $$\bar{T} = \frac{\int_0^\infty H(t)\, dt}{H_{max}} = \frac{E}{H_{max}} .$$

Thus, $\bar{T}$ is the equivalent exposure time if the pulse were a square wave of irradiance $H_{max}$. The variation of a series of E values would exhibit the repeatability of the exposure.

To integrate the pulse we imaged a 1 x 5 mm portion of the sensitometer platen onto the Photometric Data Systems microdensitometer and measured the relative irradiance with a 14 x 700 μm rectangular scanning slit. The linear amplifier used for transmission measurements was adjusted to give a 0-1.2 volt output. This analog output was displayed on an oscilloscope and fed into the digital data system. Figure 37 is a scope camera photo of the pulse showing the pulse half-width to be approximately 20 milliseconds.

The gearboxes on the microdensitometer film transport were disengaged so that a scan run could be made without physical movement of the system. The film transport provided a flat two-dimensional bench for the auxiliary optics. A scan run of about 800 milliseconds duration was performed coincidently with the sensitometer exposure cycle. The measuring increment was set at the minimum value of 2 milliseconds.

From the digital magnetic tape the programmer was able to pick off the light pulses by means of a discrimination program that separated its leading and trailing edges from sensor system noise. The relative irradiance was measured and recorded with an uncertainty of about $H_{max}/250$.

The mean value for eleven measurements of effective exposure time was 19.42 milliseconds. The standard deviation of integrated exposure

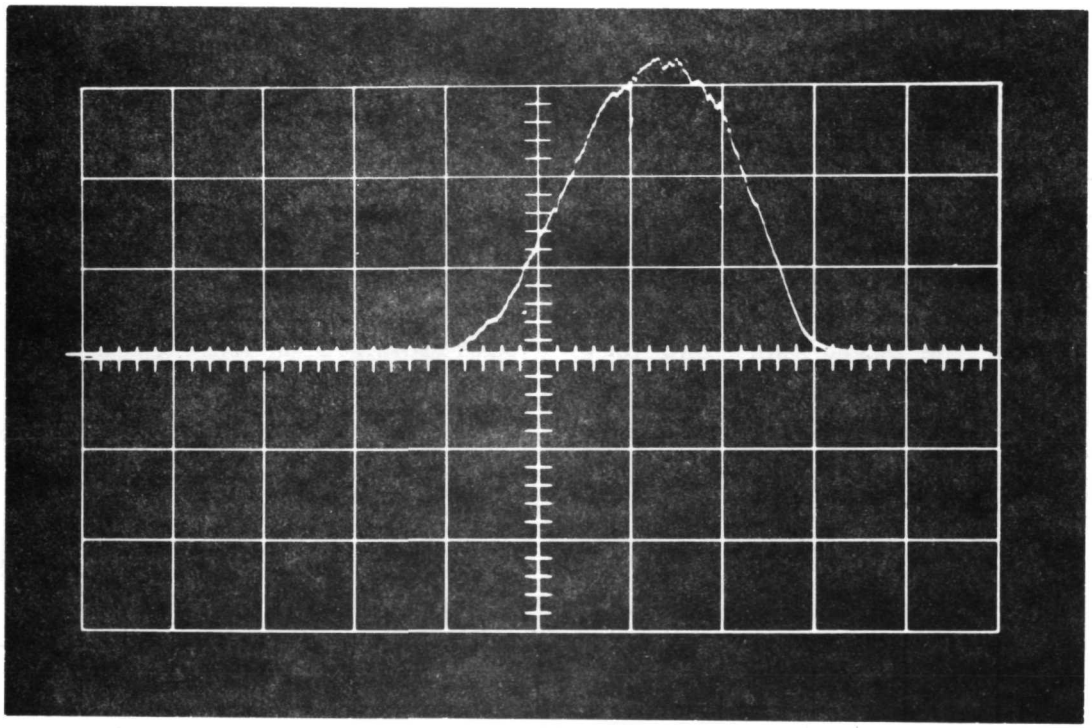

Figure 37. Oscilloscope photo of sensitometer light pulse as measured by the microdensitometer. The ordinate represents relative irradiance. The time base is 10 milliseconds for each large division.

$\sigma_E$ divided by the mean E value of all scans was 0.038. The conversion of exposure variation to approximate film density variation is made possible by equation 7:

$$(7) \qquad \partial D = \gamma \, \partial(\mathrm{Log}_{10} E), \qquad = \frac{\gamma}{2.3} \frac{\sigma_E}{E}$$

The range of gamma values encountered in our microdensity measurements of color reversal film is approximately 1.3 to 2.3. These values yield density repeatability values of 0.021 to 0.038 and are very close to the goal of 0.02. Part of the variation in exposure could actually stem from the coarseness of the time base in the pulse integration. Ideally, one might expect a more accurate measure if he could sum up the relative irradiance of a 50 ms wide pulse at 1.0 or 0.5 ms intervals.

The design work and tests discussed in this section have brought the instrumental development of film calibration nearly to completion. At least one more infrared absorbing filter is contemplated for trial in matching spectral balance to daylight. More information about the relevance of various daylight distributions will also be sought. Finally, a brief photographic test of uniformity and repeatability of the sensitometer used in conjunction with in-house processing is planned.

## APPLICATION OF SENSITOMETRIC CALIBRATION

Is film sensitometry worth all the bother? Can aerial film calibration be a useful aid to a remote sensing research group? These questions are answered affirmatively in this section as two applications of sensitometric calibrations are discussed. One deals with the testing of new film emulsions -- the other with the prospects of enhancing imagery for automatic discriminate analysis.

## AERIAL COLOR FILM TEST

As new aerial films emerge on the market, a few questions immediately come to mind. How does this new film compare with the existing film we have been using? How do we properly expose this new film from an aerial platform, and what is the best film-filter combination to use? Can we process this new emulsion with our existing equipment, and what are the processing times and procedures?

In an attempt to answer these questions we decided to run an aerial film test over an area that would simulate forestry subjects. A site was selected near San Pablo Reservoir, about 6 miles east of Berkeley, California. The test area contained stands of Monterey Pine and open areas of range vegetation (Figure 38).

Color panels and resolution targets were placed on the ground in the open range area. The targets were four-foot square panels painted to match standard Munsell system colors.[10] Standard U. S. Air Force bar targets (black bars) were painted on white panels.

This test was not intended to be a final test but rather a preliminary look to gain working knowledge of the new films. A more detailed aerial test of new films and existing films will be run at a later date.

On August 23, 1971, the test was flown with the Remote Sensing Work Unit's plane, an Aero Commander 500B. Two 70 mm Maurer KB-8 cameras with 6-inch focal length lenses were used. Flights were made at 800 feet above mean elevation to give a scale of 1:1,600. This scale was selected because it is often used in insect and disease evaluation. This large scale has

---

[10] Munsell Color Company. Munsell Book of Color. Ed. 1920-60. Baltimore, Md.

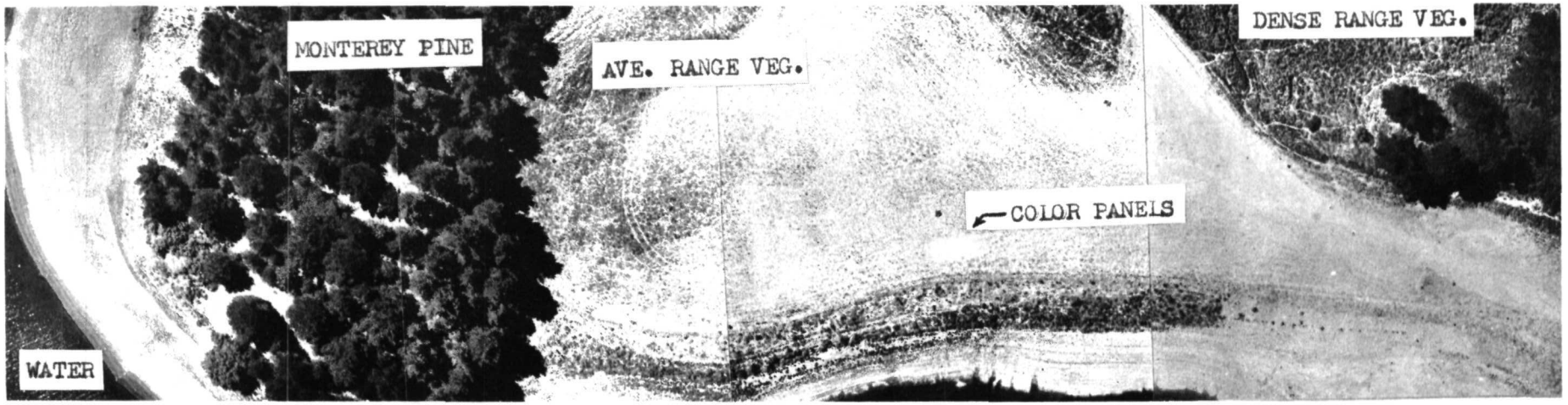


Figure 38. Film test area at San Pablo Reservoir, California. Print made from infrared color film, scale 1:1,600

the further advantage of accommodating small, easily produced and easily handled test panels.

This first test included two new emulsions of films that are presently in use on remote sensing studies and two films totally new to us. Specifically, they were as follows:

| | | |
|---|---|---|
| Anscochrome D/200 | - | Film presently in use |
| Ektachrome Infrared Aero (8443) | - | Film used in past |
| Aerochrome Infrared (2443) | - | Replaced Type 8443 |
| Ektachrome EF Aerographic (SO-397) | - | Possible future use |

When one works with new films or new emulsion numbers, the question arises, "What is the speed of this film?" From past experience we have found that the speed can vary from one emulsion number to another and is not adequately specified by the manufacturer. To each of their aerial color and infrared-sensitive films Eastman Kodak assigns an Effective Aerial Film Speed (EAFS). The effective speeds are determined empirically, usually by actual flight tests with processing under automatic, mechanized conditions. Eastman Kodak recommends determining a new EAFS for processing methods other than with automatic equipment. The EAFS is designed to be used with the Kodak Aerial Exposure Computer (8).

For low-altitude large- to medium-scale photography, we can get the best exposure by reading the subject of interest with a one degree field-of-view light meter. But in order to use a meter, we must have an ASA rating that can be used on the meter calculator.

As a starting point for determining exposure and camera settings for the aerial test, an arbitrary ASA rating of 200 was assigned to all the films in the test. On a preliminary flight over the test area a meter

reading was taken of dense range vegetation. Readings were also recorded for the average timber and average range vegetation. A normal exposure setting was determined based on ASA 200 and the light reading of dense range vegetation. To bracket the normal exposure and assure a proper exposure for both timber and range conditions, two additional camera settings were used -- one stop over the normal and one stop under normal.

Wratten No. 12 filters were used with the color infrared films; no filters were used with the color films. An additional flight was made with the Aerochrome IR (2443) with a Wratten 12 filter plus a Color Compensating Filter CC30B. The purpose of this test was to see the effects of altering the color balance.

All of the films exposed on the aerial test were processed in the Remote Sensing Work Unit's photo lab in Berkeley, California. Color film processing is handled in Nikor 70 mm film processing equipment (Figure 39), which utilizes 3 1/2-gallon capacity stainless steel tanks and spiral reels that accommodate up to 100 feet of film. Shown below are the chemical processes used, chemical volumes available from manufacturer, and the temperature recommended for each process.

| Film | Process | Unit Size | Process Temperature |
|---|---|---|---|
| Anscochrome D/200 | AR-1 | 3 1/2 gal. | 68° or 75° F. |
| Ektachrome IR - 8443 | E-3 | 3 1/2 gal. | 75° F. |
| Ektachrome EF - SO-397 | E-4 | 3 1/2 gal. | 85° F. |
| Aerochrome IR - 2443 | E-4 | 3 1/2 gal. | 85° F. |

Prior to processing, sensitometer exposures were made on each film using a Joyce-Gevaert Type 2L sensitometer with a continuous density

Figure 39. Nikor 70 mm film processing equipment in the remote sensing photo lab.

wedge. The Anscochrome and Ektachrome Infrared (8443) films were then processed according to the manufacturers' recommended processing procedures.

Aerochrome Infrared (2443) was processed in standard Ektachrome film chemicals, Process E-4. The processing of 2443 in Nikor equipment differs from the processing instructions that are packaged with the E-4 chemicals. Agitation procedures and processing times are different. The pH of the color developer was adjusted by adding 33 ml of 7N sodium hydroxide solution to the 3 1/2 gallons of developer solution. Processing times and agitation procedures are given in an Eastman Kodak Data Release (7).

The processing of Ektachrome EF (SO-397) was not as straightforward as were the other film processes. Processing procedures were requested from Eastman Kodak in Rochester, New York, and they replied that they do not actually have processing instructions for Ektachrome EF (SO-397) or processing cycles for 70 mm Nikor-type equipment. They did suggest that the instructions for Ektachrome MS Aerographic (2448) would be a good starting point, but the instructions for film 2448 are recommended processing procedures and times for rewind processing equipment. In order to get some idea of what the processing times should be for SO-397, a list was tabulated to show the processing times by step for 2448 (rewind processing), 2443 (rewind processing), and 2443 (spiral reel processing). With the exception of the first developer, the rewind times for 2448 and 2443 were the same for all steps. Rewind times were then compared with the spiral reel processing times for 2443. This comparison showed a time reduction in about half of the processing steps. On the basis of these comparisons, we felt safe in using the processing times and

agitation procedures for 2443 spiral reel processing (7). The only change we made was in the first developer time -- 5 1/2 minutes instead of 7 minutes. The 5 1/2-minute first developer time was selected by noting what relationships existed between times for the different processes, plus the fact that Nikor processing usually requires less development time than rewind processing. A short length of film, containing a series of test exposures and a continuous wedge sensitometer exposure, was processed according to our selected times. The processed sensitometer exposure appeared to have a good range of densities, and the test exposures had good color balance and exposure. The film from the aerial test was then processed in the same batch of chemicals.

An additional processing test was run to check the effects of different first developer times on the SO-397. Three 10-inch lengths of film were cut from film bearing the same emulsion number as the film used on the aerial test. Identical sensitometer exposures (with a continuous wedge) were made on each of the three strips of film. The three strips were clipped to 8- x 10-inch film hangers, and the hangers were coded with tape for easy identification in the dark. Then the test strips were processed in the Nikor tanks containing E-4 processing solutions. Processing times and agitation procedures were the same as those used on the test film. After the first two steps (Prehardener and Neutralizer) the hangers were transferred to the First Developer tank. The three developing times selected were 4 1/2, 5 1/2, and 6 1/2 minutes. At the end of the required time, a hanger was removed according to its coded number and placed in the First Stop Bath tank. For the remainder of

the processing, all three strips received identical treatment.

As one might expect, there was little change in color balance due to variation in first developer time but considerable effect on film speed. The characteristic curves using a clear scanning aperture in the Photometric Data Systems microdensitometer are shown for the three developing times in Figure 40. The speed of film developed for 4 1/2 minutes is roughly one half of that for 6 1/2 minutes developing time.

Five sets of scan runs with 100 density measurements each were performed on the film strips for the determination of film granularity. The mean density of the five runs was 1.0. The spot size was 44 μm, and the sampling interval was 48 μm x 480 μm x-y matrix on the film. No D. C. drifts in the density of the x-y arrays were seen, thereby verifying each scan run as having a sufficiently uniform exposure for granularity measurements. The standard deviation of the density multiplied by 1,000 is the usual expression of granularity. The results displayed below shown a tendency for increased granularity with developing time, but the differences are not significant.

| Developing time (m) SO-397 | Mean granularity of 5 scan runs | Standard deviation |
|---|---|---|
| 6.5 | 14.9 | 1.1 |
| 5.5 | 15.5 | 1.8 |
| 4.5 | 13.4 | 0.3 |

The indication is that for greater film speed without appreciable loss of acuity even longer developing times might be possible. Tests of resolution as well as granularity should be performed on the longer times, however.

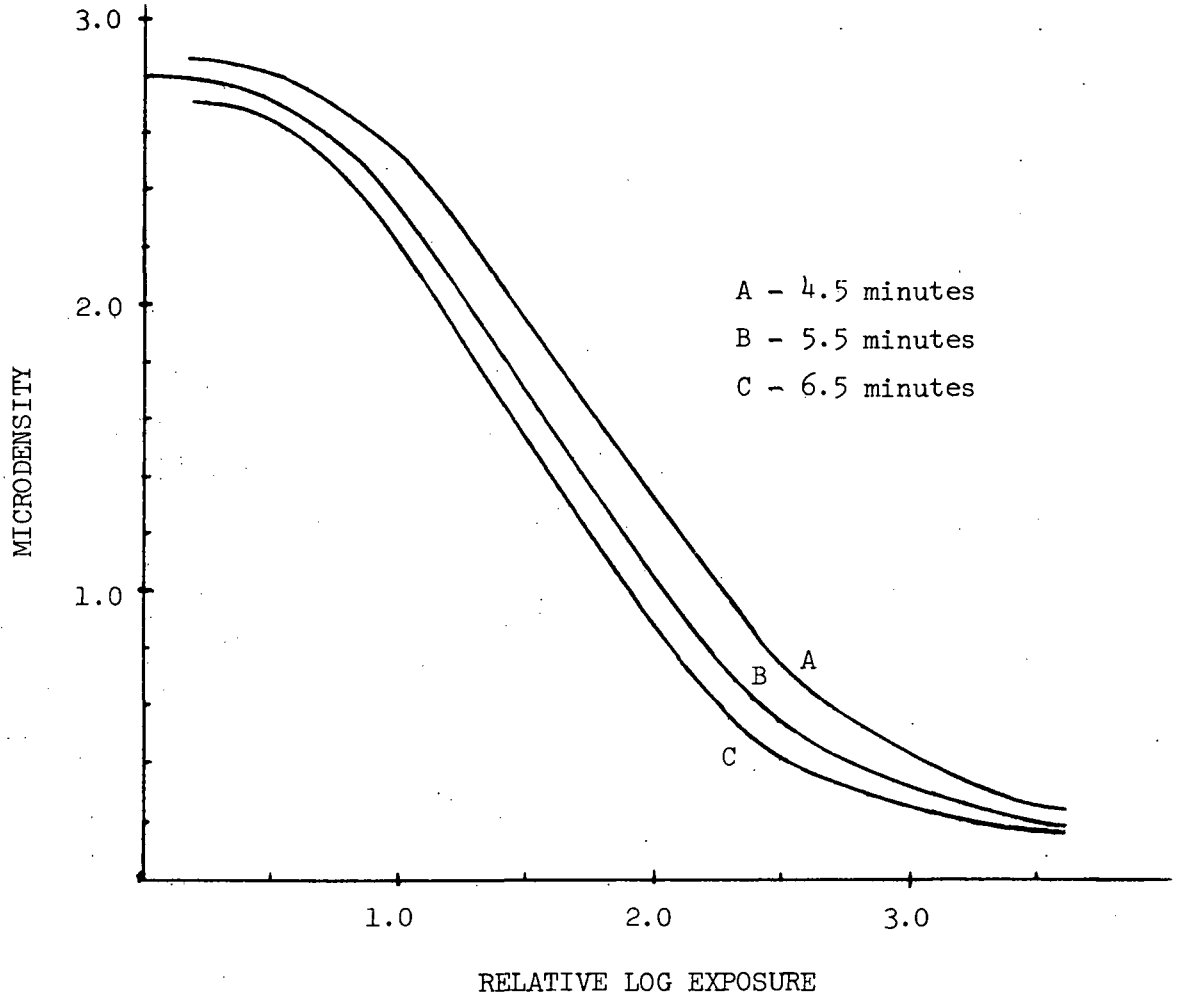


Figure 40. Characteristic curves for SO-397 processed at three different first developer times. Densitometry done with clear filter (white light).

After processing, all rolls of film were cut into shorter lengths according to exposure (normal, over, and under) or different film-filter combinations. A master list of all these film strips was compiled, and each strip was given a random number in order to eliminate as much bias as possible in the evaluation. The evaluation consisted of a group of subjective questions given to five experienced photo interpreters. The interpreters had a total of 70 years experience (ranging from 3 to 25 years) in looking at color and color infrared films on various remote sensing studies.

The questionnaire asked each interpreter to look at various numbered film strips, make certain comparisons, and give an evaluation. The flow chart (Figure 41) illustrates the various combinations and comparisons included in the interpretation. The interpreters were also asked to evaluate the color panels on the D/200 and SO-397 for color fidelity. A set of miniature color panels having the same paint as the panels displayed on the ground was used to make the comparisons.

An ASA rating was achieved for each film by evaluating the interpreters' selections as to which film strips had the best exposures. For example, the interpreters were told to look at film strips #4, #14, and #16 and select the best exposure for timber. In this particular case, three interpreters selected #4 (normal exposure) and two interpreters selected an exposure between #4 and #16 (between normal and over). From our aerial photography records we knew the camera settings and the light meter readings of timber and range vegetation. By putting these values into the meter calculator we worked backwards to a resulting ASA rating for a particular film-subject combination. This was done for all film-subject combinations looked at by each interpreter. The average ASA

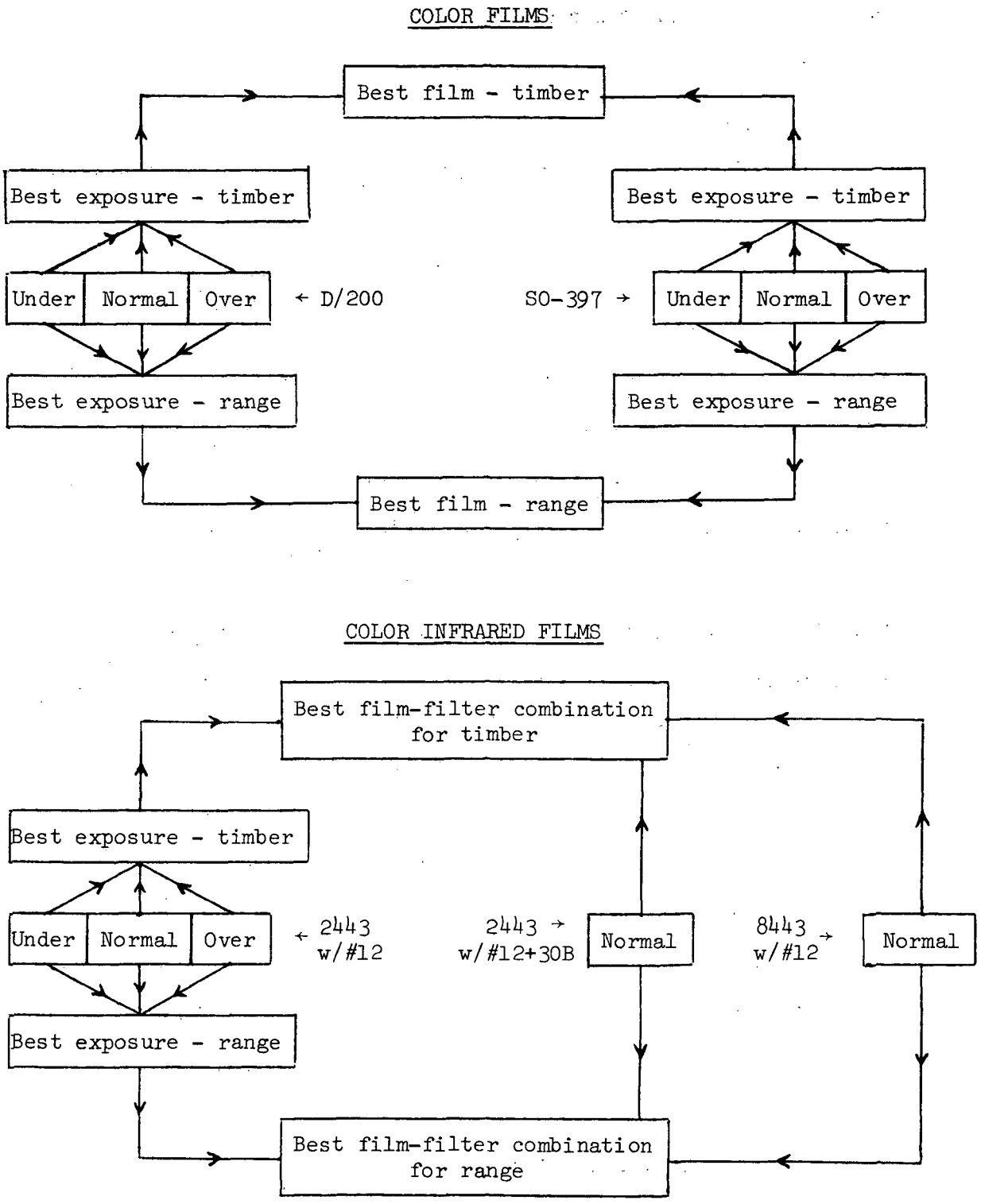


Figure 41. Flow chart showing the various combinations of film and filters on the aerial test and the comparisons made in the interpretation analysis.

ratings we arrived at are shown in the following list of ASA exposure indices.

| Film | Timber | Range |
|---|---|---|
| D/200 | 325 | 300 |
| SO-397 | 325 | 280 |
| 2443 w/#12 | 350 | 320 |

Each of these ASA ratings is actually a film speed for a particular emulsion number that is exposed at low altitude (800 feet) and is processed by the spiral reel (Nikor) equipment and procedures.

The interpreters compared the color panels on the D-200 and SO-397 films to the miniature color panels and rated the films. For overall color rendition and range of color sensitivity, the interpreters selected the SO-397. The following listing shows the composite evaluation of five interpreters for Munsell color rendition on the two color films.

| COLOR | FILM | |
|---|---|---|
| Munsell notation | D/200 | SO-397 |
| 10 R | Best | --- |
| 5 YR | Same | Same |
| 10 YR | --- | Best |
| 5 Y | Same | Same |
| 5 GY | --- | Best |
| 10 GY | --- | Best |
| 5 G | --- | Best |

Table 35 summarizes the interpreters' subjective comments on film response to natural subjects. They were asked to evaluate one film against another in terms of overall color balance and the color rendition

of timber and range based on their past experience with color and color infrared films.

The characteristic curves of the two normal color films are illustrated in Figures 42 and 43. They are three-color microdensitometer scans of sensitometer exposures that were included in the test film processing runs. The similar location of the curves along the exposure axis verifies that the films are approximately equivalent in speed. The slope of the D/200 curve is steeper in the medium density range, indicating it has greater sensitivity but less latitude than has SO-397. Although the D/200 color curves are grouped very closely together, a slight yellowish red tendency is suggested. The SO-397 color balance is definitely cast towards cyan in this example, as was also seen to be true in two other processing runs. These color balance conclusions are somewhat verified by the interpreters' opinions of color panel renditions as shown in the preceding table.

A scheme for quantitative color fidelity measurements has been devised using reflectivity measurements. Each of the color panels was subjected to diffuse reflection density measurements using a daylight source and six narrow-band analyzing filters. The same filters can be used in the microdensitometer, and the detectors in the two instruments are nearly identical in spectral response. The microdensitometer work on the film test images has not been completed, but it is hoped that these data can be correlated with the reflectivity data to rate the color accuracy of films. For example, a high correlation between film density and reflection density of a given panel should indicate that a film is very capable of reproducing that particular hue and chroma. A low correlation between

Table 35. Summary of five interpreters' evaluation of color and color infrared films.

| TASK | RESULTS | GENERAL COMMENTS OF INTERPRETERS |
|---|---|---|
| Best color film for timber | 3 out of 5 said SO-397 (vs D/200) | Better discrimination between shades of green. More color variation between trees. |
| Best color film for range vegetation | 3 out of 5 said SO-397 (vs D/200) | Good separation between green and brown vegetation. Better for separating small range plants by minor color differences. |
| Best color IR film (film-filter combination) for timber and range vegetation | All 5 agreed that 2443 w/#12 filter was best for overall vegetation | 2443 w/#12 - Good IR response. Best discrimination of vegetation, ground cover, and soils. Good range of hues - good differentiation on trees and between plant species.<br>2443 w/#12 + 30B - Oversaturated with red (especially for timber). Strong red masks subtle hue differences. No blues or greens. Areas on 2443 w/#12 that were blue are now broken into reds and purples.<br>8443 w/#12 - Weak red response, mostly magenta, blue, and purples. Fair for timber interpretation. Good hue differentiation on timber. IR response poorer than on 2443 w/#12. |
| Additional test of filters with 2443 over range area in Colorado one week after film test in California. #12 filter vs #12 + 30B. | All interpreters felt that the addition of the blue filter was the best for range conditions | 2443 w/#12 - IR response poorer for vegetation. Better discrimination between living and dead vegetation. IR response of plants is somewhat masked by an overall blue. Contrast between red vegetation and blue background not as good.<br>2443 w/#12 + 30B - Best discrimination by IR response. Best range of colors for IR response of plants (red, pink, yellow, brown, green). Better for relating plant condition (maturity and IR reflectance). Better contrast between red and the green background. Flowers show up better. |

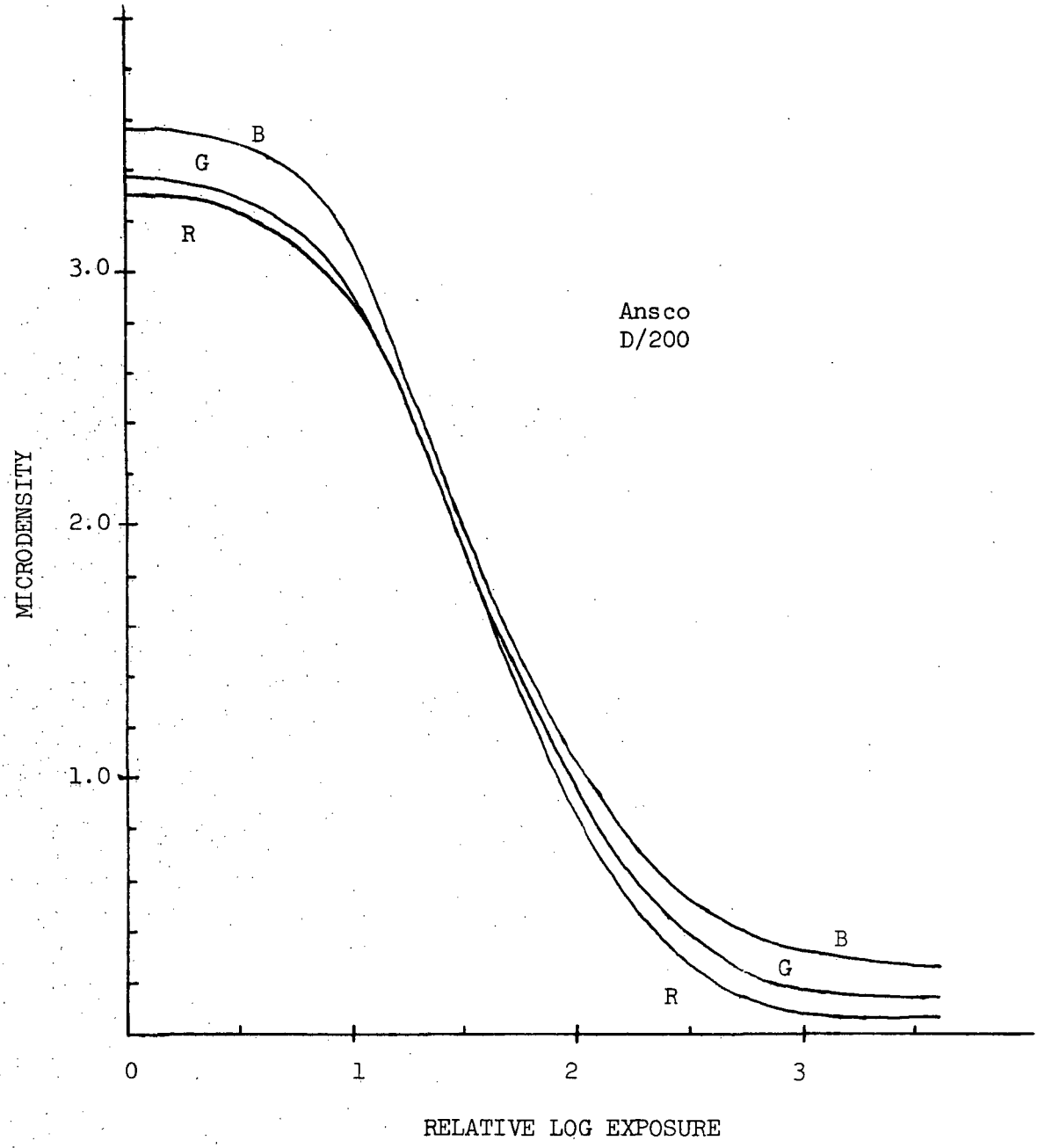


Figure 42. Color response curves of the Ansco D/200 film test emulsion. Kodak Wratten filters 92, 93, and 94 were used in the densitometry for red, green and blue response, respectively.

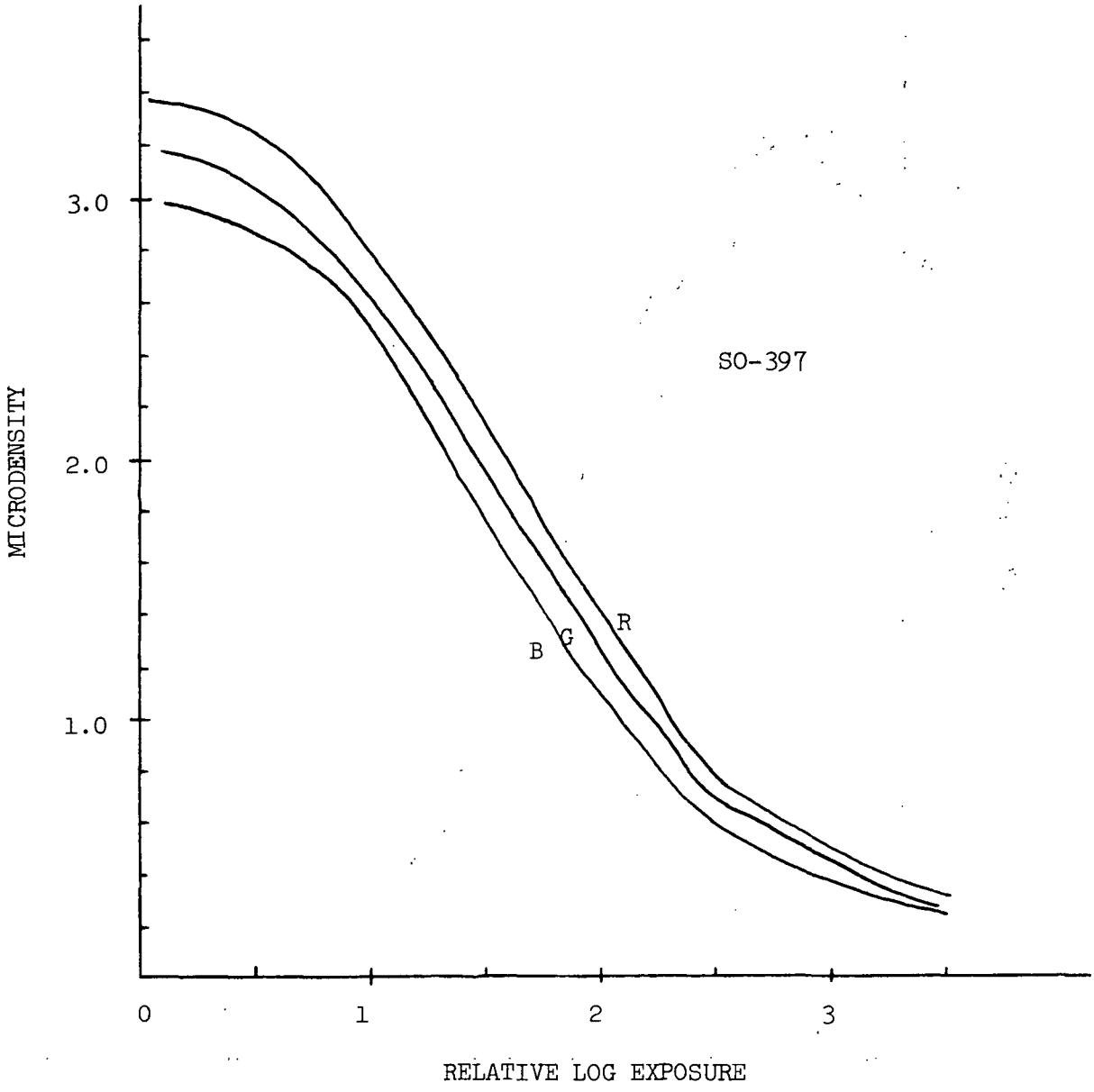


Figure 43. Color response curves of the SO-397 film test emulsion. Kodak Wratten filters 92, 93, and 94 were used in the densitometry for red, green, and blue response, respectively.

film image densities of two different panels might indicate an ability to separate those Munsell colors. Of course, exposure and sensitometry differences between films occur in the test. Therefore, one should use equivalent log E rather than film density in the regression analysis.

We are also proceeding with film and system resolution tests. The subject is too complex to discuss fully in this report, but it is sufficient to say that we intend to generate modulation transfer functions from microdensitometer edge analysis (13). Combining these functions with threshold modulation figures will give the most meaningful quantitative measure of resolution. A test of color fidelity and resolution for high-altitude applications is also planned for the near future.

## IMAGE ENHANCEMENT IN PATTERN RECOGNITON

One of the most promising aspects of the use of photographic calibrations is the possibility of enhancing photographic imagery to aid in the recognition patterns and in the automatic identification of forest and range objects. Specifically, the quantitative adjustment for exposure variations and for different color balance situations is often needed. The color balance aspect is especially important in the case of studies using infrared color film which has exhibited unpredictable variation in response. During the time period of an extended study (1) different processing techniques on film emulsions might be used, (2) different filters might be experimented with, and (3) aging changes or even manufacturing changes might take place.

The problem of exposure variations can be exemplified by considering the phenomena commonly called vignetting which is the radial fall-off of illumination on the image plane of a camera. Two effects are present

here. One is true vignetting -- the limitation of the cone of light from off-axis points by the edges of the various lens elements (11). The other is the reduction of irradiance due to aspect angle and the increased object distance for off-axis points of a flat object plane imaged on a flat image plane (5). The latter effect amounts to a $\cos^4\theta$ reduction where $\theta$ is the nadir angle for vertical aerial photography.

As an example of the $\cos^4\theta$ effect let us take n samples of optical density of images of uniform targets located at each of the nadir angles $0^\circ$, $10^\circ$, $20^\circ$, and $25^\circ$. The relative irradiance or exposure values at these angles are shown below:

| Nadir angle $\theta$ (degrees) | 0 | 10 | 20 | 25 |
|---|---|---|---|---|
| $\cos^4\theta$ | 1.00 | 0.941 | 0.780 | 0.675 |

Each group of n samples is assumed to be distributed normally about the same mean value $\bar{D}$ having a standard deviation of $\sigma$. They could be normalized to the $\theta = 0$ value using sensitometric data and lumped together as a group of 4n samples with a mean equal to $\bar{D}$ and the same standard deviation $\sigma$. However, if these samples were combined without calibration for exposure difference, the distribution would not be normal as shown in Figure 44. The mean of this bimodal distribution is $\bar{D} + 0.15$ for a uniform film gamma equal to 2.0 and for $\sigma$ equal to 0.06. The standard deviation is approximately $2\sigma$ (or 0.12).

The net effect of combining samples from different areas on the image plane is to reduce confidence in imagery that might possibly identify a target by mean density alone. One could conceivably have targets with a true standard deviation of 0.03 to 0.04 in density units and have a combined distribution almost as broad as shown above due to the great

spread in exposure values. Wherever vignetting is not precisely corrected by filtration there appears to be a need for accurate calibration in film pattern recognition, especially since combining measurements at different nadir angles in different sample sizes is often necessary and would surely result in errors for grouped mean density.

The previous example showed the effect of exposure variations of a single film layer of color film or for black-and-white film. Let us now consider the case of infrared color film which requires consideration of three spectral response curves. They can be denoted as blue, green, and red responses which are the false color representations of green, red, and infrared light, respectively, incident on the film.

In Figure 45 we have a set of sensitometric curves representing the general case of "aim" curves for imagery acquired through the NASA Earth Observation Aircraft Program (10). The green curve is a thin line, and the tolerances of the blue and red curves with respect to the green curve are expressed as stippled bands.

Let us work with a central relative log exposure level of 1.35 from a graybody and levels 1/2 stop underexposed and overexposed at 1.2 and 1.5. Assume first that the blue and red curves are the upper limits (in density) of the tolerance bands of Figure 45. The resultant density values in the three colors are shown in Table 36. The expected standard errors are shown in parenthesis and represent the approximate density reading errors one would expect. The column on the right shows the effect of combining equal-sized samples of data taken from photos exposed at the three levels 1/2 stop apart. The mean density values vary greatly from the high and low exposure values, and uncertainties of up to 0.39 are

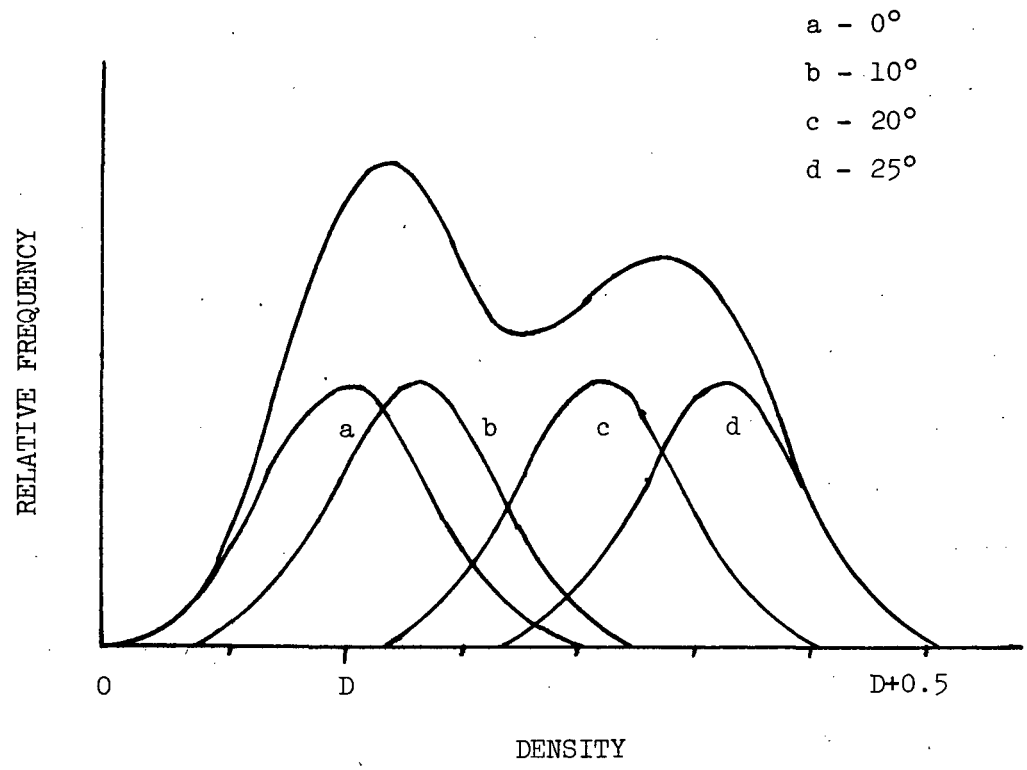


Figure 44. Bimodal distribution of density values produced by combining four equal-sized normally distributed groups without calibration. The displacement in mean density of the groups is due to the $\cos^4\theta$ reduction in exposure, where $\theta$ = 0°, 10°, 20°, 25°. Film gamma is 2.0.

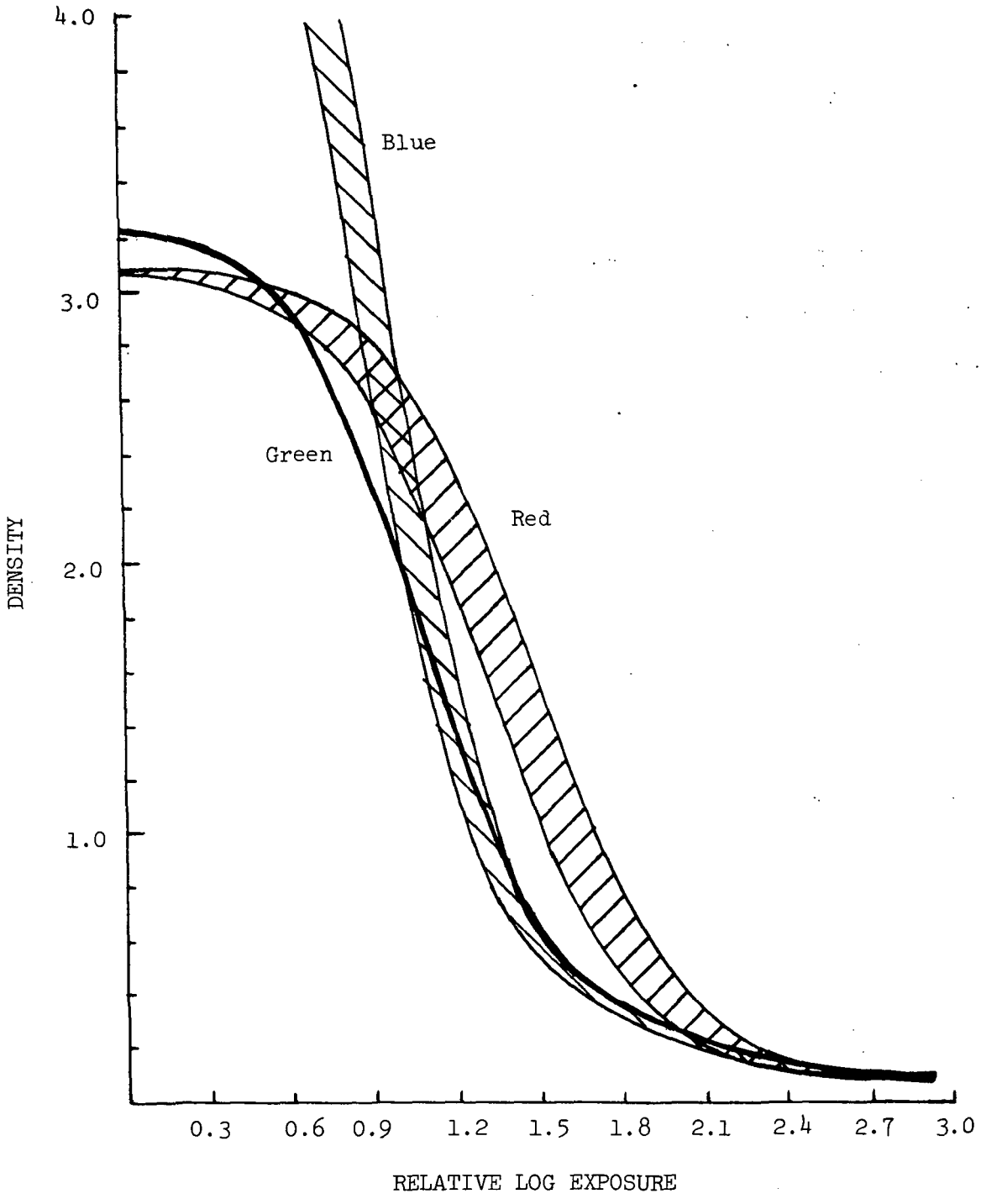


Figure 45. NASA aim curves for the general situation of Kodak 2443 infrared color film.

indicated. Note that the mean density is not close to the density value for the median exposure in the case of the blue response.

Uncertainties may be reduced considerably by normalizing the red and blue curves with respect to the green curve. There appears much less scatter in the data for blue-green and red-green, but it is still not down to the level of 0.02 that proper calibration would yield. The effects of underexposure seem to be more harmful to the averaging process than overexposures.

Now let us combine the effects of exposure with film response and processing by considering samples of different exposure and different sensitometry. Assume that four measurements are taken on film having the same three exposure levels and having four arrangements of the blue and red curves with respect to the green curve. The green curve is fixed, and green densities are the same as in the previous example but with uncertainty of zero for simplicity. The four blue-red relationships are high blue-high red, high blue-low red, low blue-high red, and low blue-low red ($D_{11}$, $D_{12}$, $D_{21}$, $D_{22}$ in the matrices of Table 37), and the values are within the tolerances of Figure 45. Mean values of each subgroup have overhead lines.

Subgroup standard deviations are large in Table 37 in terms of usual density measurement capabilities, and combining data for each exposure level again results in large standard deviations. The normalization process of subtracting the green density also fails to erase the uncertaintly.

Although the exposure and sensitometric distributions used in these examples are hypothetical and are not directly derived from actual experiments, the trends of optical film density are based on firm physical

Table 36. The effect of exposure level on the red, blue, and green density of infrared color film (2443). The density values are derived from the upper limits of the curves of Figure 44. Standard deviations are shown in parentheses.

| | Relative Log Exposure 1.20 | 1.35 | 1.50 | Exposure levels combined in equal parts |
|---|---|---|---|---|
| Green density | 1.38 (.02) | 0.94 (.02) | 0.60 (.02) | 0.97 (.32) |
| Blue density | 1.54 (.02) | 0.98 (.02) | 0.64 (.02) | 1.05 (.39) |
| Red density | 2.30 (.02) | 1.96 (.02) | 1.56 (.02) | 1.94 (.30) |
| Blue minus green density | 0.16 (.03) | 0.04 (.03) | 0.04 (.03) | 0.08 (.06) |
| Red minus green density | 0.92 (.03) | 1.02 (.03) | 0.96 (.03) | 0.97 (.04) |

Table 37. The effect of exposure, film response, and processing on the red, blue, and green density of infrared color film (2443). The results of four combinations of high and low sensitometer curves for blue and red response with respect to a stable green curve are shown in the 2 x 2 matrices. Standard deviations for groupings are in parentheses. Mean values have overhead lines.

| | Relative Log Exposure 1.20 | | 1.35 | | 1.50 | | Exposure levels combined in equal parts |
|---|---|---|---|---|---|---|---|
| Green density | 1.38 | 1.38 | 0.94 | 0.94 | 0.60 | 0.60 | $\overline{0.97}$ |
| | 1.38 | 1.38 | 0.94 | 0.94 | 0.60 | 0.60 | (.32) |
| | $\overline{1.38}$ | (.00) | $\overline{0.94}$ | (.00) | $\overline{0.60}$ | (.00) | |
| Blue density | 1.54 | 1.54 | 0.98 | 0.98 | 0.64 | 0.64 | $\overline{0.92}$ |
| | 1.12 | 1.12 | 0.72 | 0.72 | 0.52 | 0.52 | (.35) |
| | $\overline{1.33}$ | (.21) | $\overline{0.85}$ | (.13) | $\overline{0.58}$ | (.06) | |
| Red density | 2.30 | 1.84 | 1.96 | 1.46 | 1.56 | 1.02 | $\overline{1.69}$ |
| | 2.30 | 1.84 | 1.96 | 1.46 | 1.56 | 1.02 | (.41) |
| | $\overline{2.07}$ | (.23) | $\overline{1.71}$ | (.25) | $\overline{1.29}$ | (.27) | |
| Blue minus green density | 0.16 | 0.16 | 0.04 | 0.04 | 0.04 | 0.04 | $\overline{-0.05}$ |
| | -0.26 | -0.26 | -0.22 | -0.22 | -0.08 | -0.08 | (.15) |
| | $\overline{-0.05}$ | (.21) | $\overline{-0.09}$ | (.13) | $\overline{-0.02}$ | (.06) | |
| Red minus green density | 0.92 | 0.46 | 1.02 | 0.52 | 0.96 | 0.42 | $\overline{0.72}$ |
| | 0.92 | 0.46 | 1.02 | 0.52 | 0.96 | 0.42 | (.27) |
| | $\overline{0.69}$ | (.23) | $\overline{0.77}$ | (.25) | $\overline{0.69}$ | (.27) | |

principles and could easily occur. There are certainly indications that film calibrations could aid in automatic interpretation studies such as the land-use classification program. To the extent that sensitometric and other photometric data are available, these calibrations will be applied to the Apollo 9 and RB-57 imagery.

## LITERATURE CITED


1. American National Standards Institute, Inc. 1958. Sensitometric exposure of daylight-type color films. ANSI Standard PH 2.11-1958, American National Standards Institute, Inc., New York, New York.
2. Dana, R. W. 1971. Calibration of color aerial photography. Special Report for Earth Resources Survey Program, OSSA/NASA, by the Pacific Southwest Forest and Range Experiment Station. 14. p.
3. Gates, D. M. 1966. Spectral distribution of solar radiation at the earth's surface. Science 151(3710):523-529.
4. Gates, D. M. 1970. Physical and physiological properties of plants. In, Remote Sensing with Special Reference to Agriculture and Forestry, National Academy of Sciences, Washington, D. C., p. 237.
5. Jensen, N. 1968. Optical and photographic reconnaissance systems. John Wiley and Sons, Inc., New York, pp. 73-76.
6. Judd, D. B., D. L. MacAdam, G. Wyszecki. 1964. Spectral distribution of typical daylight as a function of correlated color temperature. Jour. of the Optical Soc. of America, 54(8):1031-1040.
7. Kodak Data Release. 1970. Instructions for processing Kodak Aerochrome Infrared Film 2443 using stainless steel spiral reels. Eastman Kodak Co., Rochester, N. Y.

8. Kodak Data Release. 1971. Notes on the Kodak Aerial Exposure Computer. Publication No. M-77. Eastman Kodak Co., Rochester, New York.

9. Kodak Publication No. M-29. 1971. Kodak data for aerial photography. Eastman Kodak Co., Rochester, N. Y.

10. Pierce, W. N. 1971. Earth Observations Aircraft Program Film Output Product Specifications. Technical Working Paper for NASA Contract NAS 9-10950, National Aeronautics and Space Administration, Manned Spacecraft Center, Houston, Texas.

11. Smith, W. J. 1965. Optics. In, Handbook of Military Infrared Technology, W. L. Wolfe, Ed. Office of Naval Research, Department of the Navy, Washington, D. C. p. 378.

12. Taylor, A. H. and G. P. Kerr. 1941. The distribution of energy in the visible spectrum of daylight. Jour. of the Optical Soc. of America, 31:3-8.

13. Welch, R. 1971. Modulation transfer functions. Photogram. Engng., 37(3):247-259.